Towards a complete mass spectrum of type-IIB flux vacua at large complex structure

Jose J. Blanco-Pillado,[a,b] **Kepa Sousa,**[c] **Mikel A. Urkiola**[a] **and Jeremy M. Wachter**[d]

[a] *Department of Theoretical Physics and History of Science,*
University of the Basque Country UPV/EHU,
48080 Bilbao, Spain
[b] *IKERBASQUE, Basque Foundation for Science,*
48011, Bilbao, Spain
[c] *Institute of Theoretical Physics, Faculty of Mathematics and Physics,*
Charles University in Prague,
V Holesŏvičkách 2, Prague, Czech Republic
[d] *Skidmore College Physics Department,*
815 North Broadway Saratoga Springs, New York 12866
E-mail: josejuan.blanco@ehu.eus, kepa.sousa@utf.mff.cuni.cz,
mikel.alvarezu@ehu.eus, jwachter@skidmore.edu

Abstract: The large number of moduli fields arising in a generic string theory compactification makes a complete computation of the low energy effective theory infeasible. A common strategy to solve this problem is to consider Calabi-Yau manifolds with discrete symmetries, which effectively reduce the number of moduli and make the computation of the truncated Effective Field Theory possible. In this approach, however, the couplings (e.g., the masses) of the truncated fields are left undetermined. In the present paper we discuss the tree-level mass spectrum of type-IIB flux compactifications at Large Complex Structure, focusing on models with a reduced one-dimensional complex structure sector. We compute the tree-level spectrum for the dilaton and complex structure moduli, *including the truncated fields*, which can be expressed entirely in terms of the known couplings of the reduced theory. We show that the masses of this set of fields are naturally heavy at vacua consistent with the KKLT construction, and we discuss other phenomenologically interesting scenarios where the spectrum involves fields much lighter than the gravitino. We also derive the probability distribution for the masses on the ensemble of flux vacua, and show that it exhibits universal features independent of the details of the compactification. We check our results on a large sample of flux vacua constructed in an orientifold of the Calabi-Yau $\mathbb{WP}^4_{[1,1,1,1,4]}$. Finally, we also discuss the conditions under which the spectrum derived here could arise in more general compactifications.

Contents

1   Introduction

The need to compactify the 6 or 7 extra dimensions of supersymmetric string theories leads to significant technical problems, which make the study of the phenomenological and cosmological implications of the Landscape of $4d$ Effective Field Theories (EFTs) exceedingly difficult. One of these problems is the huge number of fields arising in these EFTs, *the moduli*, which describe the geometry of the compact space. This makes the computation of the complete EFT prohibitively complex, and as a consequence it has only been obtained for simple compactifications. Another difficulty is the vast number of possible ways to compactify the extra dimensions, which makes it infeasible to characterise every possible four dimensional vacuum of the theory.

In the last few decades, several complementary strategies have been followed to overcome these technical problems. On the one hand, many efforts have been dedicated to studying explicit models where most of the moduli can be truncated or integrated out, leaving only a few fields (up to ten) for which the EFT can be computed [1–12]. In such models the observational implications can be studied in detail, and these explicit computations have been used as lampposts to guide the analysis of more complex scenarios. On the other hand, instead of attempting an exhaustive examination of all possible string compactifications, one can take a statistical perspective. In this approach one regards this set of solutions as a statistical ensemble and characterises the probability distributions of the relevant observables in such a Landscape [13–17]. It is expected (or hoped) that some of these quantities will exhibit universal properties, i.e., independent of the specific details of each particular EFT, which would partially alleviate the need to compute the effective theories. Following this approach one could try to model the complicated low-energy effective potential as a random function with some particular statistics; for example, as a multidimensional Gaussian random field. This procedure has been recently developed in the literature in relation to different aspects of the distribution of vacua of this potential as well as its applications to cosmology [18–34].

Finally, the more recent *Swampland program* is directed to find universal constraints that should be satisfied by any EFT arising in a consistent theory of quantum gravity [35–37] (see also [38, 39] and references therein). These constraints determine conditions under which the EFTs are under computational control, and serve to identify which low-energy solutions can be regarded as plausible string theory vacua. In this respect, the Swampland program sets an outermost limit for the boundaries of the Landscape.

In the present paper we will take a conservative approach and discuss one of the best studied domains of the Landscape: the tree-level flux vacua on Calabi-Yau compactifications of type-IIB superstrings at Large Complex Structure (LCS). The construction of the EFTs describing this corner of the Landscape, and the applicability of these theories, has been widely discussed in the literature [40–44] (see [45] for a review). Among this class of models, phenomenologically interesting compactifications generally involve a large number of complex structure moduli and only a few Kähler moduli (see, e.g., [12]). However, as we mentioned above, the detailed construction of the complete Effective Field Theory is prohibitive in general. Consequently, explicit constructions of flux vacua are often based on Calabi-Yau manifolds invariant under large groups of discrete symmetries which allow a consistent supersymmetric truncation of a large fraction of the complex structure moduli [6–10, 12]. These groups of symmetries arise naturally when compactifying on hypersurfaces of complex projective spaces and toric varieties, and on Complete Intersection Calabi-Yaus (see [46, 47] and references therein). Particular and prominent examples are the discrete symmetry groups which allow the Greene-Plesser construction of the mirror Calabi-Yau pairs [48]. Provided only fluxes invariant under these symmetries are turned on, it is possible to *freeze* a large set of complex structure moduli at a critical point of the resulting flux scalar potential, leaving a reduced theory for a few surviving fields [6–9]. The phenomenological and cosmological predictions of these models are then computed after including the relevant quantum corrections and supersymmetry breaking effects *in the reduced theory.* However, the fate of the truncated fields is rarely discussed in detail [10, 12].

The main objective of this work is to take a first step towards a more precise understanding of the truncated moduli sector in this class of models. Note that, in the approach we just described, the truncated moduli are not *integrated out*; instead, the resulting EFT is a *consistent supersymmetric truncation* of the complete low energy theory at tree-level, and thus there is not necessarily a mass gap between the frozen moduli and those in the reduced theory [49–51]. Actually, although the truncated sector is guaranteed to be at a stable configuration at tree-level, the spectrum might contain arbitrarily light fields. Thus, in principle the quantum corrections and the breaking of supersymmetry could render some of these light fields tachyonic. Alternatively, the fixed point of the discrete symmetry group could cease to be a critical point of the corrected scalar potential.

The perturbative stability of the complete complex structure and axio-dilaton sector has been proven using scaling arguments for generic KKLT constructions [1], and for Large Volume Scenarios (LVS) with an exponentially large compactification volume [2–4]. The case of Kähler uplifted vacua [5] and LVS scenarios with moderately large volume [52–55] is more subtle. In [56], it was argued, using statistical techniques, that these classes of vacua may contain a sizeable fraction of tachyonic fields in the truncated sector. It is

important to emphasize that, despite of all of these efforts, the complete mass spectrum in the truncated sector has never been explicitly computed.

Here we will focus on the simplest possible class of these models, those where the reduced theory contains a single complex structure modulus. Although this is a rather restrictive type of compactification, it contains plenty of examples (see, e.g., [57–61]). Furthermore, the moduli space geometry is well characterised for many of them [62–65], including the well known family of quintic hypersurfaces $\mathbb{WP}^4_{[1,1,1,1,1]}$ and its generalisations [41, 57, 58, 66]. We will prove, using only symmetry arguments and properties of the effective theory on type-IIB compactifications at LCS, that it is possible to compute the tree-level mass spectrum for the axio-dilaton and the complete set of $h^{2,1}$ complex structure moduli fields, *including the truncated ones.*

Interestingly, the resulting set of masses can be expressed entirely in terms of the known couplings of the reduced effective theory, and exhibits universal features independent on the details of the compactification. More specifically, to leading order in α' and the string coupling g_s, we find that the $2h^{2,1} - 2$ real scalar modes on the truncated sector have squared masses $\mu^2_{\pm\lambda}$ given by

$$\mu^2_{\pm\lambda} = \left(m_{3/2} \pm m_{\text{susy}} \frac{1+\xi}{\sqrt{3(1-2\xi)}}\right)^2, \qquad \text{with} \qquad \lambda = 2,\ldots,h^{2,1}.$$

This expression involves only two scales which can be computed in the reduced theory: the gravitino mass, $m_{3/2}$, and the scale of supersymmetric masses induced by the fluxes, m_{susy}. The real parameter $\xi \in [0,1/2]$ depends on the configuration of the complex structure of the reduced theory, and in particular it takes the value $\xi = 0$ at the LCS point. Analogous universal properties of the spectrum of matrices arising in the effective theory were previously reported in [67, 68], where the authors considered generic points of the moduli space, i.e., not necessarily flux vacua. The computations of the mass spectra rely on the perturbative description of the moduli space geometry at large complex structure, and thus are valid provided the exponentially suppressed instanton corrections can be neglected.

In order to illustrate our results, we have compared our analytic formulae with a numerical scan of flux vacua of type-IIB compactified on an orientifold of $\mathbb{WP}^4_{[1,1,1,1,4]}$ [57, 66]. This family of hypersurfaces has a $h^{2,1} = 149$ dimensional complex structure moduli space, which can be consistently reduced to a single field at the fixed locus of a $\mathbb{Z}_8^2 \times \mathbb{Z}_2$ symmetry. Using the known reduced effective theory, we construct a large ensemble of flux vacua and verify the validity of the formulae we derived for masses of the axio-dilaton and the complex structure field on the reduced theory. It is important to stress that, at each of these vacua, our results allow us to infer the masses of all of the truncated 148 complex structure fields, *without the need to compute the complete EFT.*

For generic vacua, the mass spectrum has a dependence on the fluxes and thus, to have a characterisation of the perturbative stability independent of the flux choice, we resort to statistical methods. More specifically, we use the techniques derived in the seminal papers [15, 16], whose only assumption is the continuous flux approximation. With this at hand, we are able to analytically compute the probability distribution for the complete

set of masses in the ensemble of flux vacua, and show that the statistical properties of the spectrum are independent of the compactification. Then, we compare the "empirical" mass distributions from the ensemble of vacua in the $\mathbb{WP}^4_{[1,1,1,1,4]}$ model with the predicted probability distributions, and show they are in good agreement within the regime of validity of both the EFT and the continuous flux approximation.

Regarding the validity of the statistical methods, our numerical scan shows a deficit in the number of generic no-scale vacua with respect to the theoretical statistical distributions in a small neighbourhood of the LCS point. This is in perfect agreement with previous analyses which predict a breakdown of the continuous flux approximation in this limit [15, 68–70]. The failure of this approximation leads to an absence of generic no-scale vacua in the LCS limit [71] of one-parameter models, other than the vacuum sitting on the LCS point itself [72] (see also [73]).

For completeness we have also compared our analysis with an alternative method aimed at describing the statistical properties of the complex structure sector in the flux ensemble: the Random Matrix Theory (RMT) approach. These models were originally proposed in [16], and further developed in [51, 56, 74, 75]. Here we show that this method, whose validity relies on the complexity of the couplings in generic string compactifications, does not correctly characterise the obtained mass spectra of the models we study here. This can easily be explained by noting that the large group of symmetries present in these models severely constrains the allowed values of couplings of the effective theory, and this resulting simplicity violates the premise on which Random Matrix Theory method is based. The failure of the RMT approach to describe the mass spectra arising in the LCS regime of more general type-IIB flux compactifications was also discussed in [67].

To conclude, we will argue that the universal spectra and mass distributions found here may also arise in more generic type-IIB compactifications. In particular we expect that our results may also apply to compactifications where no symmetry group is present, or when the reduced complex structure moduli space involves more than one field. Actually, as we shall show, provided we restrict to the LCS regime this is certainly the case if we neglect flux quantization. This motivates future works on the search for this class of vacua with universal spectrum in compactifications with large values of the $D3$ tadpole, where the continuous flux approximation is expected be more accurate.

The paper is organized as follows. In section 2 we review the effective theory for the axio-dilaton and complex structure sector on type-IIB compactifications, and collect the relevant formulae for the computation of the tree-level mass spectrum. In section 3 we revisit the effective reduction of the complex structure moduli space on a Calabi-Yau admitting a discrete group of symmetries. We also derive the restrictions that these symmetries impose on the structure of the Hessian and the fermion mass matrix. Section 4 contains the main results of the paper where we analytically derive the tree-level mass spectrum for the class of models we consider. In section 5 we present the EFT for the compactification of type-IIB in the $\mathbb{WP}^4_{[1,1,1,1,4]}$ Calabi-Yau manifold. In section 6 we analyze the statistical properties of the computed spectra in the ensemble of flux vacua, and verify our conclusions by performing a numerical scan on the $\mathbb{WP}^4_{[1,1,1,1,4]}$ model. In section 7 we discuss briefly how to extend our results to more general compactifications. We present our conclusions in section 8.

2 Flux vacua on type-IIB compactifications

In the next subsection we will summarize the relevant formulae for compactifications of type-IIB superstrings on the orientifold $\tilde{M}_3$ of a Calabi-Yau manifold M_3 (see [45, 76] for a review). We will work in units of the reduced Planck mass, $M_p^{-2} = 8\pi G = 1$.

2.1 Effective theory for type-IIB flux compactifications

The low-energy spectrum of type-IIB string theory compactified on a Calabi-Yau orientifold $\tilde{M}_3$ includes the axio-dilaton τ, the complex structure moduli z^i, where $i = 1, \ldots, h^{2,1}$, and the Kähler moduli T^ρ, where[1] $\rho = 1, \ldots, h^{1,1}$.

To leading order in α' and g_s, the Kähler potential K of the corresponding 4-dimensional effective supergravity theory reads

$$K = -2\log\mathcal{V} - \log(-\mathrm{i}(\tau - \bar{\tau})) - \log\left(\mathrm{i}\int_{M_3} \Omega \wedge \bar{\Omega}\right). \tag{2.1}$$

Here $\mathcal{V}(T^\rho, \bar{T}^\rho)$ denotes the Kähler moduli-dependent volume of $\tilde{M}_3$, measured in the Einstein frame and in units of the string length $\ell_s = 2\pi\sqrt{\alpha'}$. The holomorphic three-form of the Calabi-Yau is denoted by $\Omega(z^i)$, and it encodes the dependence of the Kähler potential on the complex structure moduli. For this Kähler potential to provide a good description of the moduli space geometry, and in particular for the α' corrections to remain under control, we will restrict ourselves to the large volume regime, $\mathcal{V} \to \infty$.

The couplings of the theory are conveniently expressed by specifying a symplectic basis of three cycles of the Calabi-Yau $\{A^I, B_I\}$, with $I = 0, \ldots, h^{2,1}$, and a dual basis of three-forms α^I and β_I such that

$$\int_{A^I} \alpha_J = \delta_J^I \quad \int_{B_I} \beta^J = -\delta_I^J, \quad \int_{M_3} \alpha_I \wedge \beta^J = \delta_I^J, \quad \int_{A^I} \beta^J = \int_{B_I} \alpha_J = 0. \tag{2.2}$$

When Ω is expressed in this basis, it reads

$$\Omega = X^I \alpha_I - \mathcal{F}_I \beta^I, \qquad \text{with} \qquad X^I = \int_{A^I} \Omega, \qquad \mathcal{F}_I = \int_{B_I} \Omega. \tag{2.3}$$

The X^I are projective coordinates in the complex structure moduli space, and the corresponding moduli fields can be defined to be $z^i \equiv -\mathrm{i}X^i/X^0$, $i = 1, \ldots, h^{2,1}$. In order to find a more convenient expression for the Kähler potential, the quantities X^I and $\mathcal{F}_I$ are grouped in a symplectic *period vector* $\Pi^T = (X^I, \mathcal{F}_I)$. Then, it is possible to write the Kähler potential of the complex structure moduli space K_{cs} as

$$\mathrm{e}^{-K_{cs}} = \mathrm{i}\int_{M_3} \Omega \wedge \bar{\Omega} = -\mathrm{i}\left(X^I \bar{\mathcal{F}}_I - \bar{X}^I \mathcal{F}_I\right) = \mathrm{i}\,\Pi^\dagger \cdot \Sigma \cdot \Pi, \tag{2.4}$$

where Σ is the symplectic matrix

$$\Sigma = \begin{pmatrix} 0 & \mathbb{1} \\ -\mathbb{1} & 0 \end{pmatrix}. \tag{2.5}$$

---

[1]On the orientifold $\tilde{M}_3$ a fraction of the deformations of M_3 are projected out, $(h^{1,1}, h^{2,1}) \to (h^{1,1}_+, h^{2,1}_-)$, but we will omit the subscripts on the Hodge numbers to keep the notation simple. We will also ignore further degrees of freedom, such as possible $h^{1,1}_-$ axion multiplets, D3- and D7-brane moduli, or matter fields.

The previous expression is invariant under transformations $\mathrm{Sp}(2h^{2,1}+2,\mathbb{Z})$ associated with different choices for the symplectic basis (2.2). These symplectic transformations act on the period vector as follows

$$\Pi \longrightarrow \mathcal{S} \cdot \Pi \qquad \text{where} \qquad \mathcal{S}^T \cdot \Sigma \cdot \mathcal{S} = \Sigma. \tag{2.6}$$

The quantities $\mathcal{F}_I$ can be expressed as the derivatives of a holomorphic function of the X^I, *the prepotential*, so that

$$\mathcal{F}_I(X) = \partial_I \mathcal{F}(X). \tag{2.7}$$

The prepotential is a homogeneous function of degree 2, i.e., $\mathcal{F}(\lambda X) = \lambda^2 \mathcal{F}(X)$, and therefore it satisfies

$$X^I \mathcal{F}_I = 2\mathcal{F}(X). \tag{2.8}$$

Setting the gauge $X^0 = 1$, and using the homogeneity of the prepotential, the period vector can be written as

$$\Pi(z^i) = \begin{pmatrix} 1 \\ \mathrm{i}z^i \\ 2\mathcal{F} - z^j \mathcal{F}_j \\ -\mathrm{i}\mathcal{F}_i \end{pmatrix}. \tag{2.9}$$

In the present paper we will consider compactifications in the LCS regime, where the prepotential $\mathcal{F}(z^i)$ admits the expansion

$$\mathcal{F} = \frac{\mathrm{i}}{6}\kappa_{ijk}z^i z^j z^k + \frac{1}{2}\kappa_{ij}z^i z^j + \mathrm{i}\kappa_i z^i + \frac{1}{2}\kappa_0 + \mathcal{F}_{\text{inst}}. \tag{2.10}$$

The terms κ_{ijk}, κ_{ij} and κ_i are numerical constants which can be computed from the topological data of the mirror manifold to M_3. In particular, for historical reasons the coefficients κ_{ijk} are often referred to as the classical *Yukawa couplings*. The constant contribution κ_0 originates from radiative α' corrections, and is determined by the Euler number $\chi(M_3) = 2(h^{1,1} - h^{2,1})$ of the Calabi-Yau:

$$\kappa_0 = \mathrm{i}\frac{\zeta(3)}{(2\pi)^3}\chi(M_3), \tag{2.11}$$

where ζ is the Riemann zeta function. Finally, $\mathcal{F}_{\text{inst}}$ denotes exponentially suppressed string worldsheet instanton contributions, which can be expressed as

$$\mathcal{F}_{\text{inst}} = -\frac{\mathrm{i}}{(2\pi)^3}\sum_{\vec{d}} n_{\vec{d}}\,\mathrm{Li}_3\left[\mathrm{e}^{-2\pi d_i z^i}\right]. \tag{2.12}$$

Here the integers $n_{\vec{d}}$ are the genus zero Gopakumar-Vafa invariants, which are labeled by the vector $d^i \in \mathbb{Z}^+$, and the function $\mathrm{Li}_3(q)$ is the polylogarithm $\mathrm{Li}_p(q) = \sum_{k>0}\frac{q^k}{k^p}$ [12]. In the LCS regime, the contribution to $\mathcal{F}$ from instantons is subleading, and in the following calculations we will neglect it entirely.

When the Kähler potential is written in terms of the prepotential, provided we discard the instanton contribution, it takes the simple form

$$K_{cs} = -\log\left(\frac{1}{6}\kappa_{ijk}(z+\bar{z})^i(z+\bar{z})^j(z+\bar{z})^k - 2\,\mathrm{Im}(\kappa_0)\right). \tag{2.13}$$

It is straightforward to check that the field space metric derived from the Kähler potential K in (2.1) is real and block-diagonal in the axio-dilaton and complex structure sectors, namely,

$$K_{\tau\bar{\tau}} = \frac{1}{2(\mathrm{Im}\,\tau)^2}\,,$$

$$K_{i\bar{j}} = -\mathring{\kappa}_{ijk}(z+\bar{z})^k + \frac{1}{4}\mathring{\kappa}_{ilm}\mathring{\kappa}_{jnp}(z+\bar{z})^l(z+\bar{z})^m(z+\bar{z})^n(z+\bar{z})^p\,, \qquad (2.14)$$

where subscripts denote the derivatives of the Kähler functions, i.e., $K_{\tau\bar{\tau}} \equiv \partial_\tau\partial_{\bar{\tau}}K$ and $K_{i\bar{j}} \equiv \partial_i\partial_{\bar{j}}K$, and the quantities $\mathring{\kappa}_{ijk} \equiv \mathrm{e}^{K_{cs}}\kappa_{ijk}$ are usually called the *rescaled Yukawa couplings* [41].

2.2 No-scale flux vacua

The presence of three-form fluxes induces the following superpotential for the dilaton and complex structure moduli [43]:

$$W = \frac{1}{\ell_s^2\,\sqrt{4\pi}}\int_{M_3} G_{(3)} \wedge \Omega\,, \qquad (2.15)$$

where $G_{(3)} = F_{(3)} - \tau H_{(3)}$, denoting by $F_{(3)}$ and $H_{(3)}$ the RR and NS-NS 3-form field strengths respectively. These fluxes satisfy the quantization conditions

$$\frac{1}{\ell_s^2}\int_{A^I} F_{(3)} = -f_A^I \in \mathbb{Z}\,, \qquad \frac{1}{\ell_s^2}\int_{B_I} F_{(3)} = -f_I^B \in \mathbb{Z}\,,$$

$$\frac{1}{\ell_s^2}\int_{A^I} H_{(3)} = -h_A^I \in \mathbb{Z}\,, \qquad \frac{1}{\ell_s^2}\int_{B_I} H_{(3)} = -h_I^B \in \mathbb{Z}\,. \qquad (2.16)$$

Here the minus signs in all expressions have been introduced for convenience. Then, these fluxes can be decomposed in the symplectic basis as

$$F_{(3)} = -\ell_s^2\,(f_A^I\alpha_I - f_I^B\beta^I), \qquad\qquad H_{(3)} = -\ell_s^2\,(h_A^I\alpha_I - h_I^B\beta^I). \qquad (2.17)$$

If we define the symplectic flux vectors $f^T = (f_A^I, f_I^B)$, $h^T = (h_A^I, h_I^B)$, and $N = f - \tau\,h$, we can write the flux superpotential in a compact way as

$$W = \frac{1}{\sqrt{4\pi}}\left[(f_A^I - \tau h_A^I)\mathcal{F}_I - (f_I^B - \tau h_I^B)X^I\right] = \frac{1}{\sqrt{4\pi}}\,N^T \cdot \Sigma \cdot \Pi\,. \qquad (2.18)$$

At tree-level, the Kähler sector satisfies the no-scale property $K^{\rho\bar{\sigma}}K_\rho K_{\bar{\sigma}} = 3$, and therefore the scalar potential of the effective supergravity action reads[2]

$$V_{\mathrm{tree}} = \mathrm{e}^K\left[K^{i\bar{j}}D_i W D_{\bar{j}}\bar{W} + K^{\tau\bar{\tau}}D_\tau W D_{\bar{\tau}}\bar{W}\right] \geq 0\,, \qquad (2.19)$$

where $D_\tau W = (\partial_\tau + K_\tau)W$ and $D_i W = (\partial_i + K_i)W$ are Kähler covariant derivatives of the superpotential. In this work we will only consider critical points, denoted by $\{\tau_c, z_c^i\}$, of the

---

[2]We denote by $K^{\rho\bar{\sigma}} = (K_{\rho\bar{\sigma}})^{-1}$, $K^{\tau\bar{\tau}} = (K_{\tau\bar{\tau}})^{-1}$ and $K^{i\bar{j}} = (K_{i\bar{j}})^{-1}$ the inverses of the field space metrics on the Kähler, axio-dilaton and complex structure sectors respectively.

no-scale potential where the axio-dilaton/complex structure sector configuration preserves supersymmetry, namely those satisfying

$$D_\tau W|_{\tau_c, z_c^i} = 0, \qquad \text{and} \qquad D_i W|_{\tau_c, z_c^i} = 0 \quad \text{for all} \quad i = 1 \ldots, h^{2,1}. \tag{2.20}$$

Note, however, that in general supersymmetry is still broken by the Kähler sector, since $D_\rho W = K_\rho W \neq 0$ unless the expectation value of the flux superpotential vanishes, $W|_{\tau_c, z_c^i} = 0$. In what follows, field configurations satisfying (2.20) will be referred to as *no-scale vacua*.

The allowed values of fluxes are subject to the tadpole cancellation condition which requires that the $D3$-brane charge induced by the fluxes, together with the contribution from $D3$-branes, cancels the negative charge from $D7-$branes and orientifold planes. The charge induced by the fluxes is given by (see [77, 78])

$$N_{\text{flux}} \equiv \frac{1}{\ell_s^4} \int_{M_3} F_{(3)} \wedge H_{(3)} = (f_I^B h_A^I - h_I^B f_A^I) = h^T \cdot \Sigma \cdot f = \frac{N^\dagger \cdot \Sigma \cdot N}{\tau - \bar{\tau}}, \tag{2.21}$$

and then, denoting by L the negative contribution from the $D7$'s and the orientifolds, we have the bound

$$N_{\text{flux}} \leq N_{\text{flux}} + N_{D3} = L, \tag{2.22}$$

where $N_{D3} \geq 0$ is the number of $D3$-branes.

Note that the expressions for the flux superpotential (2.18) and the previous one for the $D3$-charge are both manifestly invariant under the action of the symplectic group $\text{Sp}(2h^{2,1} + 2, \mathbb{Z})$, provided the flux vector also transforms as

$$N \longrightarrow \mathcal{S} \cdot N, \qquad \mathcal{S} \in \text{Sp}(2h^{2,1} + 2, \mathbb{Z}). \tag{2.23}$$

Actually, the combined actions (2.6) and (2.23) represent redundancies of the supergravity description, and therefore no-scale solutions related by these transformations should be regarded as equivalent. In addition, the previous characterisation of flux vacua is also invariant under $\text{SL}(2, \mathbb{Z})$ transformations acting simultaneously on the axio-dilaton τ and the fluxes as

$$\tau \to \frac{a\tau + b}{c\tau + d}, \qquad \begin{pmatrix} F_3 \\ H_3 \end{pmatrix} \to \begin{pmatrix} a & b \\ c & d \end{pmatrix} \cdot \begin{pmatrix} F_3 \\ H_3 \end{pmatrix}, \tag{2.24}$$

with $a, b, c, d \in \mathbb{Z}$ and $ad - bc = 1$. As in the case of symplectic transformations, these actions should also be regarded as redundancies, thus, different no-scale vacua connected by them represent the same physical state.

As a final remark, it is important to emphasize that the no-scale structure leading to the potential (2.19) is broken by α' and non-perturbative effects [1–4, 79, 80]. However, provided these corrections remain under control, they will only induce subleading contributions to the mass spectra on the axio-dilaton/complex structure sector that we compute below.[3] Regarding the Kähler moduli, the leading α' corrections generically induce a

---

[3]Here, following [1–4] we assume that no-scale configurations (2.20) represent a good classical background for the computation of quantum corrections in string theory, including the case when $W|_{\tau_c, z_c^i} \neq 0$. For a criticism of this approach see [81] (see also [82]).

run-away direction for the compactification volume, i.e. when $W|_{\tau_c, z_c^i} \neq 0$. Therefore, to have a fully stabilised vacuum would require including further ingredients, such as non-perturbative corrections. However, the stabilisation of the Kähler moduli is out of the scope of the present work.

2.3 Mass spectrum at tree-level vacua

The main focus of the present work is the study of the mass spectrum at no-scale vacua, $\{\tau_c, z_c^i\}$, satisfying (2.20). In this subsection we will enumerate the relevant properties of the Hessian of the potential (2.19) at these points and its spectrum of eigenvalues. This information will in turn determine the tree-level masses of the moduli fields.

At no-scale vacua the scalar potential vanishes identically, regardless of the configuration of the Kähler moduli, as a consequence, the Kähler moduli remain flat directions of V_{tree}. This means that to study the spectrum of excitations of these configurations, it is sufficient to focus on the axio-dilaton/complex structure sector, since all the Kähler moduli are massless. Additionally, in order to simplify the computations, we will make use of the freedom to perform a field redefinition to bring the field space metric to a canonical form at the vacuum $\{\tau_c, z_c^i\}$. To be more specific, since the Kähler metric (2.14) is real and block-diagonal in the axio-dilaton and complex structure sectors, we can redefine the complex structure fields as $z^a = e_i^a z^i$ with $e_i^a \in \mathrm{GL}(h^{2,1}, \mathbb{R})$, so that

$$(e^{-1})_a^i (e^{-1})_b^j K_{i\bar{j}}|_{\tau_c z_c^i} = \delta_{ab} \tag{2.25}$$

with $a, b = 1, \ldots, h^{2,1}$. Then, the matrices $e_a^i \equiv (e^{-1})_a^i$ can be identified with a *real* vielbein basis for the metric $K_{i\bar{j}}$ at the point $\{\tau_c, z_c^i\}$. Note that this does not completely fix the freedom to choose a matrix e_a^i, as we are still allowed to make field redefinitions $z^a \to \Lambda_b^a z^b$ (equivalently $e_i^a \to \Lambda_b^a e_i^b$) preserving the canonical form of the metric, that is with $\Lambda \in \mathrm{SO}(h^{2,1})$. Similarly, we can use the real vielbein $e_0^\tau = \mathrm{i}(\tau - \bar{\tau})$ to obtain the canonical normalisation of the axio-dilaton at the vacuum $\{\tau_c, z_c^i\}$. For convenience we will also use the index $A = 0, \ldots, h^{2,1}$ to collectively label the canonically normalized axio-dilaton and the complex structure fields, so that the full Kähler metric in the axio-dilaton/complex structure sector takes the form $K_{A\bar{B}} = \delta_{A\bar{B}}$ at the no-scale vacuum.

After bringing the field-space metric to a canonical form, it is straightforward to check that the Hessian of the scalar potential (2.19) at no-scale vacua $\{\tau_c, z_c^i\}$ has the following structure[4]

$$\mathcal{H} \equiv \begin{pmatrix} \nabla_A \nabla_{\bar{B}} V & \nabla_A \nabla_B V \\ \nabla_{\bar{A}} \nabla_{\bar{B}} V & \nabla_{\bar{A}} \nabla_B V \end{pmatrix} = \begin{pmatrix} Z_{AC} \bar{Z}^C_{\bar{B}} + \delta_{A\bar{B}} \, m_{3/2}^2 & 2m_{3/2} Z_{AB} \, \mathrm{e}^{-\mathrm{i}\alpha_W} \\ 2m_{3/2} \, \bar{Z}_{\bar{A}\bar{B}} \, \mathrm{e}^{\mathrm{i}\alpha_W} & \bar{Z}_{\bar{A}\bar{C}} Z^{\bar{C}}_B + \delta_{\bar{A}B} \, m_{3/2}^2 \end{pmatrix}, \tag{2.26}$$

where $m_{3/2} \equiv \mathrm{e}^{K/2} |W|$ is the gravitino mass, $\alpha_W = \arg(W)$ is the phase of the flux superpotential and $Z_{AB} \equiv \mathrm{e}^{K/2} D_A D_B W$. Equivalently, we can rewrite the Hessian as

$$\mathcal{H} = \left(m_{3/2} \, \mathbb{1} + \mathcal{M} \right)^2 \quad \text{with} \quad \mathcal{M} \equiv \begin{pmatrix} 0 & Z_{AB} \, \mathrm{e}^{-\mathrm{i}\alpha_W} \\ \bar{Z}_{\bar{A}\bar{B}} \, \mathrm{e}^{\mathrm{i}\alpha_W} & 0 \end{pmatrix}. \tag{2.27}$$

---

[4] Indices are here raised and lowered with the canonical form of the metric $\delta^{A\bar{B}}$ and $\delta_{A\bar{B}}$.

Since the field space metric is already in a canonical form, the eigenvalues of the matrix $\mathcal{H}$ can be identified with the squared masses of the $2(h^{2,1}+1)$ real scalar fields in the axio-dilaton/complex structure sector at $\{\tau_c, z_c^i\}$. Therefore to find the spectrum of $\mathcal{H}$ it suffices to diagonalize the matrix $\mathcal{M}$, which can be identified with the fermion mass matrix (see, e.g., [83]). Moreover, note that the eigenvalues of $\mathcal{M}$ come in pairs of opposite signs $\pm m_\lambda$, and therefore the mass spectrum of the scalar sector at tree-level is simply [51]

$$\mu_{\pm\lambda}^2 = (m_{3/2} \pm m_\lambda)^2 \geq 0 \,, \tag{2.28}$$

where $\lambda = 0, \ldots, h^{2,1}$. The positivity of the masses squared $\mu_{\pm\lambda}^2$ ensures that all no-scale vacua are perturbatively stable, which could have been anticipated by noting that the tree-level potential (2.19) is always non-negative, and vanishes at no-scale vacua.

In practice, the simplest way to find the fermion masses m_λ, and thus also the scalar mass spectrum, is to consider the $(h^{2,1}+1) \times (h^{2,1}+1)$ hermitian matrix $(ZZ^\dagger)_{AB} \equiv Z_{AC}\bar{Z}^C{}_{\bar{B}}$, whose $h^{2,1}+1$ eigenvalues m_λ^2 coincide with those of

$$\mathcal{M}^2 = \begin{pmatrix} Z_{AC}\bar{Z}^C{}_{\bar{B}} & 0 \\ 0 & \bar{Z}_{\bar{A}}{}^C Z_{CB} \end{pmatrix} . \tag{2.29}$$

Regarding the structure of the matrix Z_{AB}, it is straightforward to prove that, at no-scale vacua, we always have $Z_{00} = \mathrm{e}^{K/2}(e_0^\tau)^2 D_\tau D_\tau W = 0$. Moreover, when our model is defined in terms of a prepotential as in (2.10), we can simplify the computations with the identity [15, 40]

$$Z_{ij} = -(\tau - \bar{\tau})\mathrm{e}^{K_{cs}}\,\kappa_{ijk}\,K^{k\bar{l}}\,\bar{Z}_{\bar{\tau}\bar{l}}, \tag{2.30}$$

which we have written in a form invariant under redefinitions of the z^i fields to ease comparison with previous works. If we instead use canonically normalised fields, plus the definition of the rescaled Yukawa couplings $\mathring{\kappa}_{abc} = \mathrm{e}^{K_{cs}}\kappa_{abc}$, the previous identity takes the simpler form

$$Z_{ab} = \mathrm{i}\,\mathring{\kappa}_{abc}\,\bar{Z}_{0c}\,. \tag{2.31}$$

For later reference we will also collect here the following form of the tadpole constraint (2.22) which, at no-scale vacua, can be expressed in terms of the expectation value of the gravitino mass and the quantities Z_{0a} as (see appendix A)

$$0 \leq 4\pi\mathcal{V}^2\left(m_{3/2}^2 + |Z_{0a}|^2\right) = N_{\text{flux}} \leq L. \tag{2.32}$$

To summarise, the scalar mass spectrum $\mu_{\pm\lambda}^2$ at no-scale vacua (2.28) can be computed from the gravitino mass $m_{3/2}$, the quantities Z_{0a}, and the canonically normalised and rescaled Yukawas $\mathring{\kappa}_{abc}$, using the formulae (2.31) and diagonalising the matrix $ZZ^\dagger$. In the next section we will discuss compactifications on Calabi-Yau manifolds invariant under a group of discrete symmetries. As we shall see, at no-scale vacua preserving those symmetries, the structure of both the Yukawa couplings and Z_{0a} is severely constrained.

3 Flux vacua with enhanced symmetries

In this section we will consider the special case where the Calabi-Yau geometry is invariant under a global group of discrete isometries. As discussed in [6], provided that only fluxes which are invariant under these symmetries are turned on, the low energy action is consistent with the *supersymmetric truncation* of a subset of the complex structure fields. Indeed, in this setting the spacetime isometries act non-trivially on the complex structure fields, while leaving the low energy supergravity action invariant. Then, the consistent truncation of the theory is defined by restricting the complex structure moduli space to the fixed locus of this symmetry, in other words, a subset of the fields is *frozen* at the fixed locus. The consistency of the truncation ensures that any solution of the reduced theory obtained after freezing a subset of the fields is also a solution of the complete theory. In particular, critical points of the reduced scalar potential are also critical points in the full effective theory. Moreover, if the fields surviving the truncation are stabilized at a supersymmetric critical point, the full complex structure sector also preserves supersymmetry [6] (see also discussion in [10]).

In the next paragraphs we will review how the presence of discrete symmetries in the Calabi-Yau geometry can be used to truncate a sector of the complex structure fields. We will also discuss the restrictions that these symmetries impose on the couplings of the resulting reduced theory.

3.1 Invariant fluxes and low energy symmetries

As we mentioned in the introduction, in many interesting compactifications the Calabi-Yau geometry is invariant under the action of a discrete group of transformations, $\mathcal{G}$. These transformations act on the complex structure fields, $z^i \rightarrow \hat{z}^i$, and thus also induce a change on the period vector $\Pi(z^i)$. Since the Calabi-Yau geometry is left invariant under these symmetries, these transformations must also leave the geometry on its moduli space invariant. Therefore, the action of a transformation $g \in \mathcal{G}$ on the period vector must be of the form

$$\Pi(z^i) \longrightarrow \Pi(\hat{z}^i) = e^{\Lambda_g(z)} \, \mathcal{S}_g \cdot \Pi(z^i) \,, \tag{3.1}$$

with $\Lambda_g(z^a)$ a holomorphic function of the complex structure fields and $\mathcal{S}_g$ a constant symplectic matrix in $\mathrm{Sp}(2h^{2,1}+2, \mathbb{Z})$, both determined by the group element g. In addition, when the three-form fluxes are turned on, the invariance of the effective action under the group $\mathcal{G}$ requires that the flux vector $N = f - \tau h$ transforms as in (2.23). Then, it is easy to check that under a transformation $g \in \mathcal{G}$, the Kähler potential K_{cs} and the superpotential W experience a g-dependent Kähler transformation

$$K_{cs}(\hat{z}^i, \hat{\bar{z}}^i) = K_{cs}(z^i, \bar{z}^i) + \Lambda_g(z^i) + \bar{\Lambda}_g(\bar{z}^i) \,, \qquad W_{\hat{f}, \hat{h}}(\hat{z}^i) = e^{-\Lambda_g(z)} \, W_{f,h}(z^i) \,. \tag{3.2}$$

Here we have explicitly indicated for clarity the dependence of the superpotential on the flux vectors (f, h) and their transformed values $(\hat{f}, \hat{h})$ under (2.23). However, the symmetry groups $\mathcal{G}$ that we are considering are discrete and of finite order, and thus it is always pos-

sible to choose a Kähler gauge so that K_{cs} and W transform as scalars under[5] $\mathcal{G}$ (see [84]), that is,

$$K_{cs}(\hat{z}^i, \hat{\bar{z}}^i) = K_{cs}(z^i, \bar{z}^i), \quad W_{\hat{f},\hat{h}}(\hat{z}^i) = W_{f,h}(z^i). \tag{3.3}$$

It is important to note that despite of the behaviour (3.3) of the Kähler potential and the flux superpotential under the group of transformations $\mathcal{G}$, generically they do not constitute a proper symmetry of the low energy effective theory for the moduli fields [8]. Indeed, each choice of fluxes defines an effective theory for the moduli, where the flux integers (f, h) appear as coupling constants (see [85]). Therefore, since the group $\mathcal{G}$ generally acts non-trivially on the fluxes, i.e., the couplings of the EFT, in general it will not correspond to a low energy symmetry for the moduli effective action. On the contrary, if we restrict the flux configuration $N = f - \tau h$ to be invariant under the transformations (2.23), then $\mathcal{G}$ will be a symmetry of the low-energy action defined by this choice of fluxes. Indeed, from (3.3) we have that for an invariant set of fluxes

$$K_{cs}(\hat{z}^i, \hat{\bar{z}}^i) = K_{cs}(z^i, \bar{z}^i), \quad W_{f,h}(\hat{z}^i) = W_{f,h}(z^i), \tag{3.4}$$

so the low energy supergravity theory of the moduli is properly invariant under the action of $\mathcal{G}$.

In the following we will assume that the fluxes are invariant under the action of $\mathcal{G}$, and we will again omit the subscripts (f, h) in the superpotential in order to simplify the notation.

3.2 Consistent truncation of the moduli space

We will now discuss how the symmetry group $\mathcal{G}$ aids in the task of finding solutions to the no-scale equations (2.20). In general, for a given group $\mathcal{G}$ we can always split the complex structure fields into two sets, $z^i = \{z^\alpha, w^{\alpha'}\}$: those invariant under the action of the symmetry group, z^α with $\alpha = 1, \ldots, h_{\text{red}}^{2,1}$, and those fields which transform non trivially, $w^{\alpha'} \to \hat{w}^{\alpha'}$, where $\alpha' = h_{\text{red}}^{2,1} + 1, \ldots, h^{2,1}$.

Then, if the symmetry group $\mathcal{G}$ admits a fixed locus *on the moduli space*, i.e., a configuration of the fields $w_*^{\alpha'}$ satisfying $\hat{w}_*^{\alpha'} = w_*^{\alpha'}$, the derivatives of the scalar potential V and the Kähler potential along the non-invariant fields $w^{\alpha'}$ must vanish there

$$\partial_{w^{\alpha'}} V = 0, \quad K_{w^{\alpha'}} = 0 \quad \text{at} \quad z^i = (z^\alpha, w_*^{\alpha'}) \quad \text{for all} \quad \tau, z^\alpha. \tag{3.5}$$

To prove this it is sufficient to note that, for an invariant choice of fluxes, both the no-scale potential V and the Kähler potential transform as scalar fields under the action of $\mathcal{G}$, and thus $\partial_{z^i} V$ and K_i will transform as tensors. Then, in the case of the scalar potential, we have that a generic point of the moduli space satisfies

$$\partial_{w^{\alpha'}} V(z^\alpha, w^{\alpha'}) = \frac{\partial \hat{w}^{\beta'}}{\partial w^{\alpha'}} \partial_{\hat{w}^{\beta'}} V(z^\alpha, \hat{w}^{\beta'}). \tag{3.6}$$

---

[5]The invariant Kähler gauge $K_{cs}^{\text{inv}} = K_{cs} + \Lambda^{\text{inv}}(z) + \bar{\Lambda}^{\text{inv}}(\bar{z})$ can be found noting that under a transformation $g : z^i \to \hat{z}^i$ we must have $\Lambda^{\text{inv}}(\hat{z}) = \Lambda^{\text{inv}}(z) - \Lambda_g(z)$. It is easy to check that this condition is solved by $\Lambda^{\text{inv}}(z) = \frac{1}{[\mathcal{G}]} \sum_{g \in \mathcal{G}} \Lambda_g(z)$, where $[\mathcal{G}]$ is the order of the group $\mathcal{G}$.

At the fixed locus, where $\hat{w}_*^{\alpha'} = w_*^{\alpha'}$, the previous expression can be seen as a system of equations for $\partial_{w^{\alpha'}} V(z^\alpha, w_*^{\alpha'})$. But this system only admits the trivial solution (3.5) because, by assumption, all the fields $w^{\alpha'}$ transform non-trivially away from the fixed point implying that all equations are independent. Moreover, in the previous discussion the expectation values of the dilaton or the $\mathcal{G}$-invariant fields are irrelevant, and therefore the fixed point will always be a stationary point of the superpotential regardless of the field configuration (τ, z^α). Although our argument has been derived in the particular Kähler gauge where K_{cs} and W transform as scalars (3.3), our conclusion is a Kähler invariant statement. Different derivations can be found in [6, 10, 12].

The left condition in (3.5) implies that the fixed locus of the symmetry group $\mathcal{G}$ is always a critical point of the scalar potential, while the right one leads to a consistency condition on the geometry of the moduli space. In particular, this geometric condition implies that the moduli space metric on the fixed locus is block-diagonal in the truncated and surviving sectors $K_{z^\alpha \bar{w}^{\beta'}} = 0$. Moreover, the reduced moduli space defined by the fixed locus $w^{\alpha'} = w_*^{\alpha'}$ must be a *totally geodesic submanifold* of the full moduli space (see [51]). In other words, any geodesic on the moduli space manifold with at least one point located at the fixed locus of $\mathcal{G}$, and which is locally tangent to it, should be entirely contained in the reduced moduli space.

These are very strong requirements which ensure the consistency of freezing the moduli $w^{\alpha'}$ at the level of the EFT Lagrangian $\mathcal{L}_{\mathrm{EFT}}(\tau, z^i)$, thus defining a reduced theory involving the surviving fields alone:

$$\mathcal{L}_{\mathrm{EFT}}^{\mathrm{red}}(\tau, z^\alpha) \equiv \mathcal{L}_{\mathrm{EFT}}(\tau, z^\alpha, w^{\alpha'} = w_*^{\alpha'}) \,. \tag{3.7}$$

Indeed, the conditions (3.5) guarantee that any solution of the reduced theory given by $\mathcal{L}_{\mathrm{EFT}}^{\mathrm{red}}$ is also a solution of the complete EFT. Moreover, using (3.4) and a similar argument to the one given above, it is possible to prove that the flux potential is also extremized at the fixed locus of $\mathcal{G}$

$$D_{w^{\alpha'}} W|_{w=w_*} = \partial_{w^{\alpha'}} W|_{w=w_*} = 0 \qquad \text{for all} \qquad \tau, z^\alpha \,, \tag{3.8}$$

which means that the truncated fields $w^{\alpha'}$ preserve supersymmetry there. If supersymmetry is preserved in the reduced theory, it is also unbroken in the original EFT. Then, the process of freezing the non-invariant fields $w^{\alpha'}$ constitutes a consistent supersymmetric truncation of the theory[6] (see [50, 51, 86]).

From (3.8) it follows that compactifications admitting a discrete symmetry group are particularly convenient for the search of no-scale vacua since at the fixed locus of $\mathcal{G}$, the non-invariant fields automatically satisfy the no-scale equations (2.20). No-scale vacua located at the fixed locus of the symmetry group $\mathcal{G}$ are often called *enhanced symmetry vacua*. Moreover, provided we are interested only in this class of vacua, the consistency of the truncation ensures that it is sufficient to calculate the couplings, i.e., the period vector, of the reduced action (see, e.g., [12, 41, 87–90]), which renders the computation of the EFT tractable.

---

[6]It is important to emphasize that by this procedure the non-invariant deformations are *not projected out*, as it happens when orientifolding a Calabi-Yau or in the Green-Plesser construction of mirror Calabi-Yau duals. Here the non-invariant fields are still degrees of freedom of the EFT.

3.3 Mass matrix structure at enhanced symmetry vacua

The high degree of symmetry present in low energy theories with $\mathcal{G}$-invariant fluxes provides valuable information regarding the structure of the fermion mass matrix and the Hessian at enhanced symmetry vacua. First, as we saw above, at the fixed locus of $\mathcal{G}$ the moduli space metric is block diagonal in the truncated and surviving sectors, and from (3.5) and (3.8) it also follows that

$$D_\tau D_{w^{\alpha'}} W|_{w_*} = D_{z^\alpha} D_{w^{\beta'}} W|_{w_*} = 0, \qquad \nabla_{z^\alpha} \nabla_{w^{\beta'}} V|_{w_*} = \nabla_{z^\alpha} \nabla_{\bar{w}^{\beta'}} V|_{w_*} = 0, \qquad (3.9)$$

regardless of the configuration of the reduced moduli (τ, z^α). This, in turn, implies that the fermion mass matrix $\mathcal{M} = \mathcal{M}_{\{\tau, z^\alpha\}} \otimes \mathcal{M}_{\{w^{\alpha'}\}}$ and the Hessian of the potential $\mathcal{H} = \mathcal{H}_{\{\tau, z^\alpha\}} \otimes \mathcal{H}_{\{w^{\alpha'}\}}$ are block-diagonal in the two sectors at no-scale vacua, which means that it is consistent to study the perturbative stability of the fields (τ, z^α) and $w^{\alpha'}$ separately. Moreover, the particular structure of the fermion mass matrix on the EFTs we are considering, i.e., the identity (2.30), leads to an additional simplification. From (3.9) it is easy to see that the only non-vanishing quantities $Z_{\tau z^i}$ are those with components on the surviving sector, $Z_{\tau z^\alpha}$.

Collecting all the previous results, and using (2.31), we can see that the components of the canonically normalised matrix Z_{AB} which appears in $\mathcal{M}$ satisfy the relations

$$Z_{0w^{a'}} = Z_{z^{\tilde{a}} w^{b'}} = 0, \qquad Z_{z^{\tilde{a}} z^{\tilde{b}}} = \mathrm{i}\, \kappa_{\tilde{a}\tilde{b}\tilde{c}}\, \bar{Z}_{\bar{0}\bar{z}^{\tilde{c}}}, \qquad Z_{w^{a'} w^{b'}} = \mathrm{i}\, \kappa_{a'b'\tilde{c}}\, \bar{Z}_{\bar{0}\bar{z}^{\tilde{c}}}, \qquad (3.10)$$

where fields $z^{\tilde{a}}$ correspond to the canonically normalised fields of the reduced theory, $\tilde{a}, \tilde{b} = 1, \ldots, h^{2,1}_{\mathrm{red}}$ (see eq. (2.25)), and $w^{a'}$ to those of the truncated sector, $a', b' = h^{2,1}_{\mathrm{red}} + 1, \ldots, h^{2,1}$.

Thus, the main result of this section can be summarized as follows: at enhanced symmetry vacua the canonically normalized Hessian of the no-scale potential can be entirely expressed in terms of the derivatives of the flux superpotential *of the reduced theory*, $Z_{0z^{\tilde{a}}}$, plus $\mathring{k}_{\tilde{a}\tilde{b}\tilde{c}}$ and $\mathring{k}_{a'b'\tilde{c}}$ of the canonically normalized invariant Yukawa couplings. Furthermore, in the class of models we are interested in, the sector surviving the truncation is one dimensional (see the sample in table 1), and thus the indices $\tilde{a}, \tilde{b}$ and $\tilde{c}$ in (3.10) can only take one value, which we choose to be "1" without loss of generality. The non-vanishing components of the matrix Z_{AB} then read

$$Z_{11} = \mathrm{i}\, \mathring{\kappa}_{111}\, \bar{Z}_{\bar{0}\bar{1}}, \qquad Z_{a'b'} = \mathrm{i}\, \mathring{\kappa}_{a'b'1}\, \bar{Z}_{\bar{0}\bar{1}}. \qquad (3.11)$$

As we shall see in section 4, for the class of models we discuss here, the quantities $\mathring{\kappa}_{111}$ and $\mathring{\kappa}_{a'b'1}$ appearing in these expressions can also be completely expressed in terms of the field expectation values and the known couplings of the reduced theory.

4 Complete tree-level mass spectrum

We begin the present section by deriving certain universal properties of the type-IIB couplings which are valid in a generic Calabi-Yau compactification at LCS. We will then restrict ourselves to Calabi-Yau manifolds admitting a symmetry group which enables a

#	Manifold	$(h^{1,1}, h^{2,1})$	$\mathcal{G}$	Reference
1	$\mathbb{WP}^4_{[1,1,1,1,1]}$	$(1, 101)$	$\mathbb{Z}_5^3$, $\mathbb{Z}_{41}$, $\mathbb{Z}_{51}$, $\mathbb{Z}_5 \times \mathbb{Z}_{13}$	[41, 57, 58]
2	$\mathbb{WP}^4_{[1,1,1,1,2]}$	$(1, 103)$	$\mathbb{Z}_3 \times \mathbb{Z}_6^2$	[57, 66]
3	$\mathbb{WP}^4_{[1,1,1,1,4]}$	$(1, 149)$	$\mathbb{Z}_8^2 \times \mathbb{Z}_2$	[57, 66]
4	$\mathbb{WP}^4_{[1,1,1,2,5]}$	$(1, 145)$	$\mathbb{Z}_{10}^2$	[57, 66]
5	$\mathbb{WP}^4_{[1,1,1,1,1]}/\mathbb{Z}_5 \times \mathbb{Z}_5$	$(1, 5)$	Dic_3, Dic_5	[59]
6	$X^{20,20}$	$(20, 20)$	$\mathrm{SL}(2,3)$, $\mathbb{Z}_3 \times \mathbb{Z}_8$, $\mathbb{Z}_3 \times \mathbb{Q}_8$	[60, 63]
7	$X^{20,20}/\mathbb{Z}_3$	$(3, 3)$	$\mathbb{Q}_8$	[60, 63]

Table 1. Selection of Calabi-Yau geometries which admit a consistent supersymmetric truncation of the moduli space. The truncation is defined by the fixed locus (on the moduli space) of the symmetry group $\mathcal{G}$, and effectively reduces the number of moduli to $(h^{1,1}, h^{2,1}) \to (h^{1,1}_{\mathrm{red}} = 1, h^{2,1}_{\mathrm{red}} = 1)$. In the cases 1, 5 and 6, the fixed locus of each of the groups $\mathcal{G}$ leads to one or more distinct Calabi-Yau families. The manifold $X^{20,20}$ is the "24-cell" Calabi-Yau threefold with hodge numbers $h^{1,1} = h^{2,1} = 20$ [60], and the symbols $\mathbb{Q}_8$ and Dic_n stand for the quaternion and dicyclic groups respectively.

consistent reduction of the complex structure moduli space to a single surviving field. Using these results together with the ones in the previous sections we will show how to compute the tree-level spectrum for the complete axio-dilaton/complex structure sector at no-scale vacua.

4.1 Universal features of the type-IIB effective field theory

In this subsection we will obtain general properties satisfied by the canonically normalised Yukawa couplings in the large complex structure regime. More specifically, we will show that a subset of the rescaled Yukawas $\mathring{\kappa}_{abc}$ can be expressed in terms of a single parameter $\xi \in [0, 1/2]$, which can be defined in terms of known quantities appearing in the reduced theory as

$$\xi \equiv \frac{-2\mathrm{e}^{K_{cs}} \operatorname{Im} \kappa_0}{1 + 2\mathrm{e}^{K_{cs}} \operatorname{Im} \kappa_0}. \tag{4.1}$$

This quantity can be understood as a coordinate parametrising the complex structure moduli space, with the LCS point located at $\xi = 0$. For the models we are interested in, with a few Kähler moduli and a large complex structure sector $h^{1,1} \ll h^{2,1}$, we have from (2.11) that $\operatorname{Im} \kappa_0 < 0$. Combined with the definition (4.1), the latter condition also implies that physical configurations satisfy $\xi \geq 0$. Then, it is easy to check that field configurations with $\xi = 1/2$ are those at the boundary of the moduli space, that is, for $\xi > 1/2$ the Kähler metric has a negative eigenvalue, leading to unphysical solutions.

The argument below will proceed along the lines of [68, 91, 92], where analogous properties for the Yukawas where found strictly at the LCS point ($\xi = 0$). But here we will

only assume that the exponentially suppressed instanton contributions to the prepotential (2.10) can be entirely neglected. Therefore, the results presented below generalize those of [68, 91, 92], as the regime of validity of our analysis can be extended to the entire region of the moduli space where the polynomial approximation of the prepotential (2.10) is under control.

The starting point of the derivation is the Kähler metric (2.14) on the complex structure moduli space. Following [68] we introduce the following real vector of unit norm

$$e_1^i \equiv \frac{1}{x}(z + \bar{z})^i, \qquad K_{i\bar{j}} e_1^i \bar{e}_1^j = 1, \tag{4.2}$$

where the parameter x is a normalisation constant which has yet to be determined. Without loss of generality, and making use of the residual $\mathrm{SO}(h^{2,1})$ freedom to define the canonically normalised fields, we rotate the vielbein basis e_a^i so that the first vector coincides with e_1^i. Since the Kähler metric (2.14) has the canonical form δ_{ab} when expressed in the basis e_a^i, we find that the rescaled and canonically normalised Yukawa couplings should satisfy

$$\delta_{ab} = -\mathring{\kappa}_{ab1}x + \frac{1}{4}\mathring{\kappa}_{a11}\mathring{\kappa}_{b11}x^4. \tag{4.3}$$

Note also that from the definition of the Yukawa couplings, $\mathring{\kappa}_{abc} = \mathrm{e}^{K_{cs}}\kappa_{abc}$, and the expression for the Kälher potential (2.13), we have

$$\mathrm{e}^{-K_{cs}} = \frac{1}{6}\kappa_{111}x^3(1+\xi) \qquad \Longrightarrow \qquad \frac{1}{6}\mathring{\kappa}_{111}x^3(1+\xi) = 1. \tag{4.4}$$

Solving the two previous conditions for the Yukawas of the form $\mathring{\kappa}_{ab1}$, it is straightforward to obtain

$$\mathring{\kappa}_{111} = \frac{2(1+\xi)^2}{\sqrt{3(1-2\xi)^3}}, \qquad \mathring{\kappa}_{a'11} = 0 \quad \text{and} \quad \mathring{\kappa}_{a'b'1} = -\frac{1+\xi}{\sqrt{3(1-2\xi)}}\delta_{a'b'}, \tag{4.5}$$

with $a', b' = 2, \ldots h^{2,1}$. The rest of the rescaled Yukawa couplings $\kappa_{a'b'c'}$ are not constrained by the conditions above, and therefore a priori they can be generic. The normalisation constant x of the vielbein e_1^i is found to be

$$x^2 = \frac{3(1-2\xi)}{(1+\xi)^2}. \tag{4.6}$$

To the best of our knowledge these relations have never been presented before in the literature.

The direction specified by the vielbein e_1^i has a concrete geometrical significance. It corresponds to *the no-scale direction* of the complex structure moduli space [93, 94]

$$K_a = -\frac{1}{2}\mathring{\kappa}_{a11}x^2 = -\sqrt{3/(1-2\xi)}\delta_a^1. \tag{4.7}$$

The previous relation also implies the following generalised no-scale property

$$K_i K_{\bar{j}} K^{i\bar{j}} = 3/(1-2\xi) \geq 3, \tag{4.8}$$

which is satisfied by any type-IIB compactification with $h^{1,1} \leq h^{2,1}$ at LCS (see appendix A in [93]).

Note that in the models we are interested in, where only one field survives the truncation, the v.e.v. of the complex structure field z^a is necessarily aligned with the vector Z_{0a}, since both of them point along the unique direction of the reduced complex structure moduli space. Therefore, the Yukawa couplings $\mathring{\kappa}_{a'b'1}$ computed above are precisely those also appearing in the expression (3.11), and thus we already have all the necessary ingredients we require to compute the tree-level spectrum at a generic no-scale vacuum.

4.2 Fermion and scalar mass spectra at no-scale vacua

We begin by computing the fermion mass spectrum as described in section 2.3, that is, diagonalising the hermitian matrix $ZZ^\dagger$, and using the formula (2.28) to obtain the masses of the scalar fields. First, since the vector $Z_{0a} = \delta_{a1}Z_{01}$ is necessarily aligned with the no scale direction, from the expressions (4.5) for the rescaled Yukawa couplings, and the relations (3.11), we find that matrix Z_{AB} has the following structure

$$
Z_{AB} = \begin{pmatrix} 0 & Z_{01} & 0 \\ Z_{01} & i\mathring{\kappa}(\xi)\bar{Z}_{01} & 0 \\ 0 & 0 & -\frac{1+\xi}{\sqrt{3(1-2\xi)}}\delta_{a'b'}\bar{Z}_{01} \end{pmatrix}, \tag{4.9}
$$

where we used the shorthand $\mathring{\kappa}(\xi) \equiv \mathring{\kappa}_{111}(\xi)$. Then, after factorising an overall scale $m_{\text{susy}} \equiv |Z_{01}| = |e^{K/2}D_0 D_1 W|$, and computing the spectrum of eigenvalues m_λ^2 of $ZZ^\dagger$, we obtain

$$
m_\lambda/m_{\text{susy}} = \begin{cases} \hat{m}(\xi) & \lambda = 0 \\ 1/\hat{m}(\xi) & \lambda = 1 \\ \frac{1+\xi}{\sqrt{3(1-2\xi)}} & \lambda = 2, \ldots, h^{2,1} \end{cases}, \tag{4.10}
$$

where we defined

$$
\hat{m}(\xi) \equiv \frac{1}{\sqrt{2}} \left(2 + \mathring{\kappa}(\xi)^2 - \mathring{\kappa}(\xi)\sqrt{4 + \mathring{\kappa}(\xi)^2} \right)^{1/2}, \tag{4.11}
$$

which is shown in figure 1.

Interestingly, it can be seen that all the fermions on the truncated sector have the same mass. In particular, at the LCS point ($\xi = 0$) the fermion mass spectrum reads simply

$$
m_0/m_{\text{susy}} = \frac{1}{\sqrt{3}}, \qquad m_1/m_{\text{susy}} = \sqrt{3}, \qquad \text{and} \qquad m_{\lambda'}/m_{\text{susy}} = \frac{1}{\sqrt{3}}, \tag{4.12}
$$

with $\lambda' = 2, \ldots, h^{2,1}$.

The mass spectrum of the scalar fields can be immediately obtained from equation (2.28). To write it down, it is convenient to introduce the angular parameter θ_W (dependent on the choice of flux) as

$$
\cos\theta_W \equiv \frac{\mathcal{V}\, m_{3/2}}{\sqrt{N_{\text{flux}}/4\pi}}, \qquad \text{with} \qquad \theta_W \in [0, \pi/2], \tag{4.13}
$$

where the range of values of θ_W follows from the tadpole constraint (2.32). Despite appearances, the parameter θ_W has no dependence on the Calabi-Yau volume or the Käher
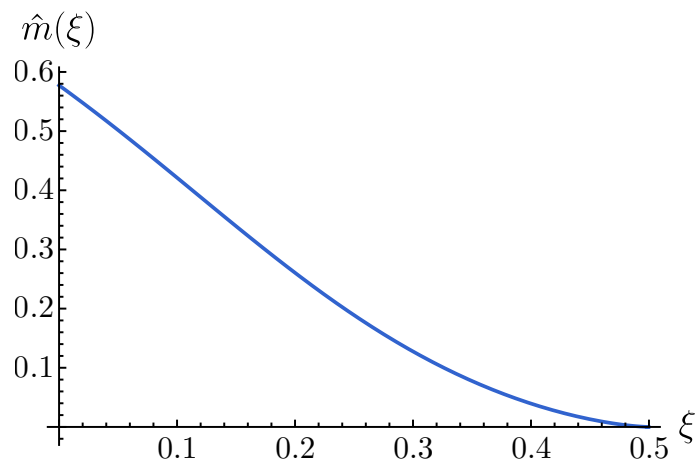
Figure 1. Plot of $\hat{m}(\xi)$, as defined in (4.11).

moduli, since the combination $\mathcal{V}m_{3/2} = \frac{1}{\sqrt{2}}e^{K_{cs}/2}\,\mathrm{Im}(\tau)^{-1/2}|W|$, often denoted by W_0 in the literature, depends solely on the axio-dilaton and complex structure fields. Furthermore, recalling that $Z_{0a'} = 0$, we find from (2.32) that the total $D3$-charge induced by fluxes is simply

$$N_{\mathrm{flux}} = 4\pi\mathcal{V}^2\left(m_{3/2}^2 + m_{\mathrm{susy}}^2\right) \qquad \Longrightarrow \qquad \tan\theta_W = m_{\mathrm{susy}}/m_{3/2}\,, \qquad (4.14)$$

and then it is straightforward to check that the complete set of scalar masses at tree-level in the axio-dilaton/complex structure sector is given by

$$\mu_{\pm\lambda}^2/m_{3/2}^2 = \begin{cases} \left(1 \pm \tan\theta_W\,\hat{m}(\xi)\right)^2 & \lambda = 0 \\ \left(1 \pm \dfrac{\tan\theta_W}{\hat{m}(\xi)}\right)^2 & \lambda = 1 \\ \left(1 \pm \dfrac{(1+\xi)\tan\theta_W}{\sqrt{3(1-2\xi)}}\right)^2 & \lambda = 2,\ldots,h^{2,1} \end{cases}. \qquad (4.15)$$

This mass spectrum is the main result of this paper. All the parameters appearing in the previous expression can easily be computed in the reduced theory, as ξ is determined by the configuration of the complex structure fields surviving the truncation, and θ_W depends only on the expectation value of the flux superpotential W_0 and the total $D3$-charge induced by fluxes N_{flux}.

It is worth noticing that this result is independent of both the specific details of the compactification and the number of moduli fields. Moreover, these masses only depend on the choice of flux via an overall scale given by the gravitino mass $m_{3/2} = W_0/\mathcal{V}$ and the angular parameter θ_W. We have chosen to present the masses normalised by the gravitino mass in order to eliminate their dependence on the Calabi-Yau volume $\mathcal{V}$, which appears as an overall multiplicative factor.

An interesting case to mention is that of the KKLT scenario [1], where the consistency of the EFT requires that the value of $W_0 \ll 1$ is very close to zero, or equivalently $\theta_W \sim \pi/2$.

In this limit the scalar spectrum simplifies to

$$\textbf{KKLT scenario:} \qquad \mu_{\pm\lambda}^2/m_{3/2}^2 \approx \begin{cases} \tan^2\theta_W\, \hat{m}(\xi)^2 & \lambda = 0 \\ \frac{\tan^2\theta_W}{\hat{m}(\xi)^2} & \lambda = 1 \\ \frac{(1+\xi)^2\tan^2\theta_W}{3(1-2\xi)} & \lambda = 2,\ldots,h^{2,1} \end{cases} , \qquad (4.16)$$

implying that all the masses in the spectrum are very large compared to the gravitino mass, $\mu_{\pm\lambda}^2 \gg m_{3/2}^2$. As discussed in detail in [95–97], in generic situations this guarantees the consistency of neglecting the complete axio-dilaton/complex structure sector in KKLT constructions, even after including quantum corrections and supersymmetry breaking effects in the theory. However, very light modes might still appear in the spectrum when considering no-scale solutions at special points of the moduli space [98, 99].

In the following two subsections we will discuss another two special cases where the value of the parameter θ_W is fixed, and thus we can write the entire (normalised) mass spectrum as a function of the parameter ξ alone.

4.3 Flux vacua with massless scalars

An important consequence of (4.15) is that at no-scale vacua we might encounter spectra with very light or even massless scalar fields, since $\tan\theta_W \in [0,\infty)$. In general the presence of those light fields is not convenient for phenomenological applications, as such vacua might become tachyonic after including quantum corrections or due to supersymmetry breaking effects. However, no-scale solutions with light (or massless) modes are still of interest for certain constructions of dS vacua [100, 101], and for implementing inflation. Thus, we will now briefly discuss the properties of their mass spectra.

Note that, for any given value of the parameter ξ, there are three values of θ_W such that the spectrum contains one, or several massless modes. They are given by

$$\tan\theta_0^W = \hat{m}(\xi)^{-1}, \qquad \tan\theta_1^W = \hat{m}(\xi), \qquad \text{and} \qquad \tan\theta_2^W = \frac{\sqrt{3(1-2\xi)}}{1+\xi}, \qquad (4.17)$$

and for each of these values the massless field(s) correspond(s) to μ_{-0}^2, μ_{-1}^2, and $\mu_{-\lambda'}^2$, respectively. The corresponding spectra associated to these branches of vacua are displayed in figures 2 and 3. In the case of the critical values $\theta_W = \theta_0^W$ and $\theta_W = \theta_1^W$, away from the LCS point ($\xi > 0$) the spectrum contains exactly one vanishing mass, corresponding to fields in the reduced theory: $\mu_{-0}^2 = 0$ and $\mu_{-1}^2 = 0$, respectively. In those two cases all the other fields have masses of at least the order of the gravitino mass. These classes of vacua might be particulary interesting to realise the construction of dS vacua of [100, 101], which required a massless field in the complex structure sector at tree-level. Regarding the last branch, $\theta_W = \theta_2^W$, away from the LCS point the spectrum contains $h^{2,1} - 1$ massless modes $\mu_{-\lambda'}^2 = 0$, that is *half of the scalar modes* in the truncated sector.

In section 6 we will discuss the statistics of this mass spectrum in the ensemble of no-scale flux vacua. This will help us to estimate how generic these classes of vacua are in the Landscape.
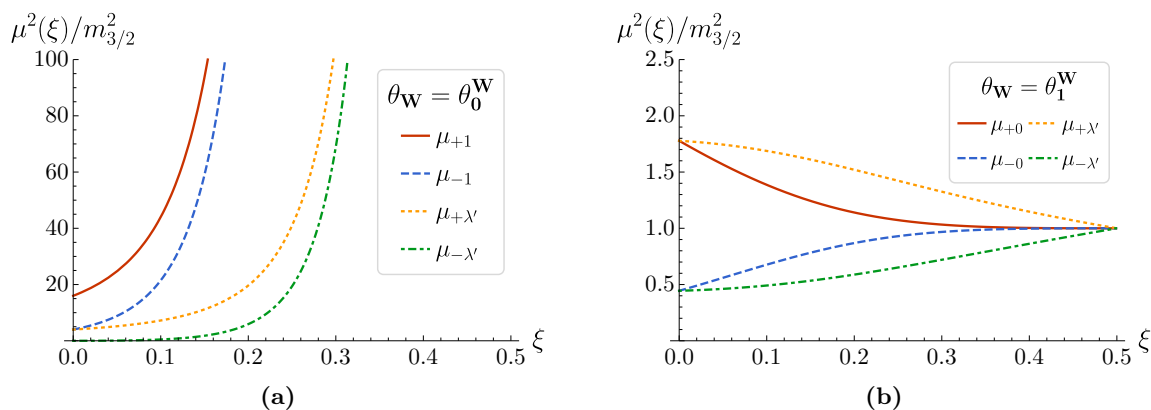
Figure 2. Scalar mass spectra associated with the critical values for θ_W (4.17) where the mass spectrum contains at least a zero mode. (a) Spectrum for $\theta_W = \theta_0^W$ where $\mu_{-0}^2 = 0$ and $\mu_{+0}^2 = 4m_{3/2}^2$. (b) Spectrum for $\theta_W = \theta_1^W$ where $\mu_{-1}^2 = 0$ and $\mu_{+1}^2 = 4m_{3/2}^2$.
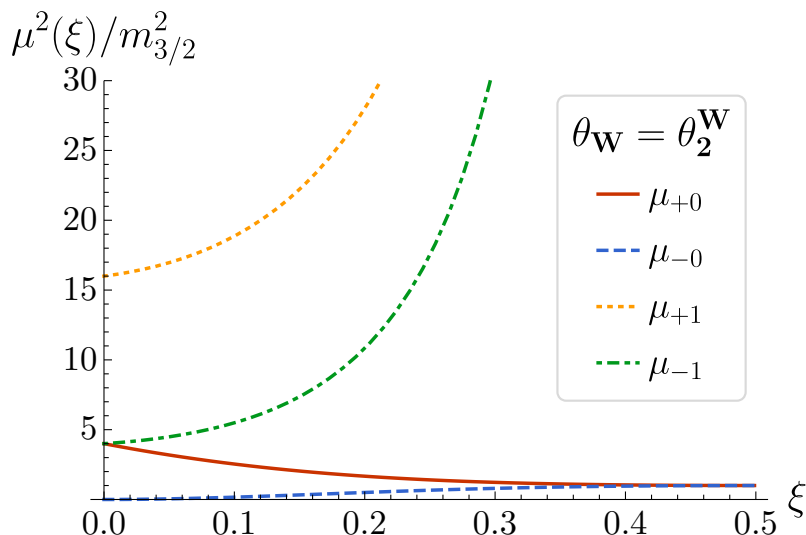

Figure 3. Scalar mass spectrum for $\theta_W = \theta_2^W$ where there are $h^{2,1} - 1$ massless modes in the truncated sector $\mu_{-\lambda'}^2 = 0$ and $\mu_{+\lambda'}^2 = 4m_{3/2}^2$.

4.4   No-scale vacua with $N_A^0 = 0$

In the present subsection we consider the second class of no-scale vacua for which the parameter θ_W is fixed in terms of ξ, namely flux vacua where the flux vector satisfies the constraint $N_A^0 = 0$. The flux N_A^0 is associated to the period (2.9) that grows without bound in the LCS limit. The main consequence of setting this flux to zero is that the terms of the superpotential which are cubic in z^i are also identically zero.

The main motivation to study this class vacua is the analyses done in [67, 68]. On the one hand, in [67] it was argued (via a numerical analysis) that for generic choices of the fluxes, and at points of the moduli space near the LCS point the cubic terms of the

superpotential typically become dominant.[7] On the other hand, as proven in [67, 68], when the cubic terms of W dominate no vacua can exist in the region of the moduli space where $\xi \approx 0$. As a consequence no-scale vacua with $N_A^0 \neq 0$ are expected to be very scarce, or even non-existent, in a small neighbourhood of the LCS point. On the contrary, the conclusions in [67, 68] cannot be applied to the class of vacua where the flux N_A^0 is set to zero, since the cubic terms of the superpotential are identically zero, and therefore can never become dominant. Thus, it is expected that the constrained class of vacua with $N_A^0 = 0$ may still be present, and even become the dominant type of vacua in a small neighbourhood of the LCS point.

To give further support to this conclusion, in appendix D we have estimated the minimal values of ξ for which it is possible to find no-scale solutions with both non-vanishing N_A^0 and when subject to the constraint $N_A^0 = 0$. We find

$$\xi_{\min}|_{N_A^0 \neq 0} \gtrsim \frac{|\operatorname{Im} \kappa_0|}{4\sqrt{N_{\text{flux}}}} \tag{4.18}$$

for $N_A^0 \neq 0$, while in the case $N_A^0 = 0$ the parameter ξ remains unbounded below. In agreement with the analyses in [67, 68], we can see that vacua with $N_A^0 = 0$ are expected to be dominant in a small neighbourhood of the LCS point. As we shall show in section 6, the numerical scan of no-scale vacua in the $\mathbb{WP}^4_{[1,1,1,1,4]}$ model confirms this expectation, and matches perfectly with the conclusions of [67, 68].

To prove that in this type of vacua the angular parameter θ_W is determined by the value of ξ, it is convenient to make use of the Hodge decomposition of the flux vector N [15]. As we review in appendix A, at any given no-scale vacuum $\{\tau_c, z_c^i\}$ the flux vector can be written in terms of the period vector Π and its Kähler covariant derivatives $D_a\Pi = (\partial_a + K_a)\Pi$ as

$$N = \sqrt{4\pi}e^{K_{cs}}\left(\mathrm{i}W\,\bar{\Pi} + D_{\bar{0}}D_{\bar{a}}\bar{W}\,D_a\Pi\right). \tag{4.19}$$

Setting $N_A^0 = 0$ in this expression, we find

$$W = iD_{\bar{0}}D_{\bar{a}}\bar{W}\,K_a\,, \tag{4.20}$$

where we have used that in the gauge (2.9) the period vector satisfies $\Pi_A^0 = 1$. Finally, taking into account the result (4.7) and the definition of the angular parameter θ_W (4.13) together with (2.32), we arrive at the constraint

$$\tan\theta_W = \sqrt{(1-2\xi)/3} \qquad \Longrightarrow \qquad \theta_W \in \left[0, \frac{\pi}{6}\right]. \tag{4.21}$$

Alternatively, this relation can be expressed in the following useful way.

$$W_0^2 = \mathcal{V}^2 m_{3/2}^2 = \frac{3N_{\text{flux}}}{8\pi(2-\xi)} \geq \frac{N_{\text{flux}}}{8\pi} \sim \mathcal{O}(10\text{--}10^3), \tag{4.22}$$

which relates the flux parameter W_0 and the total $D3$-charge N_{flux}. From here we can see immediately that these solutions are not compatible with the KKLT construction of dS

---

[7]Actually this is true even for points in field space not associated with a vacuum.
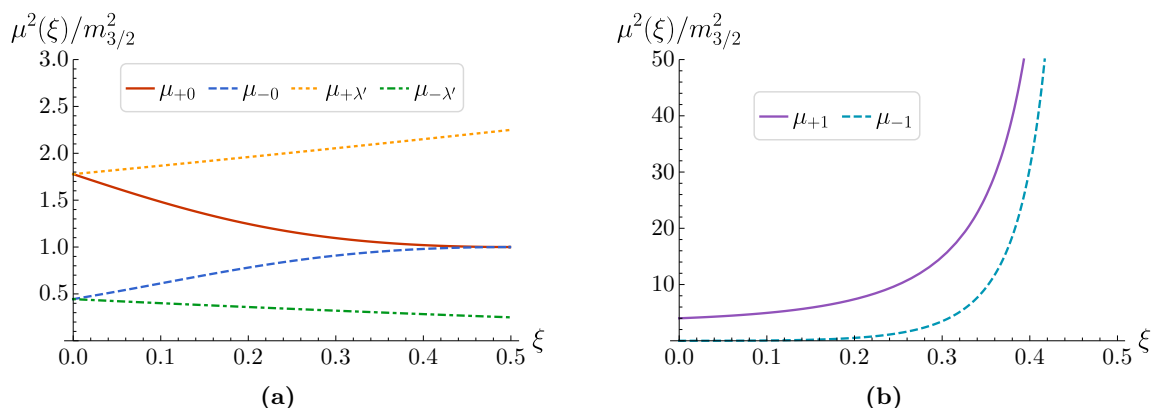
Figure 4. Spectrum of scalar masses for vacua with the restriction $N_A^0 = 0$ on the flux configuration. The masses are plotted as a function of the LCS parameter $\xi \in [0, 1/2]$ and are normalised by the gravitino mass $m_{3/2}$. (a) Branches corresponding to the masses $\{\mu_{\pm 0}^2, \mu_{\pm \lambda'}^2\}$, where $\mu_{\pm \lambda'}^2$ are the $2(h^{2,1} - 1)$ masses in the truncated sector. (b) Scalar mass branches $\{\mu_{+1}^2, \mu_{-1}^2\}$. We can see that in these branches of vacua there are no light truncated fields $\mu_{\pm 1}^2 \ll m_{3/2}^2$ in the entire LCS regime.

vacua, since that scenario requires $W_0 \ll 1$. On the contrary, this class of no-scale vacua is suitable for the construction of LVS vacua, where $W_0 \sim \mathcal{O}(1\text{–}10)$.

In order to find the scalar spectrum at these no-scale solutions, we just need to substitute the relation (4.21) into our main result (4.15), which leads to

$$
\mathbf{N_A^0 = 0}: \qquad \mu_{\pm\lambda}^2/m_{3/2}^2 = \begin{cases} \left(1 \pm \sqrt{(1-2\xi)/3}\,\hat{m}(\xi)\right)^2 & \lambda = 0 \\[2mm] \left(1 \pm \frac{\sqrt{(1-2\xi)}}{\sqrt{3}\hat{m}(\xi)}\right)^2 & \lambda = 1 \\[2mm] \left(1 \pm \frac{1+\xi}{3}\right)^2 & \lambda = 2, \ldots, h^{2,1} \end{cases} \qquad (4.23)
$$

We have displayed the dependence of these masses on the parameter ξ in figure 4. Note that the previous spectrum is independent of the details of the Calabi-Yau compactification. With the aid of (4.22), it can be computed entirely from the total $D3$-charge N_{flux}, the LCS parameter ξ, and the Calabi-Yau volume $\mathcal{V}$.

Finally, as we approach the LCS point, $\xi \to 0$, the mass spectrum (4.23) takes the universal form

$$
\mathbf{N_A^0 = 0,\ \xi = 0}: \qquad \mu_{\pm\lambda}^2/m_{3/2}^2 = \begin{cases} \left(1 \pm \frac{1}{3}\right)^2 & \lambda = 0, 2, \ldots, h^{2,1} \\[2mm] \left(1 \pm 1\right)^2 & \lambda = 1 \end{cases} \qquad (4.24)
$$

This result is reminiscent of the deterministic spectra found in [67, 68] at generic moduli configurations (not necessarily vacua) near the LCS point.

– 22 –

5 Example: the $\mathbb{WP}^4_{[1,1,1,1,4]}$ model

In order to illustrate our results we have analysed a large sample of no-scale vacua of an orientifold of the Calabi-Yau hypersurface $\mathbb{WP}^4_{[1,1,1,1,4]}$ (the *octic*). We will now briefly review the effective field theory for the compactification of type-IIB superstrings in this Calabi-Yau, and we will discuss the statistical properties of the resulting ensemble in section 6. For a more detailed description of this compactification we refer the reader to [7, 57].

5.1 Effective theory

The Calabi-Yau geometries that we will consider can be defined in terms of the following family of hypersurfaces

$$4x_0^2 + x_1^8 + x_2^8 + x_3^8 + x_4^8 - 8\psi x_0 x_1 x_2 x_3 x_4 = 0 \tag{5.1}$$

in the complex projective space $x^i \in \mathbb{WP}^4_{[1,1,1,1,4]}$ (Model 3 of table 1).

This family of hypersurfaces is characterised by a single complex deformation parameter ψ, with $\arg \psi \in [0, \frac{\pi}{4}]$. However, this Calabi-Yau three-fold has $h^{1,1} = 1$ Kähler moduli and $h^{2,1} = 149$ complex structure fields, and thus there are many other deformations that one could consider. The Calabi-Yau geometries described by (5.1) are all invariant under a large group of discrete symmetries, namely $\mathcal{G} = \mathbb{Z}_8^2 \times \mathbb{Z}_2$ with order $[\mathcal{G}] = 128$, and all the deformations that we have not included in (5.1) are those transforming non-trivially under this group [6, 7]. Thus, by retaining only the deformation parametrised by ψ, we are realizing a consistent truncation of the complex structure moduli space, just as we discussed in section 3.

In the neighbourhood of the large complex structure point, $\psi \to \infty$, the truncated action is characterised by the prepotential [57, 66]

$$\mathcal{F}(z) = \frac{\mathrm{i}}{3}z^3 + \frac{3}{2}z^2 + \mathrm{i}\frac{11}{6}z - \mathrm{i}\frac{37}{2\pi^3}\zeta(3) + \mathcal{F}_{\mathrm{inst}}, \tag{5.2}$$

where $z \approx \frac{4}{\pi}\log(4\psi)$ and $\mathrm{Im}\, z \in [-1/2, 1/2)$. Here, $\mathcal{F}_{\mathrm{inst}}$ represents exponentially suppressed instanton corrections to the prepotential. Its leading term is of the form

$$\mathcal{F}_{\mathrm{inst}} \approx -\frac{\mathrm{i}n_1}{(2\pi)^3}\mathrm{e}^{-2\pi z} + \dots, \qquad \text{with} \qquad n_1 = 29504. \tag{5.3}$$

The expansion for the prepotential (5.2) around the LCS point converges in the region $|\psi| > 1$, or equivalently $\xi \lesssim \xi_{\mathrm{cnf}} \equiv 0.39$, away from the conifold singularity at $\psi = 1$ [57, 66]. However, here we will require in addition that the instanton corrections cause small variations on the moduli space geometry and the relevant physical quantities (e.g., the Yukawa couplings $\mathring{\kappa}_{abc}$, the vielbeins e_i^a, and $m_{3/2}$). As we discuss in appendix D.3, the most restrictive bound is found when imposing that the relative corrections to the moduli space vielbein are small. Although this is checked for each particular vacuum, a simple estimate shows that the corrections remain moderately small ($< 20\%$) as long as the LCS parameter satisfies

$$\xi \lesssim \xi_{\mathrm{max}} = 0.185 < \xi_{\mathrm{cnf}}, \tag{5.4}$$

which is a more conservative bound than just requiring the convergence of (5.2).

Following [6, 7, 15], we will regard this compactification as an orientifold limit of a compactification of F-theory on the fourfold $M_4 = \mathbb{WP}^5_{[1,1,1,1,8,12]}$, where the orientifold action is defined by the transformations[8] $x_0 \to -x_0$ and $\psi \to -\psi$ [102, 103]. The advantage of considering the embedding in F-theory is that compactifications on a fourfold allow a great deal of freedom in the choice of fluxes, which is particularly appropriate for performing a statistical analysis [15]. Indeed, the tadpole constraint L is

$$L = \frac{\chi(M_4)}{24}, \tag{5.5}$$

where $\chi(M_4)$ is the Euler number of the fourfold, which typically greatly exceeds the one of the associated Calabi-Yau orientifold $\tilde{M}_3$. In the case at hand, the Euler number of the fourfold $\mathbb{WP}^5_{[1,1,1,1,8,12]}$ is $\chi(M_4) = 23,328$, and thus the upper bound on the $D3$-brane charge induced by the fluxes is $N_{\text{flux}} \leq L = 972$.

As a final remark, note that the F-theory embedding also requires including in the theory additional $D7$-brane moduli (see [104]). The problem of the stabilisation of those moduli is however beyond the scope of the present paper, and we refer the reader to [105–109] and the references therein for works on the subject.

5.2 Numerical search for flux vacua

In order to perform a numerical exploration of the flux landscape of the octic, we have used `Paramotopy` [110]. This software uses a numerical technique known as the *Polynomial Homotopy Continuation* (PHC) method [111, 112], which efficiently finds all roots of non-linear polynomial systems, such as the no-scale equations (2.20) (see appendix B). Therefore, given a flux ensemble satisfying the tadpole condition (2.22), the PHC method allows for an exhaustive search of all the solutions to the no-scale equations (2.20) [113, 114].

As described in detail in appendix B, we have constructed two separate ensembles of no-scale vacua: one with generic fluxes satisfying the tadpole constraint, and one where fluxes additionally satisfy the condition $N_A^0 = 0$, as considered in section 4.4. We shall refer to them as the *generic* and *constrained* ensembles, respectively. The starting point for the construction of each of the ensembles is a collection of fluxes f and h randomly selected from a uniform distribution with support $[-50, 50]$. This starting set consists of 10^7 choices of flux for the generic ensemble, and 10^6 choices for the constrained one.

For each choice of flux, the corresponding set of no-scale vacua were found using the PHC method. We then selected all solutions which have a small string coupling constant $g_s = (\operatorname{Im} \tau)^{-1} < 1$ and small instanton corrections, i.e., which satisfy (5.4). In addition, when constructing the ensemble we checked that there was no double-counting of vacua related by either an $\mathrm{SL}(2, \mathbb{Z})$ action (2.24), or the symplectic transformations (2.6) and (2.23). Regarding the symplectic transformations, as proposed in [8], all no-scale solutions have been mapped to the fundamental domain of the axio-dilaton, where the redundant copies

---

[8]As shown in [6], it is possible to turn on the three-forms $F_{(3)}$ and $H_{(3)}$ on the four periods of the reduced theory consistently with the orientifold action.
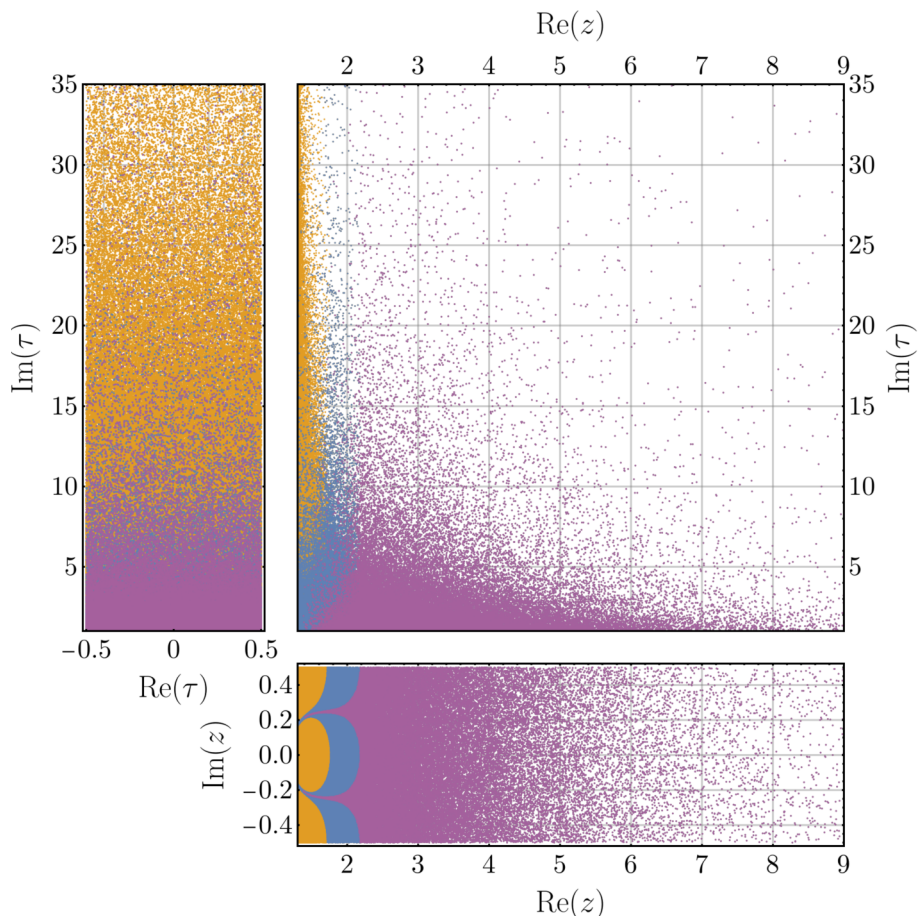
Figure 5. Distribution of the numerically generated set of generic no-scale solutions on the (τ, z) field space. We have represented in orange vacua with large instanton corrections $> 20\%$ (leading term in (5.3)), in blue when corrections are in the range $1 - 20\%$, and in purple when corrections are $< 1\%$. The $(\text{Re}\,z, \text{Im}\,\tau)$ plane exhibits nicely delineated regions, which are nevertheless likely to be blurred by higher order contributions to (5.3). The generic ensemble of vacua analysed in the text is comprised of those solutions with small instanton corrections $< 20\%$, and small string coupling $g_s = (\text{Im}\,\tau)^{-1} < 1$ (blue and purple, 119,139 solutions).

have been identified and discarded.[9] As for symplectic transformations, there is the monodromy around the LCS point [57, 66] which we have treated similarly, by mapping all solutions to a fundamental domain of the complex structure modulus z and eliminating duplicate solutions.

The ensemble of vacua with unconstrained fluxes that we obtained with this method contains $119,139$ solutions, while the constrained ensemble has $57,487$. The results of this procedure for the generic ensemble are displayed in figure 5, where we show the distribution of no-scale vacua in the fundamental domain of the axio-dilaton τ, in the complex structure

---

[9] We avoided imposing conditions on the fluxes to eliminate the redundancies, as done, e.g., in [113, 114]. In particular, our analysis showed that the constraints on the fluxes proposed in [113] to deal with the $SL(2, \mathbb{Z})$ symmetry lead to spurious correlations arising in the statistical analysis, and which are incompatible with the predictions derived from the continuous flux approximation [15].
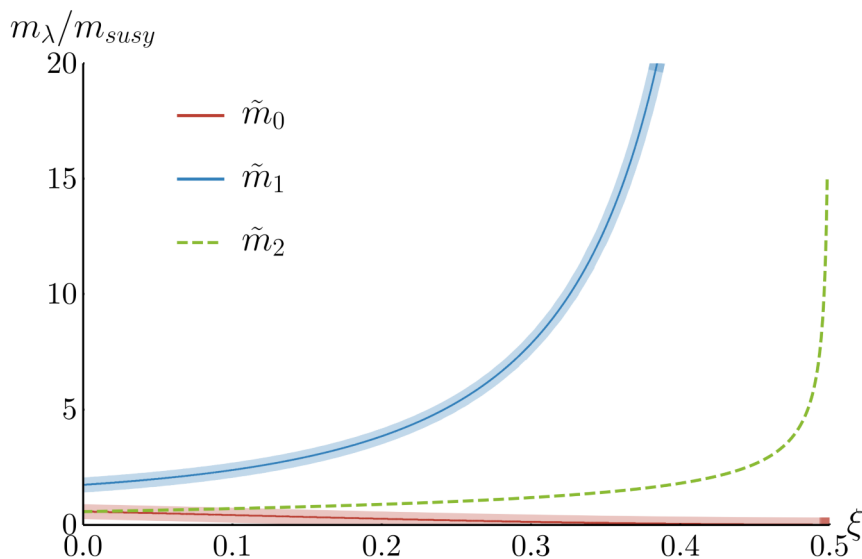
Figure 6. Fermion masses in the $\mathbb{WP}^4_{[1,1,1,1,4]}$ compactification versus the LCS parameter ξ at no-scale vacua. The fermion masses are normalised by the supersymmetric mass scale, $\tilde{m}_\lambda \equiv m_\lambda / m_{\text{susy}}$. The uppermost and lowermost thick curves represent the analytic result in (4.10) for the two fermions in the reduced theory. The thin solid curves, composed of (indistinguishable) data points, show masses obtained diagonalising numerically the fermion mass matrix (2.29) at each vacuum of the ensemble. The middle dashed curve represents the mass of the 148 fermions in the truncated sector (with a priori unknown EFT couplings), which was computed via the third equation in (4.10).

field z, and in the $(\operatorname{Re} z, \operatorname{Im} \tau)$. For completeness, let us mention that more conservative constraints could be imposed on the vacua, e.g., $g_s < 0.1$ and instanton corrections below $< 1\%$, leading to a considerably smaller ensemble with 427 vacua. However, in order to have a sufficiently large sample to perform the statistical analysis, in the following we will consider all vacua in the weak coupling regime $g_s < 1$ and with moderately small instantons corrections $< 20\%$.

In order to check the validity of our main result, (4.10), at each of the no-scale solutions, we computed the eigenvalues of the fermion mass matrix (2.27) for the reduced theory (involving only τ and z) using two different methods: first via the direct diagonalisation of the mass matrices obtained numerically, and then using the analytic formula (4.10). We display the outcome of these computations in figure 6, which demonstrates the perfect the agreement of both methods. Regarding the 148 truncated complex structure moduli, although the EFT given above has no specific information about them, the expressions (4.10) allowed us to determine the fermionic masses corresponding to this sector at each no-scale solution. Finally, the scalar mass spectra in the whole axio-dilaton/complex structure sector for the ensemble of no-scale solutions were computed via (2.28). We checked that these masses coincide with those obtained by diagonalizing the Hessian (2.26) at each no-scale vacuum. The statistical properties of these spectra will be analysed in the next section.

6 Statistics of vacua

As we discussed in section 4, the no-scale mass spectrum will depend in general on the flux configuration. To determine the properties of the spectra that may arise in the ensemble of flux vacua, we will adopt the statistical approach of [15], and derive the probability distributions for the masses and other quantities of interest. We begin by presenting the relevant formulae for general compactifications before using them to study the particular models we consider.

Our starting point for this analysis will be the formula for the density of flux vacua derived in [15] using the continuous flux approximation. This approximation is based on the assumption that for large tadpoles, $L \gg 1$, flux quantisation can be neglected, and thus it is possible to replace the sums over flux configurations by integrals.

$$\sum_{N_A^I, N_I^B} \longrightarrow \int d^{2n} N_A d^{2n} N^B \,, \tag{6.1}$$

where $n = h^{2,1} + 1$ and each component of $N = f - \tau h$ is a complex number parametrized by the two tuples of integers f and h. Furthermore, as was proven in [15] and reviewed in appendix A, by using the Hodge decomposition of the flux vector, it is possible to establish a one-to-one correspondence between the $2n$ *continuous* flux complex variables $\{N_A^I, N_I^B\}$ and the $2n$ complex quantities $\{Z_A, F_A\}$ $(A = 0, \ldots, h^{2,1})$ given by

$$Z_0 \equiv \mathcal{V}\mathrm{e}^{K/2}W \,, \qquad Z_a \equiv \mathcal{V}Z_{0a} \,, \qquad F_0 \equiv \mathcal{V}\mathrm{e}^{K/2}D_0 W \,, \qquad F_a \equiv \mathcal{V}\mathrm{e}^{K/2}D_a W \,. \tag{6.2}$$

These variables are particularly convenient choices for describing the flux ensemble, as no-scale vacua can be equivalently characterised as flux configurations satisfying the conditions $F_A = 0$. Thus, assuming a flat probability distribution on the fluxes, and using a generalisation of the Kac-Rice formula [115, 116] (see [117] for a review), the *density function* for no-scale vacua follows as [15]

$$d\mu_{vac}(Z_A, u^A) = \mathcal{N} \cdot |\det \mathcal{H}|^{1/2} |\det g| \mathrm{e}^{-|Z|^2} \cdot d^{2n} Z \cdot d^{2n} u \,, \tag{6.3}$$

where we denote the fields collectively by $u^A = \{\tau, z^a\}$, g is the moduli space metric, and $\mathcal{H}$ is the canonically normalised Hessian of the no-scale potential given by (2.26) and (2.31) (see appendix C). Here, and throughout the text, $\mathcal{N}$ indicates some normalization constant which must be computed for each particular distribution. The previous formula should not be confused with the *index density* of flux vacua,[10] first derived in [118] and subsequently verified numerically in [7] and [119].

In the class of models we are interested in, the number of complex structure moduli can be arbitrarily high but only one survives the truncation. In addition, as explained in section 3, the truncation requires that only the components $I = 0, 1$ of the flux vector $N = \{N_A^I, N_I^B\}$ are turned on (8 flux integers). Therefore, the statistics of these models can be described by (6.3), setting $h^{2,1} = 1$ $(n = 2)$. In this case, the determinant of the Hessian $\mathcal{H}$ takes the particularly simple form

$$|\det \mathcal{H}|^{1/2} = ||Z_0|^4 + |Z_1|^4 - (2 + \mathring{\kappa}^2)|Z_0|^2|Z_1|^2| \,, \tag{6.4}$$

which will considerably simplify the computation of the mass distributions.

---

[10]The index density obtained in [118] counts vacua weighted with the sign of $\det(\mathbb{1} + \mathcal{M})$.
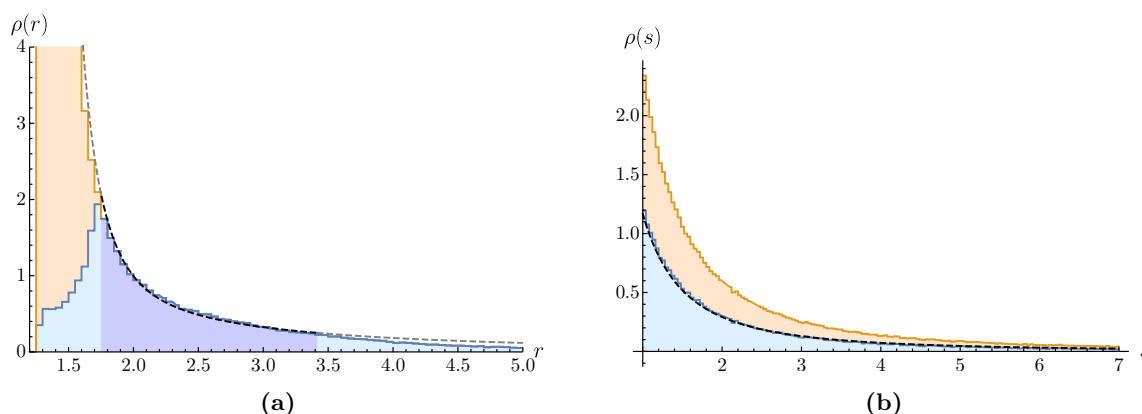
Figure 7. (a) Marginalised density of no-scale vacua on the complex structure sector (6.5) (dashed line), and numerically obtained histogram of generic no-scale solutions in the $\mathbb{WP}^4_{[1,1,1,1,4]}$ flux ensemble. The quantity $r \equiv (2\kappa_{zzz}/3|\operatorname{Im}\kappa_0|)^{1/3} \operatorname{Re} z$ represents the complex structure field at the vacua, with the boundaries of the moduli space located at $r = 2^{1/3}$ and $r \to \infty$ (the LCS point). The orange area represents excluded solutions with large instanton corrections ($> 20\%$). In dark blue we indicate the subset of the remaining vacua well described by (6.5) (normalised in $r \in [1.75, 3.42]$). (b) Marginalised distribution (6.5) for the imaginary part of the axio-dilaton, $s \equiv \operatorname{Im}\tau$ (dashed line), and histogram of solutions in the generic ensemble of no-scale vacua.

6.1 Moduli space distribution of generic no-scale vacua

Integrating (6.3) over the flux parameters Z_A (with $h^{2,1} = 1$) one obtains the following density distribution of no-scale vacua [15]:

$$d\mu(z,\tau) = \mathcal{N} \cdot |\det g| \cdot \left(2 - \mathring{\kappa}^2 + \frac{2\mathring{\kappa}^3}{\sqrt{4 + \mathring{\kappa}^2}}\right) d^2\tau d^2 z \,, \tag{6.5}$$

where

$$|\det g| = \frac{3}{16}\left(\frac{2\kappa_{zzz}}{3|\operatorname{Im}\kappa_0|}\right)^{2/3} \frac{(r^3 - 2)r}{(r^3 + 1)^2 s^2} \tag{6.6}$$

is the determinant of the moduli space metric, with κ_{zzz} denoting Yukawa coupling for the (non-canonically normalised) field z. We have also introduced the shorthands

$$s \equiv \operatorname{Im}\tau \qquad \text{and} \qquad r \equiv 1/\xi^{1/3} = (2\kappa_{zzz}/3|\operatorname{Im}\kappa_0|)^{1/3} \operatorname{Re} z\,. \tag{6.7}$$

Thus the quantity $\mathring{\kappa}$, defined in (4.5) in terms of ξ, should be understood as a function of $\operatorname{Re} z$ in the expression (6.5) for the no-scale vacua density function. The corresponding marginal probability distributions for $\operatorname{Re} z$ and $\operatorname{Im}\tau$ are displayed in figure 7. The plots show a remarkable agreement with the histograms obtained from the numerical scan of the octic model. Combining (6.5) and (6.7) it is also straightforward to find the probability distribution function for the LCS parameter ξ,

$$d\mu(\xi) = \mathcal{N} \cdot \frac{(1 - 2\xi)}{(1 + \xi)^2 \xi^{2/3}} \left(2 - \mathring{\kappa}(\xi)^2 + \frac{2\mathring{\kappa}(\xi)^3}{\sqrt{4 + \mathring{\kappa}(\xi)^2}}\right) d\xi\,, \tag{6.8}$$
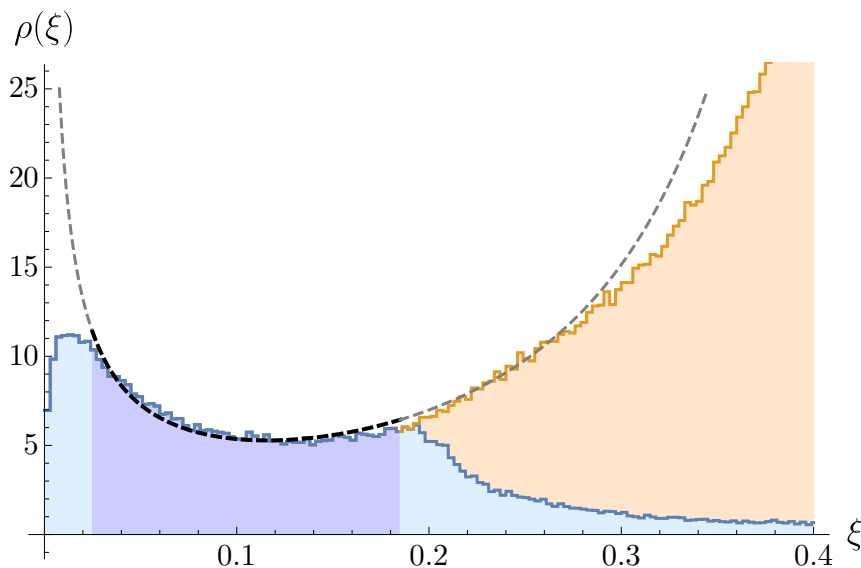
Figure 8. Distribution for the LCS parameter ξ (6.8) in the flux ensemble with unconstrained N_A^0 (dashed line), and histogram of solutions obtained from the numerical scan in the $\mathbb{WP}^4_{[1,1,1,1,4]}$ model. The colours are the same as in figure 7.

which we have displayed in figure 8, together with the histogram obtained from the direct computation from the octic flux ensemble data.

It is interesting to note that the density of vacua grows without bound as we move towards small values of r (i.e., $\xi \to 1/2$), where the conifold point is located, $r_{\rm cnf} \approx 1.37$ ($\xi_{\rm cnf} = 0.39$). This is consistent with the expectation that the density of vacua is enhanced in regions of large moduli space curvature [7, 118, 119]. Actually, the marginalised density functions for $\mathrm{Re}\, z$ obtained from (6.5) are not normalisable when we define its support to be the entire range[11] $r \in [2^{1/3}, \infty)$. This property of the ensemble has an observable effect: as the underlying distribution from which we are extracting the vacua is not normalisable, regardless of the size of the sample, the histograms will always exhibit a deficit of vacua in with respect to the probability distribution (see region $\xi \gtrsim 0.3$ in figure 8). Nevertheless, the complications due to the distribution being non-normalisable can be easily avoided: recall that the EFT for the octic can only be trusted in the region where the instanton corrections can be safely neglected, that is, in the region given by the bound (5.4), or equivalently with $r \in [1.75, \infty)$. Thus, as long as the support of (6.5) is taken to be the region of validity of the EFT, the probability distribution will be finite and normalizable, and thus well defined.

In figure 8, it can also be seen that the density of generic no-scale vacua near the LCS point ($\xi \approx 0$) is considerably lower that the statistical prediction based on the continuous flux approximation (dashed line). This to be expected from the analyses in [67, 68], where it was shown that the statistics of generic no-scale vacua (with unconstrained N_A^0) can

---

[11]Recall that we obtained the condition $\xi < 1/2$, satisfied away from the moduli space boundaries, neglecting completely the instanton contributions, and thus it gives no information about the position of the conifold point at $\xi_{\rm cnf} = 0.39$.

not be described with the continuous flux approximation in the strict LCS limit, and that actually in a small neighborhood of the LCS point there are no no-scale solutions with $N_A^0 \neq 0$. Such behavior was also anticipated in [16], where the authors argued that the techniques presented there could fail to describe vacua statistics restricted to small regions of the moduli space. In appendix D.2 we derive an estimate for the region of validity of the continuous flux approximation (eq. (4.18)) which, in the present ensemble, leads to the additional constraint on the LCS parameter

$$\xi \geq \xi_{\min} = 0.025 \,. \tag{6.9}$$

In the following section we will discuss the statistics of the mass spectrum in the regime where the EFT is under control and, in addition, where the continuous flux approximation is a good characterisation of the flux ensemble. That is, in the moduli region determined by the bounds (5.4) and (6.9).

Before we end this subsection let us comment briefly on the distribution of the string coupling constant g_s. Both the analytical result in eq. (6.5), and the numerical histogram displayed in figure 7(b), indicate that the probability density for $\mathrm{Im}(\tau)$ has the form $\rho(\mathrm{Im}\,\tau) \propto 1/(\mathrm{Im}\,\tau)^2$. Therefore, it is straightforward to check that the string coupling $g_s = (\mathrm{Im}\,\tau)^{-1}$ is uniformly distributed. This conclusion is relevant in the computation in [120] of the distribution of the supersymmetry breaking scale in the Landscape which relies on g_s having a uniform distribution.

6.2 Mass distributions at generic no-scale vacua

With the joint probability distribution (6.3) at hand it is now straightforward to compute probability distributions for the masses, both the fermions and the scalar modes, at the no-scale vacua in our flux ensemble.

In particular, at a given vacuum with LCS parameter ξ and angular parameter θ_W, the fermion mass spectrum normalised by the gravitino mass $m_\lambda/m_{3/2}$ is given by

$$x_\lambda \equiv m_\lambda/m_{3/2} = \begin{cases} \zeta\,\hat{m}(\xi) & \lambda = 0 \\ \zeta\,\hat{m}(\xi)^{-1} & \lambda = 1 \\ \zeta(1+\xi)/\sqrt{3(1-2\xi)} & \lambda = 2,\dots,h^{2,1} \end{cases}, \tag{6.10}$$

where we have used (4.10) in combination with (4.14), with $\zeta \equiv \tan^2\theta_W \in [0,\infty]$. Then, in order to find the distribution for these masses, we need the joint distribution for $\{\xi,\zeta\}$. This distribution can be obtained from (6.3) and (6.4) by integrating over the phases $\arg(Z_0)$ and $\arg(Z_1)$, the total $D3$-charge induced by fluxes $|Z_A|^2 = N_{\mathrm{flux}}$, and the field space directions τ and $\mathrm{Im}\,z$. Using the ζ and ξ variables, this yields

$$d\mu(\zeta,\xi) = \mathcal{N} \cdot \frac{(1-2\xi)}{\xi^{2/3}(1+\xi)^2(1+\zeta)^4}\left|\zeta - \hat{m}(\xi)^2\right|\left|\zeta - \hat{m}(\xi)^{-2}\right| \cdot d\zeta\, d\xi \,. \tag{6.11}$$

From (6.10) we can see that given a fixed value of ξ, we can establish is a one-to-one correspondence between ζ and each of the rescaled fermion masses x_λ. Therefore, by

performing a change of random variables $\{\zeta, \xi\} \rightarrow \{x_\lambda, \xi\}$ in (6.11), we can derive three separate distribution functions, each involving a different scaled mass x_λ. After integrating over the LCS parameter on the interval $\xi \in [\xi_{\min}, \xi_{\max}]$ given by (5.4) and (6.9), the resulting marginal distributions for the fermion masses in the reduced theory read

$$\rho_0^f(x_0) = \mathcal{N} \left| x_0^2 - 1 \right| x_0 \int_{\xi_{\min}}^{\xi_{\max}} d\xi \frac{(1 - 2\xi)\,\hat{m}(\xi)^2}{\xi^{2/3}(1 + \xi)^2(\hat{m}(\xi)^2 + x_0^2)^4} \left| x_0^2 - \hat{m}(\xi)^4 \right|, \qquad (6.12)$$

and

$$\rho_1^f(x_1) = \mathcal{N} \left| x_1^2 - 1 \right| x_1 \int_{\xi_{\min}}^{\xi_{\max}} d\xi \frac{(1 - 2\xi)\,\hat{m}(\xi)^2}{\xi^{2/3}(1 + \xi)^2(1 + x_1^2\,\hat{m}(\xi)^2)^4} \left| x_1^2\,\hat{m}(\xi)^4 - 1 \right|. \qquad (6.13)$$

Without further computations, we can already see that the probability of finding vacua with $m_{\lambda=0,1} = m_{3/2}$ (equivalently $x_{\lambda=0,1} = 1$) is suppressed, i.e., $\rho_{\lambda=0,1}^f(1) = 0$. This is a direct consequence of the generalized Kac-Rice formula (6.3). To see this, note that density of vacua is proportional to the square root of the Hessian determinant $|\det \mathcal{H}|^{1/2}$. This means that the probability of finding no-scale solutions with massless scalar modes in the flux ensemble should vanish. Since according to (2.28) massless scalar modes occur precisely whenever one fermion mass equals that of the gravitino, we conclude that no-scale vacua with $m_\lambda = m_{3/2}$ are quite rare in the Landscape. It is important to emphasize that this does not preclude vacua with $m_{\lambda=0,1} = m_{3/2}$ from existing, it just means they represent a very small fraction of the total number of vacua. Actually, the suppression of critical points with of zero eigenvalues on the Hessian, which also leads to an apparent repulsion between critical points, is a generic feature of random functions (see, e.g., [117]), and has already been observed in other characerisations of the Landscape [121, 122].

Regarding the rescaled mass of the truncated fermions $x_{\lambda'} = m_{\lambda'}/m_{3/2}$, we find the distribution

$$\rho_{\lambda'}^f(x_{\lambda'}) = \mathcal{N} x_{\lambda'} \int_{\xi_{\min}}^{\xi_{\max}} d\xi \frac{(1 - 2\xi)f(\xi)^{-2} \left| x_{\lambda'}^2 f(\xi)^{-2} - \hat{m}(\xi)^2 \right| \left| x_{\lambda'}^2 f(\xi)^{-2} - \hat{m}(\xi)^{-2} \right|}{\xi^{2/3}(1 + \xi)^2(1 + x_{\lambda'}^2 f(\xi)^{-2})^4}, \quad (6.14)$$

where $f(\xi) \equiv \frac{1+\xi}{\sqrt{3(1-2\xi)}}$. Note that for generic values of ξ there appears to be no suppression on the probability of finding $x_{\lambda'} = 1$ in the truncated sector; in other words, $\rho_{\lambda'}^f(1) \neq 0$. This in turn shows that massless scalar modes on the truncated sector are *not suppressed*. This is a surprising result that is at odds with what would be expected from the analysis of generic random functions. This reflects the important role that symmetries of the EFT play in shaping the flux Landscape. In particular, this observation is of importance for the construction of dS vacua proposed in [100, 101], which relies on the existence of no-scale solutions with massless modes at tree-level.

A common feature to the three distributions (6.12), (6.13) and (6.14), is that they all vanish for $m_\lambda = 0$ (equivalently $x_\lambda = 0$). That is, the probability of finding no-scale solutions with massless fermions also appears to be suppressed in the ensemble of flux vacua. This result can be traced back to the structure of the fermion mass matrix $\mathcal{M}$ given
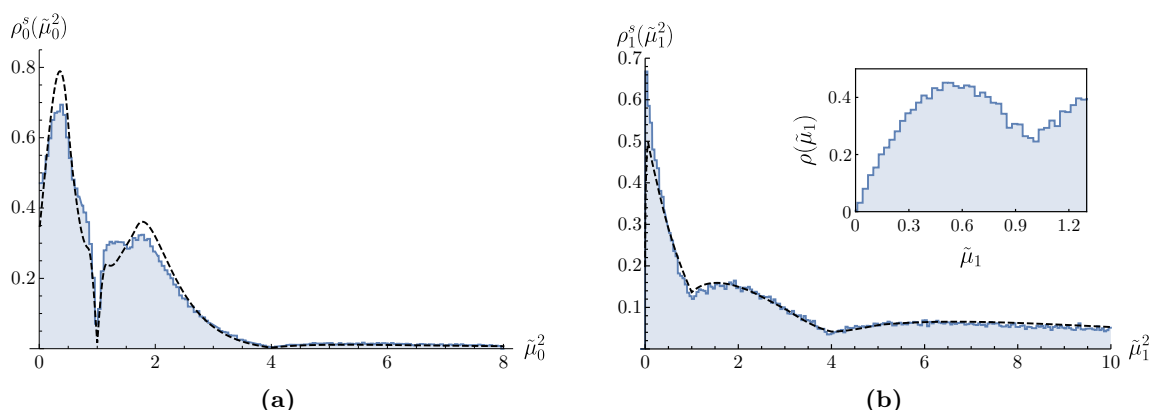
Figure 9. Distribution of the squared scalar masses normalised by the gravitino mass, $\tilde{\mu}_\lambda^2 \equiv \mu_\lambda^2/m_{3/2}^2$, in the ensemble with unconstrained fluxes. The dashed lines in (a) and (b) correspond to the probability distribution (6.15) (evaluated with (6.12) and (6.13), resp.) for the masses of the scalars in the reduced theory. We also show the mass histograms obtained numerically from the flux ensemble of the $\mathbb{WP}_{[1,1,1,1,4]}^4$ model (blue). The inset in (b) shows the obtained distribution $\rho(\tilde{\mu}_1)d\tilde{\mu}_1$ near the origin, which presents a suppression for the massless mode.

in (2.26), whose eigenvalues come in pairs $\pm m_\lambda$, and the well known *eigenvalue repulsion* effect [123], which is characteristic of random matrix ensembles[12] (see [124] for a review).

With the above distributions for $m_\lambda/m_{3/2}$ at hand, the probability density functions for the scalar masses can be easily obtained with a simple change of variables. Indeed, for each λ the probability distribution for the combined two branches of scalar masses $\mu_{\pm\lambda}^2$ reads

$$\rho_\lambda^s(\tilde{\mu}_\lambda^2)d\tilde{\mu}_\lambda^2 = \mathcal{N} \cdot \tilde{\mu}_\lambda^{-1} \left[\rho_\lambda^f(1+\tilde{\mu}_\lambda) + \rho_\lambda^f(|1-\tilde{\mu}_\lambda|) \right] d\tilde{\mu}_\lambda^2, \tag{6.15}$$

where $\tilde{\mu}_\lambda^2 \equiv \mu_\lambda^2/m_{3/2}^2$. These theoretical distributions are plotted in figures 9 and 10, along with the scalar mass histograms obtained from the numerical scan. As described in section 5, the masses of the scalar modes in the sector surviving the truncation, $\mu_{\lambda=0,1}^2$ are obtained via the diagonalisation of the fermion mass matrix (2.29) at each vacuum together with the formula (2.28), while those associated to the truncated modes $\mu_{\lambda'}^2$ are computed from the formula (4.15). The plots show a remarkable agreement of the numerical results and analytical predictions in the regime where both the low energy EFT and the continuous flux approximation are expected to provide a good description of the theory.[13]

It is interesting to note that the spectra in the surviving sector of figure 9 show a suppressed probability of no-scale solutions with scalar masses[14] $\mu_\lambda^2/m_{3/2}^2 = 0, 1, 4$. This is

---

[12]The collection of mass matrices $\mathcal{M}$ associated with the ensemble no-scale vacua can be regarded as an statistical ensemble of matrices with random entries [16, 51, 56, 74, 75].

[13]The histograms in figures 9 and 10 show slight deviations with respect to the theoretical distributions. As argued in [15], the discrepancies might be due to restricting the vacua to lie in a bounded region of moduli space, i.e., within the limits (5.4) and (6.9).

[14]Note that the $\mu_\lambda^2/m_{3/2}^2 = 0$ suppression is not evident in the main plot of figure 9(b). This is due to the factor $1/\tilde{\mu}_1$ in (6.15), which makes it difficult to resolve the suppression in the numerical histogram. The inset of this figure shows the histogram for $\tilde{\mu}_1$, which does present clearly the suppressed probability of the massless modes.
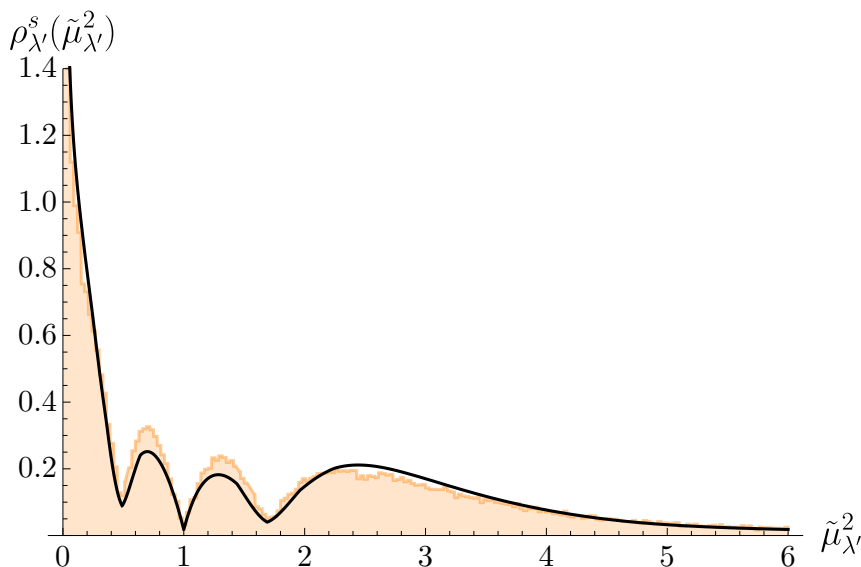
Figure 10. The theoretical prediction for the probability distribution of the normalised squared masses $\tilde{\mu}_{\lambda'}^2 = \mu_{\lambda'}^2/m_{3/2}^2$ of the truncated scalar fields (solid line), eqs. (6.15) and (6.14). For comparison we also show in orange a histogram of scalar masses generated with (4.15).

consistent with our discussion above, as the first and third cases correspond to vacua with one or more fermion masses equal to $m_{3/2}$ (see relation (2.28)), and the second case to vacua with massless fermions. Therefore, making contact with our discussion in section 4.3, we can see that the branches of solutions corresponding to $\theta_W = \{\theta_0^W, \theta_1^W\}$ have a low probability to occur, since they are respectively the vacua where the masses μ_{-0} and μ_{-1} vanish.

By contrast, in the spectra for the truncated sector, figure 10, we see a suppression of vacua with masses $\mu_\lambda^2/m_{3/2}^2 = 1$ (i.e., with massless fermions), while the distribution function *diverges* in the limit $\mu_\lambda^2/m_{3/2}^2 \to 0$, that is, for the branch of solutions with $\theta_W = \theta_2^W$ discussed in section 4.3. In other words, for a large fraction of no-scale solutions, half of the scalar modes in the truncated sector have masses much lower than the gravitino. It is precisely these vacua which are in danger of developing tachyonic instabilities upon including quantum effects (α' corrections or instanton effects). In particular we observe that approximately 11% of the vacua contain modes with masses satisfying $\mu_{\lambda'}^2 \lesssim 10^{-2} m_{3/2}^2$, and about 3% with masses $\mu_{\lambda'}^2 \lesssim 10^{-3} m_{3/2}^2$. Moreover, a closer examination of the mass spectra in the ensemble reveals the presence of vacua with large mass hierarchies, with modes as light as $\mu_{\lambda'}^2 \sim 10^{-10} m_{3/2}^2$.

Note also that the suppressions seen in figure 10 around $\mu_{\lambda'}^2 \approx 0.5 m_{3/2}^2$ and $\mu_{\lambda'}^2 \approx 1.7 m_{3/2}^2$ are due to modes of the reduced theory becoming massless, i.e., the branches of vacua with $\theta_W = \{\theta_0^W, \theta_1^W\}$. Indeed, recall that due to the form of the spectrum (4.15) the mass distributions for all the modes arise from the same probability density function (6.11), and thus the suppression of any particular branch of vacua can also be observed in the statistics of all the other masses.

As a final remark, let us point out that equation (6.3) and (6.4) imply that the masses (4.15) and g_s are statistically independent from each other. As a consequence,

although the ensemble discussed here involves vacua with a marginally small string coupling $g_s \leq 1$, the statistical properties of the spectrum would not be affected by restricting the analysis to vacua with very small string coupling $g_s \ll 1$. As a consistency check, we also computed the numerical histograms represented in figures 9 and 10 for the subset of vacua in our ensemble with $g_s \leq 0.1$ (~ 5000 vacua), but no significant changes where observed, and thus, we will not present them here.

6.3 Statistical properties of the constrained ensemble

We will now turn to the statistics of the constrained ensemble of vacua, where $N_A^0 = 0$. As we show in appendix C the statistical methods in [15] can easily be adapted to describe this ensemble. In particular, the density of flux vacua with is found to be

$$d\mu_{\text{vac}}(z,\tau)\big|_{N_A^0=0} = \mathcal{N} \cdot \frac{(1+\xi)\xi^{2/3}}{(2-\xi)^2(\text{Im}\,\tau)^2}d^2z\, d^2\tau \,, \qquad (6.16)$$

where ξ should be understood here as a function of $\text{Re}\,z$. It is worth noting that, provided we consider only the weak coupling regime $\text{Im}\,\tau > 1$, the density of no-scale vacua is normalisable within the whole moduli space, even near the conifold point $\xi \to \xi_{\text{cnf}}$ where the EFT is known to become inaccurate. Indeed, contrary to the generic case, the density (6.16) is not enhanced (and remains finite) as we approach the conifold point, and as a result the distribution is well defined in the whole range of z (i.e., in $\xi \in [0, 1/2]$). Furthermore, as we show in appendix C, for this sub-ensemble, flux quantisation and a finite tadpole do not lead to the breakdown of the statistical description near the LCS point.[15] As a consequence, in contrast with the case of generic no-scale solutions, the continuous flux approximation provides an excellent characterisation of the ensemble in the strict LCS regime. As we shall see next, these features of the model will lead to an almost perfect agreement between the statistical description and the results of the numerical scan in the octic model.

As in the previous section, we begin by computing the probability distribution for the LCS parameter ξ, which takes the simple form

$$\rho(\xi)d\xi = \frac{2^{1/3}(1+\xi)}{(2-\xi)^2\xi^{2/3}}d\xi \,. \qquad (6.17)$$

This distribution, together with the histogram obtained from the numerical scan, is plotted in figure 11. As is evident, the analytic formula perfectly matches the histogram over the whole range of ξ. The histogram includes all of the no-scale solutions at points where the moduli space metric is well defined, $\xi \in [0, 1/2]$, however only those shaded in light and dark blue correspond to vacua with small instanton corrections. Excluding solutions with sizeable corrections (orange) leads to the fall-off (light blue) observed around $\xi \approx 0.2$. The statistical description does not incorporate the effects of truncating the ensemble, and therefore it can only provide a good description in the region of ξ where few vacua (or none)

---

[15]This observation relies on the fact that when $N_A^0 = 0$, the flux N_B^0 is not bounded by the flux tadpole. However, in practice the flux integers are extracted from a uniform distribution in $[-50, 50]$, which results in deviations from the continuous flux approximation in the range $\xi \lesssim \xi_{\text{min}} = 5 \cdot 10^{-5}$.
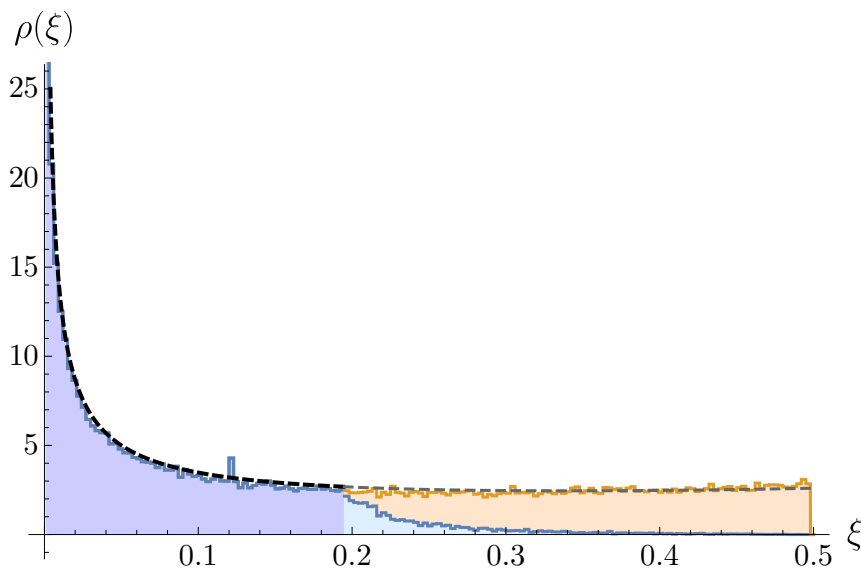
Figure 11. Distribution for the LCS parameter for the constrained flux ensemble. The dashed line represents the theoretical distribution 11 normalized for data in the range $5.10^{-5} \leq \xi \leq 0.185$ (see footnote 15). We also show the histogram of ξ at no-scale vacua, with colours the same as in figure 7.

are excluded from the ensemble. This region of ξ, which we shaded in dark blue, represents the set of vacua we will use next to characterise the statistics of the mass spectra, both numerically and using the continuous flux approximation.

As a curiosity, it is worth mentioning the small enhancement[16] on the number of vacua with $\xi \approx 0.12$. An examination of these solutions reveals that they all correspond to flux configurations satisfying the relation $N_A^1 = N_B^0$ and Im $z = 0$. Although we have not made further inquiries regarding the origin of the enhancement, it seems plausible that this particular choice of fluxes leads to a new symmetry in the EFT (exact or approximate), which is known to produce accumulations of no-scale solutions at special points of the moduli space [8].

In complete analogy with the previous section, the density function (6.17) can be used to derive the distributions for the rescaled fermion masses $m_\lambda/m_{3/2}$. Performing a change of variables from ξ to each of the normalised masses, and using (6.10) with $\tan \theta_W = \sqrt{(1 - 2\xi)/3}$ (see section 4.4), we obtain

$$\rho_\lambda^f(x_\lambda) dx_\lambda = \frac{2^{1/3}(1 + \xi)}{(2 - \xi)^2 \xi^{2/3} \left(dx_\lambda(\xi)/d\xi\right)}\Big|_{\xi(x_\lambda)} dx_\lambda \,, \tag{6.18}$$

where we use the shorthand $x_\lambda = m_\lambda/m_{3/2}$ which was introduced above. The distributions for the squared scalar masses can then be found using (6.15), which are displayed along with the histograms derived from the numerical scan in figures 12 and 13. As in the case of the generic ensemble, the mass histograms of the scalar modes in the reduced theory, $\mu_{\pm 0}^2$ and $\mu_{\pm 1}^2$, have been obtained first by computing the eigenvalues of the fermion mass

---

[16]This spike in the histogram of ξ induces similar enhancements in the mass distributions displayed in figures 12 and 13, as they all depend on the former.
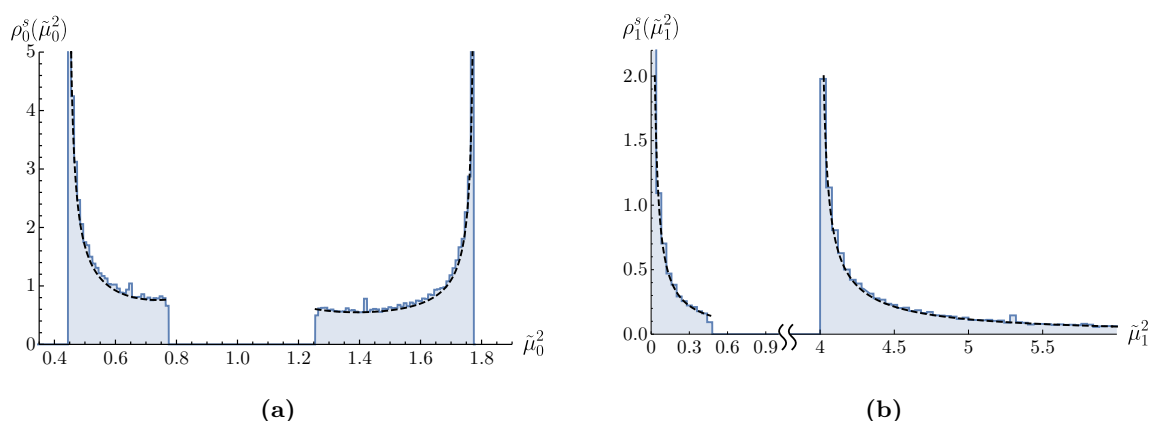
Figure 12. Distribution for the squared scalar masses with constrained fluxes $N_A^0 = 0$ normalised by the gravitino mass $\tilde{\mu}_\lambda^2 = \mu_\lambda^2 / m_{3/2}^2$, with $\lambda = 0, 1$ in (a) and (b), respectively. The dashed lines correspond to the theoretical mass distributions of fields in the reduced theory, (6.15) evaluated with (6.18). We compare with the histograms obtained numerically from the flux ensemble of the $\mathbb{WP}_{[1,1,1,1,4]}^4$ model.

matrix (2.29), and then via (2.28). The histogram for the masses in the truncated modes $\mu_{\pm\lambda'}^2$ were found using (4.23) instead. Here again we can observe the excellent agreement between the analytical predictions and the direct numerical computation of the masses in the octic. It is important to mention that, as in the case of the generic ensemble described above, it can be checked that the string coupling g_s is statistically independent from the masses in (4.23). Thus, while the numerical histograms presented here correspond to an ensemble of marginally weakly coupled vacua $g_s \leq 1$, our conclusions remain valid also for very weakly coupled vacua with[17] $g_s \ll 1$.

The most important feature of these distributions is the divergence of the probability density for the masses $\mu_{\pm 1}^2 \ll m_{3/2}^2$ (see figure 12 (b)). This implies that in this ensemble the branch of solutions with $\theta_W = \theta_1^W$, defined in (4.17), occurs with relatively high frequency. This contrasts with the results obtained for the generic ensemble, where the same branch was shown to have a suppressed probability to appear.

Finally, for completeness we have also studied the dependence of the mass spectrum on the distance of vacua from the LCS point. For this purpose, we obtained the mass histograms for subsets of no-scale solutions restricted to be in neighbourhoods of the LCS point of varying sizes. The results are displayed in figure 14, where we have plotted the histograms for four sets of vacua with $\xi \leq \xi_{\max}$, where $\xi_{\max} = \{0.15, 0.1, 0.05, 0.01\}$. As it can be seen in the plots, the closer the solutions are to the LCS point, the more deterministic the mass distributions become. Note also that in the case $\xi \leq 0.01$ the spectrum is already very peaked at the values given in (4.24), which correspond to the strict limit $\xi \to 0$. Interestingly, in this regime the spectrum always contains a (nearly) massless field, $\mu_{-1}^2 \approx 0$, which belongs to the reduced moduli space (i.e., $\theta_W \approx \theta_1^W$).

---

[17]We checked explicitly that this is indeed the case by computing the numerical mass histograms for the subset of solutions in the constrained ensemble with $g_s \leq 0.1$ (~ 2500 vacua).
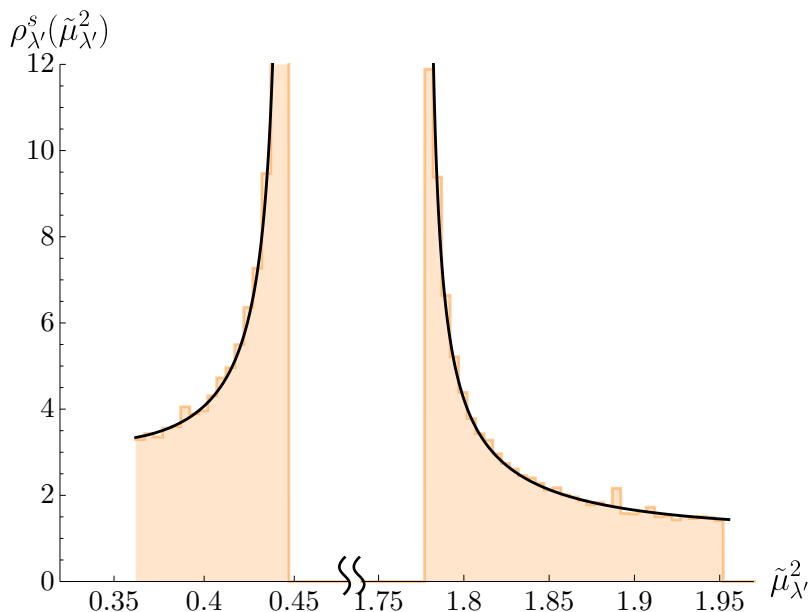
Figure 13. Theoretical prediction (solid line) for the probability distribution of the normalised squared masses of the truncated scalar fields $\tilde{\mu}_{\lambda'}^2 = \mu_{\lambda'}^2 / m_{3/2}^2$, eqs. (6.15) and (6.18), in the constrained ensemble. For comparison we display the histogram of values obtained by applying (4.15) to the vacua ensemble.

6.4 Comparison with Random Matrix Theory

Before we conclude this section let us comment on one further simplification, proposed in [16] to study the statistical properties of the flux ensemble. The statistical method we used above to analytically compute the probability distributions of the masses relies solely on the continuous flux approximation, but at the theory level it still requires the knowledge of the couplings of the (reduced) EFT. In other words, the prepotential (2.10) needs to be computed. As we mentioned in the introduction, in typical Calabi-Yau compactifications the number of moduli fields in the complex structure sector can be of the order of hundreds, and in the absence of symmetries to simplify the analysis as done here, the computation of the prepotential can be prohibitively difficult.

To address this problem, in [16] Denef and Douglas argued that for *sufficiently complex compactifications* with a *large number of moduli fields*, the mass spectrum of perturbations could be well described in the framework of the 4d EFT using methods of Random Matrix Theory (RMT). Since the universality theorems of RMT ensure that the statistical properties of the mass spectrum are independent of the distributions of couplings in the EFT, such a characterisation would avoid the challenges posed by a detailed computation. These ideas where developed in [74, 75], and RMT models designed specifically to describe no-scale vacua of type-IIB compactifications were presented in [51, 56].

Let us consider for definiteness the normalised fermion mass matrix $\mathcal{M}/m_{3/2}$. The main prediction of RMT is the expectation value of the eigenvalue spectrum, which can be given in terms of the collection of $n = h^{2,1} + 1$ rescaled fermion masses, $x_\lambda \equiv m_\lambda / m_{3/2}$,
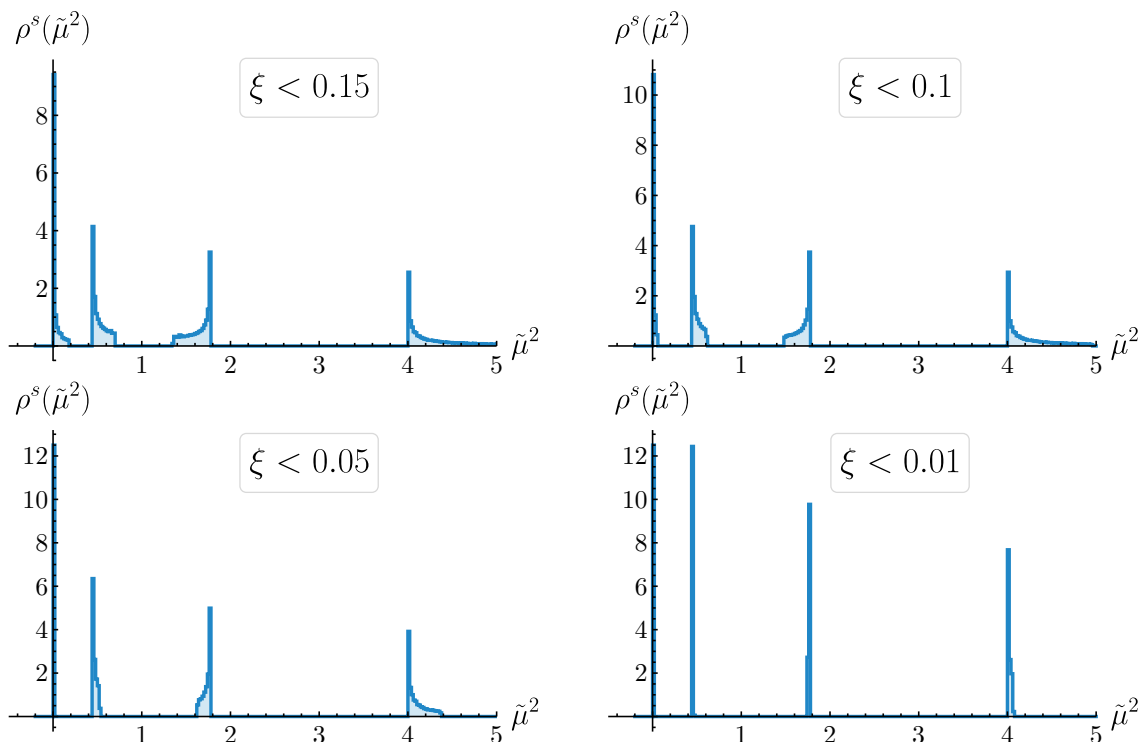
Figure 14. Histograms for the normalized squared masses $\tilde{\mu}^2_{\lambda=0,1} = \mu^2_{\lambda=0,1}/m^2_{3/2}$ of the scalars in the reduced theory. The plots represent vacua in the constrained ensemble, with varying upper bounds on the LCS parameter ξ. Note that as the upper bound on ξ decreases the distributions become increasingly deterministic, peaking at the limiting $\xi \to 0$ values given in (4.24). The plots also show the presence of a light mode $\mu_{-1} \ll m_{3/2}$ in all vacua, whose mass becomes zero $\mu_{-1} \to 0$ in the limit $\xi \to 0$.

sorted as $x_0 \leq x_2 \leq \ldots \leq x_{n-2} \leq x_{n-1}$. More specifically, the spectrum of random matrices is usually characterised by the empirical eigenvalue density function $\rho(x)$, or its alternative (non-standard) definition $\sigma(x)$, which are defined as

$$\rho(x) \equiv \frac{1}{n}\Big\langle \sum_{\lambda=0}^{n-1} \delta(x - x_\lambda) \Big\rangle, \qquad \sigma(x) \equiv \frac{1}{n} \sum_{\lambda=0}^{n-1} \delta(x - \langle x_\lambda \rangle), \qquad (6.19)$$

with the average taken over a finite sample of vacua randomly drawn from the ensemble. The alternative definition will be useful below.

The $\rho(x)$ and $\sigma(x)$, which are randomly distributed in the ensemble of flux vacua, become increasingly deterministic as the number of fields grows (as $n \to \infty$). The RMT models [51, 56, 75] describing the axio-dilaton/complex structure sector of type-IIB compactifications predict the fermion mass spectrum at no-scale vacua to be

$$\lim_{n\to\infty} \rho(x) = \lim_{n\to\infty} \sigma(x) = \frac{4}{\pi x_h^2}\sqrt{x_h^2 - x^2}, \qquad x \leq x_h, \qquad (6.20)$$

where x_h is a free (model dependent) parameter which determines the typical ratio of the fermion masses to the gravitino mass.[18]

_____
[18]The parameter x_h is closely related to $\tan\theta_W$, or equivalently to the typical value of W_0 [51, 56].
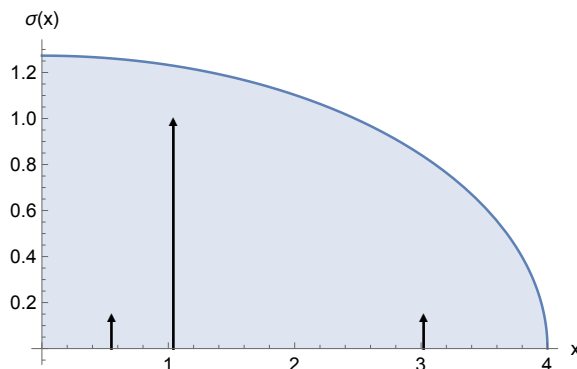
Figure 15. Eigenvalue density function $\sigma(x)$ for the rescaled fermion mass matrix $\mathcal{M}/m_{3/2}$, with $x = m/m_{3/2}$. The blue shaded area represents the density function $\sigma(x)$ predicted by Random Matrix Theory (6.20) ($x_h = 4$). The arrows represent the averaged spectral density obtained numerically for the octic model, which is composed of three Dirac-delta contributions at $\langle x_\lambda \rangle \approx \{0.55, 1.04, 3.02\}$ with weights $\{\frac{1}{150}(\times 20), \frac{148}{150}, \frac{1}{150}(\times 20)\}$.

In figure 15 we have displayed the RMT prediction together with result of evaluating $\sigma(x)$ on the numerical ensemble of generic no-scale vacua constructed above for the octic model. The plot clearly shows that RMT is not an appropriate choice to represent the fermion mass spectrum in the model at hand. In particular, while RMT predicts a spectrum continuously distributed on its support $x \in [0, x_h]$, the expectation value of density function (6.19) on the octic flux ensemble consists of three Dirac deltas centered at $\langle x_\lambda \rangle \approx \{0.55, 1.04, 3.02\}$ with weights given by $\{\frac{1}{150}, \frac{148}{150}, \frac{1}{150}\}$ respectively. The values $\langle x_\lambda \rangle$ are just the averages of the three distinct masses of the spectrum (6.10). Similar discrepancies were previously reported in [67, 68].

This negative result is in stark contrast with the successful characterisation provided by the continuous flux approximation observed in the previous section. The reason underlying the failure of RMT is that the first assumption on which it is based is not applicable here: the large degree of symmetry of the model yields a great simplification of the EFT, which is at odds with the requirement of complexity.[19] The very same property that allowed us to perform a fully analytical characterisation of the octic model prevents RMT from accurately describing the eigenvalue density.

In view of this result, it would be therefore interesting to analyse the statistics of more complicated models, and check if the RMT tools become more useful there. By contrast, the present work has already shown that the continuous flux approximation works remarkably well, even in simple models with only a moderately large number of active fluxes (only 8 flux integers in the octic).

7 More general compactifications

The main focus of this paper is the study of compactifications invariant under a group of symmetries which effectively reduce the complex structure moduli sector to a one-parameter

---

[19]Note, e.g., that in our numerical example all the truncated 148 fermions have the exact same mass.

space. In the present section we will discuss the possibility of finding the universal spectrum (4.15) derived above in more general models. This could include cases where the reduced theory involves more than one complex structure field, or where there are no symmetries to reduce the number of moduli.

The fundamental property that has allowed us to derive the spectrum (4.15) for the compactifications discussed above is the possibility of truncating all complex structure fields except one. As a direct consequence of this, the vector of derivatives of the superpotential Z_{0a} points along the no-scale direction e_1^a. This fact, together with some generic properties of type-IIB compactifications at large complex structure, led us to the full mass spectrum. Thus, in order to generalise this result to more general compactifications we just have to find out under which circumstances it is possible to find vacua where Z_{0a} aligns with the no-scale direction.

We will now show that, provided we neglect the quantisation of fluxes, it is possible to find no-scale vacua with the spectrum (4.15) in the LCS regime of any compactification of type-IIB superstrings. More specifically, *at any point of the moduli space* $\{\tau_0, z_0^i\}$ parametrised by the axio-dilaton and the $h^{2,1}$ complex structure moduli, it is possible to find a two complex dimensional family of fluxes $\{N_A^I, N_I^B\}$ such that the point $\{\tau_0, z_0^i\}$ is a no-scale vacuum, where the corresponding set of $2(h^{2,1}+1)$ tree-level masses is given by (4.15).

To see this we can begin with the Hodge decomposition of the flux vector N (see appendix A), which allows us to express this vector as a linear combination of the period vector and its Kähler covariant derivatives. This decomposition holds at any generic point of the moduli space $\{\tau, z^i\}$, excluding certain singular field configurations known as D-limits [118]. In particular, at no-scale vacua where $D_0 W = D_a W = 0$ the decomposition has the simpler form given in (4.19). Conversely, at any given point of the moduli space $\{\tau_0, z_0^a\}$, any flux configuration which can be expressed as a linear combination

$$N = \bar{a}^0 \bar{\Pi} + a^a \, D_a \Pi, \tag{7.1}$$

is guaranteed to satisfy the no-scale vacuum equations (2.20) at that point. In other words, given an arbitrary point in the moduli space, we can always choose a flux vector to make that point a no scale vacuum. The possible choices of flux in that case are in one-to-one correspondence with a set of $h^{2,1} + 1$ complex parameters $\{a^0, a^a\}$ which can be freely chosen. In particular, we can use this freedom to make the complex vector a^a point along the no scale direction e_1^a. Then, comparing (7.1) with equation (4.19) we see that the vector Z_{0a} will also point along e_1^a, which is precisely the condition that guarantees that total the tree-level spectrum is given by (4.15).

To find such a choice of flux explicitly we can use (4.7), which implies that the vector K^a points along the no-scale direction. Choosing the direction of a^a accordingly, and using the definitions of θ_W and $m_{3/2}$ we obtain the following parametrisation for fluxes consistent with the no-scale spectrum (4.15)

$$N = m_{3/2} \left(\mathrm{i} e^{\mathrm{i}\alpha_W} \bar{\Pi} - \frac{1}{\sqrt{3}} e^{-\mathrm{i}\alpha_K} \tan\theta_W \sqrt{(1 - 2\xi)} K^i D_i \Pi \right) \frac{\sqrt{\pi} \mathcal{V} \, e^{K_{cs}/2}}{g_s}, \tag{7.2}$$

where $\alpha_W = \arg(W)$ and $\alpha_K = \arg(D_0 D_1 W)$. Note that in this formula the Calabi-Yau volume $\mathcal{V}$, the string coupling g_s, the expectation value of the Kähler potential and the LCS parameter are all determined by the configuration of moduli fields. Nevertheless, we are still free to select the gravitino mass scale $m_{3/2}$, the angular parameter θ_W and the phases α_W and α_K. Thus, as anticipated above, for a given Calabi-Yau geometry the set of fluxes compatible with the spectrum (4.15) has complex dimension two.

It is important to emphasize that the vector N obtained by this method will not be in general compatible with the quantisation of fluxes. Our ability to tune the parameters $\{a^0, a^a\}$ in (7.1) will be limited by the maximum value of the flux $D3$-charge, which is set by the tadpole constraint. Indeed, since the fluxes can only be changed in integral steps, and the maximum value they can attain is of the order of $\sqrt{N_{\text{flux}}} \leq \sqrt{L}$, we expect that the maximum accuracy that may be achieved in aligning Z_{0a} to the no scale direction, i.e., making $Z_{0a'}$ small, is given by

$$|Z_{0a'}|/|Z_{01}| \sim \mathcal{O}(1/\sqrt{N_{\text{flux}}}) \gtrsim \mathcal{O}(1/\sqrt{L}) \sim \mathcal{O}(10^{-1} - 10^{-2}). \tag{7.3}$$

Therefore, in generic compactifications we will only be able to find no-scale vacua with quantised fluxes that satisfy (7.2) approximately. Still, with a large flux tadpole, and provided the moduli space is non-singular at the point of interest so that the Yukawa couplings $\mathring{\kappa}_{abc}$ have a finite value, it might be possible to find vacua where the corrections to the spectrum (4.15) are small, $\delta m_{\lambda'} \ll m_{\lambda'}^{(0)}$. To estimate the magnitude of these corrections we can consider the diagonalisation of the fermion mass matrix

$$(Z^\dagger Z)_{A\bar{B}} = (Z^\dagger Z)_{A\bar{B}}^{(0)} + \delta(Z^\dagger Z)_{A\bar{B}} + \dots \tag{7.4}$$

to first order in perturbation theory, where $(Z^\dagger Z)^{(0)}$ is the matrix obtained setting $Z_{0a}^{(0)} = \delta_a^1 Z_{01}$, and we regard the remaining components $Z_{0a'}$ as small deformation. The perturbed eigenvalues are then given by $\delta m_\lambda^2 = \delta(Z^\dagger Z)_{\lambda\bar{\lambda}}$. A straightforward computation shows that the first-order corrections to the rescaled fermion masses $\tilde{m}_\lambda = m_\lambda/m_{\text{susy}}$ are

$$\delta\tilde{m}_0 = \delta\tilde{m}_1 = 0, \qquad \delta\tilde{m}_{\lambda'} = -\mathring{\kappa}_{\lambda'\lambda'a'} \, \text{Re}\left(\frac{\delta Z_{0a'}}{Z_{01}}\right), \tag{7.5}$$

where we made use of (4.5), and for simplicity we define $m_{\text{susy}} = |Z_{01}|$. Without further computations we can already see that generically, these corrections will lift the degeneracy of the fermion masses in the truncated sector.

To understand under which circumstances these deformations can be regarded as small corrections, it is fundamental to have some estimate of the size of the Yukawa couplings. We will further investigate these issues in future publications.

8 Conclusions

No-scale vacua of type-IIB flux compactifications are an essential stepping stone in the construction of dS vacua and inflationary models in KKLT and Large Volume Scenarios. Guaranteeing the validity of these constructions requires a good understanding of the

perturbative spectrum of the no-scale solutions. Indeed, while the no-scale property ensures the absence of tachyons in the axio-dilaton/complex structure sector at tree-level, this does not prevent the existence of arbitrarily light fields, which may turn tachyonic upon including quantum corrections, uplifting terms, or the effect of matter fields [56, 125]. These light modes might also lead to difficulties when implementing viable inflationary models in these scenarios, as the backreaction effects caused by the inflaton might also result in their destabilisation.

In generic situations, the absence of such light fields can be argued using scaling arguments in the KKLT and LVS settings, as done in [95–97] and [2, 3], respectively. However, the most interesting vacua for phenomenological applications are often those in the neighbourhood of special (and thus non-generic) points of the moduli space, such as the conifold or the LCS points, where the presence of light fields may become unavoidable [98, 99]. Moreover, as argued in [56], in the specific case of LVS vacua with an only moderately large compactification volume [52–55], typical vacua might still contain a sizeable fraction of light modes susceptible to becoming tachyonic.

Despite its importance, a complete analytic understanding of the perturbative spectrum at no-scale vacua has remained elusive, primarily due the complexity of the corresponding EFTs and the large number of fields involved. In the present paper we have considered a particular class of Calabi-Yau compactifications with an arbitrary number of moduli fields, and computed *analytically* the complete mass spectrum of the axio-dilaton/complex-structure sector at no-scale vacua in the LCS regime (see (4.15)). The Calabi-Yau geometries we considered here are invariant under large discrete isometry groups, which allows for a consistent reduction of the complex structure sector to a single field. An important feature of this class of models is that the Calabi-Yau symmetries make the computation of an EFT for the unique complex structure modulus surviving the truncation feasible [40, 41, 57, 66]. Then, using only symmetry arguments, together with certain universal properties satisfied by the EFT couplings at LCS, we derived the mass spectrum of the full axio-dilaton/complex structure sector, including the truncated fields. Remarkably, the full spectrum can be expressed solely in terms of the couplings of the reduced EFT theory, which can be determined. This result applies to plenty of interesting compactifications such as: the family of quintic hypersurfaces in $\mathbb{WP}_{[1,1,1,1,1]}$ [41] admitting the discrete symmetry groups discussed in [58]; the close relatives to the quintic (i.e., the sextic, octic and dectic) with analogous symmetric configurations [57, 66] and quotients thereof [57, 59]; or the Complete Intersection Calabi-Yau described in [60] and its quotients (see table 1). Moreover, we can also use these results to describe the LCS regime of the hundreds of one-parameter models listed in [61]. We should remark that these discrete global symmetries are nevertheless expected to be broken upon including all sub-leading α' and quantum effects [126–128], what will induce small corrections in the spectrum (4.15), lifting, in particular, the large degeneracy of the truncated sector.

A crucial step in the derivation of the spectrum is the computation of the Yukawa couplings which determine the fermion masses at LCS. While the universal behaviour of the canonically normalised Yukawa couplings in the strict LCS limit has been well known for a long time [91], here we have extended those results to the complete LCS regime.

That is, we have computed the relevant subset of these couplings in the whole region of moduli space where the instanton corrections to the complex structure Kähler potential and flux superpotential can be safely neglected.[20] As in the strict LCS limit, we found that the Yukawa couplings exhibit a universal behaviour, independent of the details of the compactification or the number of complex structure fields (see (4.5)). It is important to emphasize that this result applies to any Calabi-Yau compactification, and does not require the invariance of the manifold under a large discrete isometry group.

In the class of models that we consider here, the strict LCS/weak-coupling limit is of particular interest, as it is the region of moduli space where one has the best perturbative control of the EFT. In [67, 68], the authors considered compactifications of type-IIB and F-theory at the strict LCS limit where the superpotential was dominated by its cubic or quartic terms, and proved the absence of vacua (AdS, dS or Minkowski) in this region of moduli space. More specifically, the no-scale potential was shown to satisfy the relation $|\nabla V| = (\sqrt{7}/2)\, V > 0$, consistent with the de Sitter conjecture in [36], which forbids the existence of de Sitter vacua when approaching an infinite distance limit in moduli space (see [35] for the necessary second-derivative conditions).

These conclusions can nevertheless be avoided by setting to zero the flux associated with the period which grows without bound in this limit ($N_A^0 \equiv f_A^0 - \tau h_A^0 = 0$ in (2.18)). Indeed, in this case the higher order terms in the flux superpotential are identically zero, and thus the above no-go theorem does not apply. In section 4.4 we computed the mass spectrum at this class of no-scale vacua for the models described above, and proved it to have the universal form in the strict LCS limit. Namely, the spectrum of squared masses in the axio-dilaton/complex structure sector is given by

$$\text{Spectrum at the \textit{strict LCS limit}:} \qquad \mu_\lambda^2 = \left\{ 0,\, \frac{4}{9}m_{3/2}^2,\, \frac{16}{9}m_{3/2}^2,\, 4m_{3/2}^2 \right\}, \qquad (8.1)$$

with the first and last masses appearing with multiplicity 1, and each of the other two with multiplicity $h^{2,1} + 1$. In particular it can be observed that the spectrum always contains exactly one massless field, while the rest of the moduli have masses of the order of the gravitino mass $m_{3/2}$. It is also worth mentioning that closely related classes of vacua surviving in the strict LCS limit were also discussed in [71, 72], and in particular those of [99] also present a massless field in the no-scale spectrum, which is nevertheless lifted by instanton corrections.

The previous results are consistent with [73, 129], where it was argued that obtaining vacua parametrically close to the LCS point requires turning on *unbounded fluxes*, that is, fluxes not contributing to the total $D3$-charge and therefore unconstrained by the tadpole condition. Furthermore, as discussed in [73], the contribution to the flux potential due to the unbounded fluxes must also be asymptotically vanishing in the strict LCS limit. Interestingly, the class of no-scale solutions (and thus Minkowski vacua) described above satisfies both of these conditions, and is therefore consistent with the no-go theorems derived in [73] (see section 4.4). On the one hand, setting to zero the flux $N_A^0 \equiv f_A^0 -$

---

[20]This regime is sometimes referred to as the *nilpotent orbit* approximation, and the strict-LCS as the *sl*(2)-*orbit* approximation [73].

– 43 –

τh_A^0 on the diverging period implies that the flux on the dual B-cycle, i.e., $N_0^B \equiv f_0^B - \tau h_0^B$, does not contribute to the tadpole. On the other hand, as the term in the flux superpotential associated to N_0^B is just a constant, it also follows that its contribution to the no-scale potential is asymptotically vanishing at the LCS point. Note that the analyses in [73, 129] only refer to the strict LCS limit, while the results presented here also allow one to characterise the properties of the no-scale potential away from the LCS point, i.e., over a region of moduli space not captured in those works.

For generic flux vacua, not necessarily close to the LCS point, the mass spectrum will not have the deterministic form of (8.1), and thus will in general be dependent on the choice of fluxes. Therefore, in order to obtain a characterisation of the spectrum independent of the choice of flux we have studied the statistical properties of the moduli masses in the ensemble of flux vacua. More specifically, using the continuous flux approximation, we computed analytically the probability distributions for the density of vacua and the masses, both for the generic ensemble of vacua and for the constrained ensemble with vanishing flux N_A^0. Moreover, we verified the validity of the obtained distributions by comparing them with the result of a numerical scan on the octic model $\mathbb{WP}^4_{[1,1,1,1,4]}$. As can be seen in figures 7–13, the analytical and empirical distributions show an excellent agreement in the expected regime of applicability of the continuous flux approximation.

Regarding the density of vacua, for the generic ensemble the result of the numerical scan in the octic model shows a suppression on the density of vacua close to the LCS point with respect to the statistical predictions (see figure 8). This discrepancy with the theoretical distributions was nevertheless already anticipated in [67, 68] (see also [15]), due to a breakdown of the continuous flux approximation. In the generic ensemble, vacua with $N_A^0 = 0$ represent only 0.08% of total vacua and, as we mentioned above, the results of [67, 68] show that only vacua with vanishing flux N_A^0 may be found parametrically close to the LCS point. By contrast, as can be seen in figure 11, the constrained ensemble exhibits no suppression near the LCS point, indicating that this subclass of solutions will dominate in this region of the moduli space.

Away from the LCS point, the computed probability distributions based on the continuous flux approximation describe very accurately the result of the numerical scan. Therefore, we can use these results to have a precise analytic understanding of the features displayed by the mass spectra observed in the flux ensemble. In the case of the generic ensemble, when considering only the reduced theory, we observe that vacua with modes much lighter than the gravitino appear with very low frequency (figure 9), $\mathrm{Prob}(\mu_{\mathrm{red}}^2 < 0.01 \, m_{3/2}^2) \approx 2\%$. This result is actually a well-known consequence of the generalized Kac-Rice formula, which characterises the density of critical points in random fields (see [117, 122]). However, when considering the truncated sector, the situation changes: the mass distribution of the truncated fields diverges in the limit $\mu^2 \ll m_{3/2}^2$ (see figure 10), indicating that a sizeable fraction of vacua contain light fields in this sector, $\mathrm{Prob}(\mu_{\mathrm{trunc}}^2 < 0.01 \, m_{3/2}^2) \approx 11\%$, with masses as low as $\mu_{\mathrm{trunc}}^2 \sim 10^{-10} \, m_{3/2}^2$. The reason for this is that, in the models we consider, only the critical points of the reduced scalar potential can be described as extrema of random fields, and thus appropriately characterised by the Kac-Rice formula. By contrast, the expectation values of the fields in the truncated sector are fully determined by the

action of the Calabi-Yau symmetry group, and thus the Kac-Rice formula cannot be used to obtain the distribution of extrema for these moduli, or their mass spectra.

Concerning the statistics of vacua in the constrained ensemble, our results show that the mass spectra change significantly due to the condition imposed on the fluxes. In particular, contrary to the generic ensemble, in this class of vacua the lightest field is always in the reduced moduli space (see figure 12). In order to understand the dependence of the spectra on the distance to the LCS point, we considered subsets of vacua constrained to be in neighbourhoods of this point with varying sizes. This analysis showed that the smaller the neighbourhood around the LCS point, the more deterministic the mass spectrum becomes, recovering the limiting form (8.1) in the strict LCS limit. In other words, for the dominant class of vacua near the LCS point, the spectrum was always observed to contain a very light (and asymptotically massless) field in the reduced moduli space (see figure 14).

Finally, let us comment on the applicability of our results. As we mentioned above, our results can be used to describe no-scale vacua in compactifications invariant under a large discrete isometry group. Therefore, it would be desirable to understand if the class of vacua with an analytic spectrum discussed here can be embedded in more general compactifications. As we discussed in section 7, as long as we neglect the quantisation of the fluxes, in *any Calabi-Yau compactification*, and *for every point of the moduli space at the LCS regime*, it is possible to find an 4-real-dimensional family of ISD fluxes (i.e., satisfying the no-scale condition), such that the mass spectrum in the axio-dilaton/complex structure sector is given by (4.15). This already suggests that these vacua might be encountered in compactifications where the $D3$-charge tadpole is large, as in type-IIB compactifications arising as the orientifold limit of F-theory compactified on a fourfold. Embedding this class of vacua in generic compactifications, while retaining the flux quantisation condition, is an interesting problem that we will address in future work. To conclude we will briefly comment on the possible extension of our results to other regimes away from the LCS limit. In general, such an analysis would require a specific treatment which is beyond the reach of the present analysis, as our derivations depend crucially on the universal properties satisfied by the couplings of the EFT at LCS. However, in the specific case of conifold limits of the moduli space, it might be possible to make some progress following an analogous procedure to the one described in [130, 131] (see also [132]). In those works, it was explicitly demonstrated that one can stabilise a subset of the complex structure moduli near a conifold point, while fixing the rest near the LCS point, i.e., at a *conifold-LCS regime*. As shown in [130, 131], provided the moduli at LCS are sufficiently massive, the stabilisation of this sector can be treated independently, ignoring consistently the presence of moduli near the conifold limit to leading order. Therefore, another interesting future direction would be to study the application of our results to characterise the spectrum of those complex structure at LCS for compactifications in a conifold-LCS regime, such as those described in [130, 131].

Acknowledgments

A Hodge decomposition of the flux vector

In this appendix we review the Hodge decomposition of the flux vector N [16]. This decomposition was used in sections 4.4 and 7 of the main text, and is also the starting point for the derivations of the probability distributions of the type-IIB flux ensemble.

The flux vector N has complex dimension $2h^{2,1} + 2$ and transforms non-trivially under the symplectic group $\mathrm{Sp}(2h^{2,1} + 2, \mathbb{Z})$, i.e., it is a *symplectic section*. As we reviewed in section 2, the set of $2h^{2,1} + 2$ vectors $\mathcal{B} = \{\Pi, \bar{\Pi}, D_a\Pi, D_{\bar{a}}\bar{\Pi}\}$ evaluated at any given point $\{\tau, z^a\}$ is also composed of symplectic sections, which can be shown to be linearly independent. In other words, the set $\mathcal{B}$ forms a basis in the space of sections. To prove the linear independence of the elements of $\mathcal{B}$ we introduce the symplectic product $\langle A, B \rangle$ of two sections A and B,

$$\langle A, B \rangle = A^T \cdot \Sigma \cdot B, \tag{A.1}$$

where Σ is the symplectic invariant matrix (2.5). Then, it can be checked from the definition of Π that the elements of $\mathcal{B}$ satisfy the orthogonality relations

$$\begin{aligned}
\langle \Pi, \bar{\Pi} \rangle &= \mathrm{i}e^{-K_{cs}}, \\
\langle \bar{\Pi}, \bar{\Pi} \rangle &= 0, \\
\langle \Pi, D_a\Pi \rangle &= 0, \\
\langle \Pi, D_{\bar{a}}\bar{\Pi} \rangle &= 0, \\
\langle D_a\Pi, D_b\Pi \rangle &= 0, \\
\langle D_a\Pi, D_{\bar{b}}\bar{\Pi} \rangle &= -\mathrm{i}e^{-K_{cs}}\delta_{a\bar{b}},
\end{aligned} \tag{A.2}$$

from which the linear independence of the set $\mathcal{B}$ follows. In this setting the Hodge decomposition of the flux vector can be obtained as the decomposition in the basis of sections $\mathcal{B}$,

$$N = \sqrt{4\pi}\left(a_0\Pi + \bar{b}_0\bar{\Pi} + a^a D_a\Pi + \bar{b}^a D_{\bar{a}}\bar{\Pi}\right). \tag{A.3}$$

Using these orthogonality relations it is straightforward to find that the coefficients $\{a_0, a^a, b_0, b^a\}$ are determined by the values of the superpotential and its derivatives at the point $\{\tau, z^a\}$

$$a^0 = -e^{K_{cs}}D_{\bar{0}}\bar{W}, \quad \bar{b}^0 = \mathrm{i}e^{K_{cs}}W, \quad a^a = e^{K_{cs}}D_{\bar{0}}D_{\bar{a}}\bar{W}, \quad \bar{b}^a = -\mathrm{i}e^{K_{cs}}D_aW. \tag{A.4}$$

Therefore, the basis elements Π, $D_a\overline{\Pi}$, $D_{\bar{a}}\Pi$ and $\overline{\Pi}$ correspond to the $(3,0)$, $(1,2)$, $(2,1)$ and $(0,3)$ components of the flux $G_3 = F_3 - \tau H_3$, respectively. In particular, at no-scale vacua (2.20), which is the moduli space locus where the parts $(3,0)$ and $(1,2)$ of G_3 vanish (i.e., G_3 is "imaginary self-dual"), the Hodge decomposition reduces to

$$N = \sqrt{4\pi}\mathrm{e}^{K_{cs}}(\mathrm{i}W\,\bar{\Pi} + D_{\bar{0}}D_{\bar{a}}\bar{W}\,D_a\Pi). \tag{A.5}$$

Substituting this expression into (2.21) we can obtain an expression for the $D3$-charge induced by imaginary self-dual fluxes:

$$\begin{aligned}
N_{\text{flux}} &= -\mathrm{i}4\pi\mathrm{e}^{2K_{cs}+K_d}\left(|W|^2\left\langle\Pi,\bar{\Pi}\right\rangle + |D_0D_1W|^2\left\langle D_{\bar{1}}\bar{\Pi}, D_1\Pi\right\rangle\right.\\
&\qquad\qquad\qquad\left. +2\,\mathrm{Im}\left[\bar{W}D_{\bar{0}}D_{\bar{1}}\bar{W}\left\langle\Pi, D_1\Pi\right\rangle\right]\right)\\
&= 4\pi\mathrm{e}^{K_{cs}+K_d}\left(|W|^2 + |D_0D_1W|^2\right),
\end{aligned} \tag{A.6}$$

where, in the last step, we have applied the identities (A.2). Finally, using the definitions of the gravitino mass and m_{susy}, we find N_{flux} to be positive semidefinite, and given by

$$0 \leq N_{\text{flux}} = 4\pi\mathcal{V}^2\left(m_{3/2}^2 + m_{\text{susy}}^2\right) \leq L. \tag{A.7}$$

B   Numerical method: Paramotopy

In this appendix we describe in detail the numerical method used in this work to obtain the ensemble of no-scale solutions for the $\mathbb{WP}^4_{[1,1,1,1,4]}$ model, also known as the octic. As discussed in section 5, this model features a single complex structure modulus and an axio-dilaton, which we seek to stabilize at no-scale configurations (2.20).

It can easily be checked, using the machinery described in section 2, that the no-scale conditions can be expressed as a system of non-linear polynomial equations near the LCS point, where the instanton contributions to the prepotential (5.2) (or, more generally, (2.10)) can be neglected [113]. In the following we will denote this polynomial form of the no-scale conditions (2.20) by

$$P_i(z, \bar{z}, \tau, \bar{\tau}; f, h) = 0, \quad i = \{1, 2\}, \tag{B.1}$$

where f and h are the *quantized* flux vectors defined in (2.16), and which are subject to the *tadpole condition* (2.22). The main numerical difficulty of this problem lies in solving the polynomial system of equations (B.1) for the huge number of allowed choices of f and h.

B.1   Polynomial homotopy continuation and Paramotopy

In recent years, one of the most outstanding algorithms to solve systems of the form of (B.1) has been that of *polynomial homotopy continuation* (PHC), coined within the field of numerical algebraic geometry [111, 112]. Schematically, this method works as follows:

1. Given the set of polynomial equations to be solved, $P(x) = 0$, the first step is to construct an auxiliary system of equations, $Q(x) = 0$, which is easily solvable and that has the same maximal number of solutions. We then define

$$H(x,t) = \gamma(1-t)Q(x) + tP(x), \tag{B.2}$$

which is known as the *homotopy* function, where $t \in [0,1]$ and γ is a random complex number.[21]

Note that the roots of $H(x,0)$ correspond to those of $Q(x)$, while the roots of $H(x,1)$ are those of $P(x)$, the ones we are interested in.

2. Once the roots of $Q(x) \propto H(x,0)$ are determined, it can be shown that, as t increases, the roots of $H(x,t)$ will be continuously deformed from their original values [112]. Thus, we can easily track the path each solution takes as we vary t up to $t = 1$, where the solutions correspond to the solutions to our problem.

Many different implementations of the PHC method can be found in the literature, such as `phcpy` [133], `StringVacua` [134], and `Bertini` [135]. In this work, we have used `Paramotopy`[22] [110], a highly efficient PHC-based algorithm specially suited for polynomial systems like (B.1) which depend on parameter tuples.

In short, `Paramotopy` works in two steps. Given a certain parametrically-dependent polynomial system $P(x;p)$, it first performs the above PHC algorithm for a random p_0. Once that has been solved, it performs the same algorithm for the homotopy

$$H(x,t;p_0,p) = \gamma(1-t)P(x;p_0) + tP(x;p) \tag{B.3}$$

where p corresponds to one of the parameter choices we are interested in. However, in this second run, the number of paths that have to be tracked is qualitatively smaller than in the first step, as only those paths that led to proper solutions of $P(x;p_0)$ have to be followed. In cases where the number of well-behaved paths is orders of magnitude lower than the maximum number of solutions, this second step proves to be crucial for an efficient solution [110].

B.2 Construction of the flux ensemble and search for no-scale solutions

In order to perform a consistent exploration of the moduli space vacua of the octic, we took random integer flux values from a uniform distribution, that the components of the flux vectors satisfy $f, h \in [-f_{\max}, f_{\max}]$. Only those flux tuples satisfying the tadpole condition

$$0 < h \cdot \Sigma \cdot f \leq L \tag{B.4}$$

were kept where, for our purposes, we took $L = 972$, and chose $f_{\max} = 50$ to be sufficiently large for the distribution of the $D3$-charge N_{flux} (2.21) to converge to a flat distribution.

---

[21]This parameter ensures no singularities will occur during the deformation of $Q(x)$ into $P(x)$. For more detail, see [112].

[22]Software available at www.paramotopy.com.

This way, we avoid artificially induced boundary effects associated to having set a finite value for $f_{\max}$.

For the case of generic flux vacua, we generated 10^7 flux tuples consistent with the tadpole condition. On the other hand, for the constrained case, we generated 10^6 consistent flux tuples[23] following the algorithm above, while manually keeping $f_A^0 = h_A^0 = 0$.

With these parameter choices in hand, we employed `Paramotopy` to solve the system of no-scale conditions given by (2.20). Note that (2.20) involves both τ, z and $\bar{\tau}, \bar{z}$. One possibility to deal with this would be to solve for the real and imaginary parts of each variable. However, here we solved for barred and unbarred variables separately, and then only kept those solutions which actually satisfied the conjugation relation between the variables. We found that this second choice was easier to solve by the software, and kept the equations simple. The whole process took around 5 hours in a 46-core machine for the constrained ensemble (10^6 tuples) and 50 hours for the generic ensemble (10^7 tuples).

From the resulting ensemble of no-scale solutions, we only considered (in section 6) those with moderately small instanton corrections. When performing this cut in our ensemble data, we made sure that the EFT we used to describe the octic model is indeed reliable. The sizes of these corrections were considered *a posteriori*, once the tree-level equations had been solved. More specifically, at each of the obtained solutions, we computed the Kähler potential and Kähler metric, both neglecting entirely the instanton contributions to the prepotential and considering the leading correction (5.3). First, we selected only those solutions for which the Kähler metric was still well defined after including the corrections, i.e., where it was non-degenerate and positive. Then, with these solutions, we computed the gravitino mass $m_{3/2}$, rescaled Yukawa coupling $\mathring{\kappa}$, and Kähler metric (with and without considering the leading instanton), and selected those vacua where the relative corrections were $< 20\%$. The resulting ensemble of solutions is represented in blue in the histograms of figures 7, 8 (generic ensemble), and 11 (constrained ensemble).

B.3 Redundancies of the EFT and solution duplicates

As discussed in sections 2 and 5, the low energy supergravity description of type-IIB string compactifications has two inherent redundancies: one associated with the modular $\mathrm{SL}(2,\mathbb{Z})$ transformations (2.24), and one associated with the symplectic transformations acting as in (2.6) and (2.23). Thus, no-scale solutions which can be related to each other by any combination of these transformations should be regarded as equivalent.

To avoid double-counting no-scale solutions related by the $\mathrm{SL}(2,\mathbb{Z})$ symmetry, we transported each solution to the fundamental domain of the modular group, given by the complex upper half-plane with $|\tau| > 1$ and $|\mathrm{Re}(\tau)| < 1/2$. This operation can be easily performed by successively applying the generators of the group, given by

$$
T_b = \begin{pmatrix} 1 & b \\ 0 & 1 \end{pmatrix} \quad , \quad R = \begin{pmatrix} 0 & -1 \\ 1 & 0 \end{pmatrix}.
$$

$$
\tau \to \tau + b \qquad \tau \to -1/\tau
$$

(B.5)

---

[23]Random fluxes are more prone to high corrections as opposed to those with $N_A^0 = 0$, mostly due to the difference in the number of solutions near the LCS point. Thus, to keep a considerable amount of solutions in the former case, we generated more flux tuples.

Note that while these transformations change the value of f and h, it can be shown that the quantity N_flux remains invariant, so the transported solutions will nevertheless satisfy the tadpole condition.

As for the symplectic transformations, at large complex structure the corresponding source of redundancy comes from the monodromy around the LCS point, which acts on the complex structure field z and the fluxes as [8, 57, 66, 119]

$$z \to z - i\, n \qquad \equiv \qquad \begin{cases} N \to A^n \cdot N \\ \Pi \to A^n \cdot \Pi \end{cases} , \tag{B.6}$$

where $n \in \mathbb{Z}$ and

$$A = \begin{pmatrix} 1 & 0 & 0 & 0 \\ 1 & 1 & 0 & 0 \\ 4 & -2 & 1 & -1 \\ -4 & -2 & 0 & 1 \end{pmatrix} \tag{B.7}$$

for the octic.[24] This symmetry allows us to define a fundamental domain on the z plane, which we chose to lie at $|\text{Im}(z)| \le 1/2$.

Both sets of transformations, (B.5) together with (B.6) and (B.7) can be used to transport τ and z to their respective fundamental domains. Vacua with the same flux and moduli values (up to 10^{-8}, corresponding to the error estimate of `Paramotopy`) are then removed to avoid double-counting solutions in the numerical scan.

C Density distribution of no-scale flux vacua

In this appendix we present a derivation of the theoretical probability distributions for the density of no-scale vacua (6.3) and (6.16), which describe the generic ensemble and the one constrained by the condition $N_A^0 = 0$, respectively

The proof below relies only on the continuous flux approximation, and closely follows the one presented in [15]. We begin by deriving the probability distribution for the variables (6.2) at no-scale vacua using the Hodge decomposition (A.3). We then combine the result with a generalised version of the Kac-Rice formula to derive the density of flux vacua. In each of these two steps, we will present the argument first for the generic ensemble, as obtained in [15], and then we will adapt the it to the case the constrained ensemble.

C.1 Derivation of the Denef-Douglas distribution

Following [15], our starting point is a flat distribution for the $4m = 4(h^{2,1} + 1)$ integer flux parameters

$$\left\{ f_A^I, h_A^I, f_I^B, h_I^B \right\}. \tag{C.1}$$

Note that this distribution also matches the numerical procedure we followed to obtain the ensemble in the $\mathbb{WP}^4_{[1,1,1,1,4]}$ model, where flux realisations are drawn from a flat distribution.

---

[24]See [57] for more detail on this and other one-parameter models.

In addition, we will also consider the situation when the tadpole constraint is large, $L \gg 1$. In this case the typical values of these flux parameters are also large, and can be regarded as a continuous random variables. The corresponding probability distribution is therefore

$$d\mu_{\text{flux}}(f, h) = \mathcal{N} (df \, dh)^{4m}. \qquad (C.2)$$

Begin by switching variables to the complex flux parameters $N = f - \tau h$ and their conjugates $\bar{N} = f - \bar{\tau} h$. The associated Jacobian is

$$J = \frac{\partial(N_A, \bar{N}_A, N^B, \bar{N}^B)}{\partial(f_A, h_A, f^B, h^B)} = \begin{pmatrix} \frac{\partial(N_A, \bar{N}_A)}{\partial(f_A, h_A)} & 0 \\ 0 & \frac{\partial(N^B, \bar{N}^B)}{\partial(f^B, h^B)} \end{pmatrix}, \qquad (C.3)$$

where

$$\frac{\partial(N_A, \bar{N}_A)}{\partial(f_A, h_A)} = \frac{\partial(N^B, \bar{N}^B)}{\partial(f^B, h^B)} = \begin{pmatrix} \mathbb{1} & \mathbb{1} \\ -\tau \mathbb{1} & -\bar{\tau} \mathbb{1} \end{pmatrix}. \qquad (C.4)$$

Then,

$$\det(J) = \det \begin{pmatrix} 1 & 1 \\ -\tau & \bar{\tau} \end{pmatrix}^{2m} = (-2\mathrm{i} \, \mathrm{Im} \, \tau)^{2m}, \qquad (C.5)$$

implying that the resulting probability distribution for $\{N, \bar{N}\}$ reads

$$d\mu_{\text{flux}}(N, \bar{N}) = \mathcal{N} (dN \, d\bar{N})^{4m} \mathrm{e}^{2mK_d}. \qquad (C.6)$$

Next, we consider the change of variables between $\{N, \bar{N}\}$ and $\{Z_0, F_a, F_0, Z_a, c.c.\}$, defined by[25]

$$\begin{aligned}
F_0 &\equiv \mathrm{e}^{K/2} D_0 W = -\mathrm{i} \mathrm{e}^{K/2} N^\dagger \cdot \Sigma \cdot \Pi, \\
F_a &\equiv \mathrm{e}^{K/2} D_a W = \mathrm{e}^{K/2} N^T \cdot \Sigma \cdot D_a \Pi, \\
Z_0 &\equiv \mathrm{e}^{K/2} W = \mathrm{e}^{K/2} N^T \cdot \Sigma \cdot \Pi, \\
Z_a &\equiv \mathrm{e}^{K/2} D_0 D_a W = -\mathrm{i} \mathrm{e}^{K/2} N^\dagger \cdot \Sigma \cdot D_a \Pi,
\end{aligned} \qquad (C.7)$$

where the components of the vectors have been expressed in a canonically normalised basis. Note that these definitions coincide with those in the main text, (6.2), up to a volume factor $\mathcal{V}$. Since the volume is independent of the complex structure moduli or the dilaton, the effect of the rescaling necessary to make contact with (6.2) amounts to a redefinition of the normalisation constant, and thus we will ignore the volume prefactor in the following. The Jacobian $J = \partial(Z_0, F_a, F_0, Z_a, c.c.)/\partial(N, \bar{N})$ of the transformation above reads

$$J = \mathrm{e}^{K/2} \begin{pmatrix} \Sigma \cdot \Pi & \Sigma \cdot D_a \Pi & 0 & 0 & 0 & 0 & \mathrm{i} \Sigma \cdot \bar{\Pi} & \mathrm{i} \Sigma \cdot D_{\bar{a}} \bar{\Pi} \\ 0 & 0 & -\mathrm{i} \Sigma \cdot \Pi & -\mathrm{i} \Sigma \cdot D_a \Pi & \Sigma \cdot \bar{\Pi} & \Sigma \cdot D_{\bar{a}} \bar{\Pi} & 0 & 0 \end{pmatrix}. \qquad (C.8)$$

Then,

$$\det(J) = \mathrm{e}^{2mK} |\det M|^2, \qquad (C.9)$$

---

[25]In the following derivations, in order to simplify the notation, we will ignore the overall $1/\sqrt{4\pi}$ factor in the definition of W (2.18), since it plays no role in the final result.

where

$$M \equiv \left(\Sigma \cdot \Pi, \ \Sigma \cdot D_a \Pi, \ i\Sigma \cdot \bar{\Pi}, \ i\Sigma \cdot D_{\bar{a}} \bar{\Pi} . \right) \tag{C.10}$$

To compute the determinant, we use the trick

$$|\det M|^2 = |M^\dagger M| = |M^\dagger \cdot \Sigma \cdot M|, \tag{C.11}$$

since $|\Sigma| = 1$. Then, using the orthogonality properties of the basis $\{\Pi, \bar{\Pi}, D_a \Pi, D_{\bar{a}} \bar{\Pi}\}$ for the space of symplectic sections under the product defined by Σ, we obtain [15]

$$M^\dagger \cdot \Sigma \cdot M = \begin{pmatrix} e^{-K_{cs}} & 0 & 0 & 0 \\ 0 & -i e^{-K_{cs}} \delta_{a\bar{b}} & 0 & 0 \\ 0 & 0 & e^{-K_{cs}} & 0 \\ 0 & 0 & 0 & i e^{-K_{cs}} \delta_{a\bar{b}} \end{pmatrix}. \tag{C.12}$$

The determinant of this matrix is then $\det(M^\dagger \cdot \Sigma \cdot M) = e^{-2mK_{cs}}$. Using this result we find that the determinant of the Jacobian of the change of variables is

$$\det(J) = e^{2m(K_d + K_k)}, \tag{C.13}$$

and therefore, noting that the factor e^{2mK_d} cancels with that of (C.6), we find that the probability distribution on the variables $\{F_0, F_a, Z_0, Z_a\}$ is flat

$$d\mu_{\text{flux}}(F_A, Z_A, \bar{F}_A, \bar{Z}_A) = \mathcal{N} \, (dF_A d\bar{F}_A dZ_A d\bar{Z}_A)^{4m} e^{-2mK_k}. \tag{C.14}$$

In these variables no-scale vacua correspond to those configurations with $F_A = 0$, and the tadpole constraint requires

$$N_{\text{flux}} = Z_A \bar{Z}_A \equiv |Z|^2 \le L. \tag{C.15}$$

The no-scale conditions can be imposed by introducing a delta function $\delta^{2m}(F_A, \bar{F}_A)$ in (C.14), which is equivalent to considering simply the distribution

$$d\mu_{\text{flux}}(Z_A, \bar{Z}_A)|_{\text{no-scale}} = \mathcal{N} \, (dZ_A d\bar{Z}_A)^{2m}. \tag{C.16}$$

In other words, the variables $Z_A = \{e^{K/2}W, e^{K/2}D_0 D_a W\}$ and their complex conjugates form a set of $2(h^{2,1} + 1)$ independent complex variables uniformly distributed on the sphere (C.15) defined by the tadpole constraint. We refer to the previous probability density function as the *Denef-Douglas distribution*.

C.2 Constrained flux distribution

We will now repeat the above computation for the constrained ensemble of vacua. We begin by noting that this constraint can be implemented in the continuous flux approximation with Dirac delta functions as

$$d\mu_{\text{flux}}(f, h) = \mathcal{N} \, (df \, dh)^{4m} \, \delta(f_A^0) \delta(h_A^0). \tag{C.17}$$

After changing to complex flux coordinates, we obtain

$$d\mu_{\text{flux}}(N, \bar{N}) = \mathcal{N} \, (dN d\bar{N})^{4m} e^{2mK_d} \delta(N_A^0) \delta(\bar{N}_A^0) |J_0|, \tag{C.18}$$

where

$$|J_0| = \det \frac{\partial(N_A^0, \bar{N}_A^0)}{\partial(f_A^0, h_A^0)} = \det \begin{pmatrix} 1 & 1 \\ -\tau & -\bar{\tau} \end{pmatrix} = -2\mathrm{i}\,\mathrm{Im}\,\tau\,, \qquad (\text{C.19})$$

and so

$$d\mu_{flux}(N, \bar{N}) = \mathcal{N}\,\mathrm{i}(dN d\bar{N})^{4m}\mathrm{e}^{(2m-1)K_d}\delta(N_A^0)\delta(\bar{N}_A^0)\,. \qquad (\text{C.20})$$

Using the Hodge decomposition of the flux vector

$$N = \mathrm{e}^{\frac{1}{2}(-K_k - K_d + K_{cs})}(-\bar{F}_0\Pi + \mathrm{i}Z_0\bar{\Pi} + \bar{Z}_a D_a\Pi - \mathrm{i}F_a D_{\bar{a}}\bar{\Pi})\,, \qquad (\text{C.21})$$

we can obtain the form of the constraint in terms of the variables $\{Z_A, F_A, \bar{Z}_A, \bar{F}_A\}$. It is given by

$$N_A^0 = \mathrm{e}^{\frac{1}{2}(-K_k - K_d + K_{cs})}(-\bar{F}_0 + \mathrm{i}Z_0 - \sqrt{3/(1-2\xi)}\bar{Z}_1 + \sqrt{3/(1-2\xi)}\mathrm{i}F_1) = 0\,. \qquad (\text{C.22})$$

We can implement this condition as a constraint on the variables

$$Z_0 = Z_0^*(Z_a, F_A)\,, \qquad \bar{Z}_0 = \bar{Z}_0^*(Z_a, F_A) \qquad (\text{C.23})$$

with the aid of Dirac delta functions, so that the final density function, written in terms of $\{Z_A, F_A, \bar{Z}_A, \bar{F}_A\}$, reads

$$d\mu_{\text{flux}} = \mathcal{N}\,\mathrm{i}(dF_A d\bar{F}_A dZ_A d\bar{Z}_A)^{4m}\mathrm{e}^{-K_{cs}}\delta(Z_0 - Z_0^*)\delta(\bar{Z}_0 - \bar{Z}_0^*)\,. \qquad (\text{C.24})$$

Here we have absorbed the Calabi-Yau volume factor, which is independent of the axio-dilaton and complex structure fields, in the normalisation constant.

C.3 Density of generic no-scale vacua

We now turn to the computation of the density of flux vacua in the generic ensemble. The number of no-scale vacua $\mathcal{C}_{\text{vac}}(N)$ for a given choice of flux N can be obtained using the generalised Kac-Rice formula [115, 116]

$$\mathcal{C}_{\text{vac}}(N) = \int d^{2m}u\,\delta^{2m}(DW)\,|\det D^2 W|\,, \qquad (\text{C.25})$$

with $u^A = \{\tau, z^i\}$ and

$$\delta^{2m}(DW) = \delta^m(D_A W)\,\delta^m(D_{\bar{A}}\bar{W}), \qquad D^2 W = \begin{pmatrix} D_A D_{\bar{B}}W & D_A D_B W \\ D_{\bar{A}} D_{\bar{B}}\bar{W} & D_{\bar{A}} D_B \bar{W} \end{pmatrix}\,. \qquad (\text{C.26})$$

Let us now consider the total number of no-scale vacua in the ensemble of fluxes satisfying the tadpole constraint $N_{\text{flux}} \leq L$, which is given by

$$\mathcal{C}_{\text{vac}}(N_{\text{flux}} \leq L) = \sum_N \Theta(N_{\text{flux}} - L) \int d^{2m}u\,\delta^{2m}(DW)|\det D^2 W|\,. \qquad (\text{C.27})$$

Note that here we have chosen to count all choices of flux with equal weight, consistent with our initial assumption that fluxes are drawn from an underlying uniform distribution.

As discussed in [15], using the integral representation of the Heaviside theta function we can rewrite the previous formula as

$$\mathcal{C}_{vac}(N_{\text{flux}} \leq L) = \frac{1}{2\pi i} \int_C \frac{d\alpha}{\alpha} e^{\alpha L^*} \mathcal{C}(\alpha) \tag{C.28}$$

with

$$\mathcal{C}(\alpha) \equiv \sum_N \int d^{2m}u \; e^{-\alpha N_{\text{flux}}} \; \delta^{2m}(DW)|\det D^2W|$$

$$\approx \int (dNd\bar{N})^{4m} \int d^{2m}u \; e^{-\alpha N_{\text{flux}}} \; \delta^{2m}(DW)|\det D^2W| e^{2mK_d}, \tag{C.29}$$

where in the last line we have approximated the sum over the integer fluxes by an integral with measure given by (C.6).

Expressing the gradient, DW, and the Hessian of the superpotential, D^2W, in a canonically normalised basis, we find

$$\mathcal{C}(\alpha) = \int (dNd\bar{N})^{4m} \int d^{2m}u|\det g| \; e^{-\alpha N_{\text{flux}}} \; \delta^{2m}(D_a W)|\det \mathcal{H}|^{1/2} e^{2mK_d}$$

$$= \int (dZdF)^{4m} \int d^{2m}u|\det g| \; e^{-\alpha \mathcal{V}^2|Z|^2} \; \delta^m(F_A)\delta^m(\bar{F}_A)|\det \mathcal{H}|^{1/2} e^{-2mK_k}$$

$$= \mathcal{V}^{4m} \int (dZd\bar{Z})^{2m} \int d^{2m}u|\det g| \; e^{-\alpha \mathcal{V}^2|Z|^2} \; |\det \mathcal{H}|^{1/2}. \tag{C.30}$$

In the second line, the term of the form e^{mK} arises as a result of the change of variables (C.7) in the argument of the delta function, which then is reabsorbed when expressing $\det D^2W$ in terms of $\mathcal{H}$.[26] Rescaling $Z_A \rightarrow Z_A/(\mathcal{V}\sqrt{\alpha})$, it is possible to see that $\mathcal{C}(\alpha) = \mathcal{C}(1, \mathcal{V} = 1)\alpha^{-2m}$ and the overall volume factor disappears, so we can explicitly perform the integral in α to give

$$\mathcal{C}_{vac}(N_{\text{flux}} \leq L) = \Lambda(L, m) \cdot \int d^{2m}u|\det g| \int (dZd\bar{Z})^{2m} \; e^{-|Z|^2} \; |\det \mathcal{H}|^{1/2}, \tag{C.31}$$

where $\Lambda(L, m)$ is a constant depending on the tadpole parameter L and the moduli space dimension m. Consistent with the previous equation, the density of flux vacua is then defined by

$$d\mu_{\text{vac}}(z, \tau) = \mathcal{N} \cdot d^{2m}u \, |\det g| \left[\int (dZd\bar{Z})^{2m} \; e^{-|Z|^2} \; |\det \mathcal{H}|^{1/2} \right]. \tag{C.32}$$

C.4 Density of constrained vacua

For the ensemble with constrained fluxes the argument proceeds as before, but when changing to the variables (C.7) in (C.30), we should use the measure (C.24) rather than (C.16). As a result, the density of no-scale vacua is given by

$$d\mu_{\text{vac}}(z, \tau) = \mathcal{N} \cdot d^{2m}u \, |\det g| \left[\int (dZd\bar{Z})^{2(m-1)} \; e^{-|Z|^2} \; |\det \mathcal{H}|^{1/2} e^{-K_{cs}} \right], \tag{C.33}$$

---

[26]Recall that in canonically normalized coordinates we have the relation $\mathcal{H} = e^K(D^2W)^2 = (m_{3/2}\mathbb{1} + \mathcal{M})^2$, from (2.27).

where the integral is over the subspace of $\{Z_A, \bar{Z}_A\}$ defined by the constraints (C.23) with $F_A = \bar{F}_A = 0$ (no-scale conditions). In the case when the complex structure moduli space is one dimensional ($m = 2$), the integral appearing in the previous equation reduces to

$$\int dZ_1 d\bar{Z}_1 e^{-\frac{2(2-\xi)}{1-2\xi}|Z_1|^2} |Z_1|^4 \Big|1 + \frac{9}{(1-2\xi)^2} - \frac{3(2+\mathring{\kappa}^2)}{(1-2\xi)}\Big| \frac{\xi+1}{\xi}\,, \qquad (C.34)$$

where we used the relation $|Z_0| = \sqrt{3/(1-2\xi)}|Z_1|$ (given in (4.21)) and the definition of the LCS parameter $e^{-K_{cs}} = |2\,\mathrm{Im}\,\kappa_0|(\xi + 1)/\xi$. Integrating the previous expression over the complex variable Z_1, and over the directions $\mathrm{Im}\,z$ and $\mathrm{Re}\,\tau$ we find

$$d\mu_{\mathrm{vac}}(z, \tau) = \mathcal{N} \cdot \frac{(1+\xi)}{(2-\xi)^2} \frac{1}{r^2 s^2} dr ds\,, \qquad (C.35)$$

expressed in terms of the variables (6.7), which agrees with (6.16).

D   Bounds on the LCS parameter

The theoretical distributions (6.3) and (6.16) were derived in order to have an analytical description of the ensemble of no-scale vacua, constructed as described in section 5 and appendix B. However, this characterisation is only a faithful representation of the Landscape in the regime of moduli space where both the EFT and the continuous flux approximation are valid.

Indeed, vacua with large instanton corrections should be discarded, since the EFT we used cannot be trusted in those cases. As the vacua density functions (6.3) and (6.16) contain no information regarding the size of the instanton contributions, they are bound to be inaccurate in the regime where these corrections are large. Furthermore, from [67, 68], we know that in the generic ensemble the density of vacua should be suppressed with respect to the theoretical distribution (6.3), due to the breakdown of the continuous flux approximation. In this appendix we discuss the parameter space where the statistical description can be applied, providing an analytic estimate for this region in terms of the LCS parameter ξ.

D.1   No-scale equations near the LCS point

We begin by rewriting the no-scale equations (2.20) in the LCS limit in a more convenient way for the derivations below.

In this regime, $\xi \to 0$, the Kähler potential of the complex structure sector can be expressed as

$$Y \equiv e^{-K_{cs}} \approx \frac{1}{6}\kappa_{ijk}(z^i + \bar{z}^i)(z^j + \bar{z}^j)(z^k + \bar{z}^k)\,, \qquad (D.1)$$

and the canonically normalized Yukawa couplings satisfy [67, 68]

$$\kappa_{111} = \frac{2}{\sqrt{3}}Y\,, \qquad \kappa_{11\tilde{a}} = 0\,, \quad \kappa_{1\tilde{a}\tilde{b}} = -\frac{1}{\sqrt{3}}Y\delta_{\tilde{a}\tilde{b}}\,, \qquad (D.2)$$

where the direction "1" corresponds to the no-scale direction (4.7) and $\tilde{a}, \tilde{b} = 2, \dots h^{2,1}$. We also have

$$z^a = \frac{\sqrt{3}}{2}\delta_1^a + i\lambda^a, \qquad K_a = -\sqrt{3}\delta_1^a, \qquad (D.3)$$

where z^a (with $a = 1, \dots, h^{2,1}$) are the canonically normalised fields at the vacuum, and $\lambda^a = \text{Im}(z^a)$. After some algebra, it can be shown that the superpotential has the form

$$W = -\frac{i}{6}\kappa_{abc}N_A^0 z^a z^b z^c + \frac{1}{2}\kappa_{abc}N_A^a z^b z^c + i\left(\kappa_a N_A^0 - \kappa_{ab}N_A^b - N_a^B\right)z^a$$
$$+ \kappa_0 N_A^0 + \kappa_a N_A^a - N_0^B, \qquad (D.4)$$

while the no-scale conditions (2.20) read

$$D_0 W = -\frac{1}{6}\kappa_{abc}\bar{N}_A^0 z^a z^b z^c - \frac{i}{2}\kappa_{abc}\bar{N}_A^a z^b z^c + \left(\kappa_a \bar{N}_A^0 - \kappa_{ab}\bar{N}_A^b - \bar{N}_a^B\right)z^a$$
$$- i\kappa_0\bar{N}_A^0 - i\kappa_a\bar{N}_A^a + i\bar{N}_0^B = 0,$$
$$D_a W = -\frac{i}{2}\kappa_{abc}N_A^0 z^b z^c + \kappa_{abc}N_A^b z^c + i\kappa_a N_A^0 - i\kappa_{ab}N_A^b - iN_a^B - \sqrt{3}W\delta_a^1 = 0. \qquad (D.5)$$

To analyse these equations it is convenient to introduce the flux parameter redefinitions

$$\hat{N}_0^B \equiv -\frac{1}{6}\kappa_{abc}N_A^0 \lambda^a \lambda^b \lambda^c - \frac{1}{2}\kappa_{abc}N_A^a \lambda^b \lambda^c - \left(\kappa_a N_A^0 - \kappa_{ab}N_A^b - N_a^B\right)\lambda^a$$
$$+ \kappa_0 N_A^0 + \kappa_a N_A^a - N_0^B, \qquad (D.6)$$
$$\hat{N}_a^B \equiv -\frac{1}{2}\kappa_{abc}N_A^0 \lambda^b \lambda^c - \kappa_{abc}N_A^b \lambda^c - \kappa_a N_A^0 + \kappa_{ab}N_A^b + N_a^B. \qquad (D.7)$$

Note that the flux parameters $\hat{f}_I^B$ and $\hat{h}_I^B$ in $\hat{N} = \hat{f} - \tau\hat{h}$ are still real, but are not integers in general. Using these new parameters, the superpotential now reads

$$W = \hat{N}_0^B - i\frac{\sqrt{3}}{2}\hat{N}_1^B + \left[\left(\frac{\sqrt{3}}{4}\lambda^1 - \frac{i}{8}\right)N_A^0 + \frac{\sqrt{3}}{4}N_A^1\right]Y \qquad (D.8)$$

and the no-scale conditions are given by

$$\left[\left(\frac{1}{2}\lambda^1 + \frac{i}{4\sqrt{3}}\right)N_A^0 + \frac{1}{2}N_A^1\right]Y + i\hat{N}_1^B = -\frac{2}{\sqrt{3}}\hat{N}_0^B, \qquad (D.9)$$

$$\left[\left(\frac{1}{2}\lambda^1 - \frac{i\sqrt{3}}{4}\right)N_A^0 + \frac{1}{2}N_A^1\right]Y + i\hat{N}_1^B = 2\sqrt{3}\hat{N}_0^B, \qquad (D.10)$$

$$\left[\frac{1}{2}\lambda^{a'}N_A^0 + \frac{1}{2}N_A^{a'}\right]Y + i\hat{N}_{a'}^B = 0. \qquad (D.11)$$

These expressions can be rewritten in a more compact way as

$$\hat{N}_0^B = -\frac{i}{8}Y N_A^0, \qquad \hat{N}_a^B = \frac{i}{2}Y\left(N_A^0 \lambda^a + N_A^a\right). \qquad (D.12)$$

The second equation can be equivalently written, after contracting it with the vielbein e_i^a, as

$$\hat{N}_i^B = \frac{i}{2}Y\left(N_A^0 \lambda^j + N_A^j\right)g_{ji}, \qquad (D.13)$$

where we have used that $\hat{N}_a^B e_i^a = \hat{N}_i^B$, and $N_A^a e_i^a = N_A^j e_j^a e_i^a = N_A^j g_{ji}$, and similarly for the terms involving λ^a. The redefined fluxes can also be rewritten as

$$\hat{N}_0^B \equiv -\frac{1}{6}\kappa_{ijk}N_A^0\lambda^i\lambda^j\lambda^k - \frac{1}{2}\kappa_{ijk}N_A^i\lambda^j\lambda^k - \left(\kappa_i N_A^0 - \kappa_{ij}N_A^j - N_i^B\right)\lambda^i$$
$$+ \kappa_0 N_A^0 + \kappa_i N_A^i - N_0^B\,, \tag{D.14}$$

$$\hat{N}_i^B \equiv -\frac{1}{2}\kappa_{ijk}N_A^0\lambda^j\lambda^k - \kappa_{ijk}N_A^j\lambda^k - \kappa_i N_A^0 + \kappa_{ij}N_A^j + N_i^B\,. \tag{D.15}$$

D.2 Lower bound on the LCS parameter

We will now determine the regime of applicability of the continuous flux approximation near the LCS point on the generic flux ensemble, expressed as a lower bound for the LCS parameter ξ.

Let us first discuss the equation in (D.12) for $\hat{N}_0^B$ in the $\xi \to 0$ limit when $N_A^0 \neq 0$. From the definition of the LCS parameter ξ (4.1), we can rewrite Y as

$$Y = 2\left|\mathrm{Im}\,\kappa_0\right|\frac{1+\xi}{\xi} \approx 2\left|\mathrm{Im}\,\kappa_0\right|\xi^{-1} \tag{D.16}$$

in the LCS limit, that is, $\xi \to 0$. On the other hand, from the definition of N_A^0, we can obtain the following lower bound:

$$\left|N_A^0\right|^2 = (f_A^0 - \mathrm{Re}(\tau)h_A^0)^2 + \mathrm{Im}^2(\tau)(h_A^0)^2 \geq 1\,, \tag{D.17}$$

where in the last step we used $\mathrm{Im}(\tau) > 1$, as required for the vacua to be in the weak string coupling regime. This implies that at no-scale vacua near the LCS limit, we must have

$$|\hat{N}_0^B| \approx \frac{|\mathrm{Im}\,\kappa_0|\,|N_A^0|}{4\xi}\,. \tag{D.18}$$

Note that, since by assumption $|N_A^0| \neq 0$, the right hand side blows up when $\xi \to 0$, and so $|\hat{N}_0^B| \gtrsim \mathcal{O}(\xi^{-1})$, which will require some contributions in (D.7) to become large. From (D.17) we can see that the previous condition will be the least restrictive when $|N_A^0|$ and $\mathrm{Im}\,\tau$ are both $\mathcal{O}(1)$, leading to

$$|\hat{N}_0^B| \gtrsim \frac{|\mathrm{Im}\,\kappa_0|}{4\xi}\,. \tag{D.19}$$

In order to solve this condition, one could try to tune the parameters $\lambda^i = \mathrm{Im}\,z^i$ to be large, $\lambda^i = \mathcal{O}(\xi^{-1/3})$; however, in that case the cubic terms in (D.7) would dominate, and the first equation in (D.12) would become

$$\frac{1}{6}\kappa_{ijk}\lambda^i\lambda^j\lambda^k \overset{!}{\approx} \mathrm{i}\frac{|\mathrm{Im}\,\kappa_0|}{4\xi}\,, \tag{D.20}$$

which cannot be solved, as the left hand side is real and the right hand side purely imaginary. This conclusion is in agreement with the results of [67, 68], where it was shown that if the superpotential is dominated by its cubic term, the no-scale equations (2.20) cannot admit solutions in a neighbourhood of the LCS point.

As a consequence, we need terms with different powers of λ^i in (D.7) to be comparable and, assuming the constant coefficients of the prepotential to be $\mathcal{O}(1)$, due to the tadpole condition (2.21) we will typically have $|\hat{N}_0^B| = \mathcal{O}(\sqrt{N_{\text{flux}}})$. Combining all of this, we arrive at the bound we were looking for:

$$\xi \gtrsim \xi_{\min}\big|_{N_A^0 \neq 0} \equiv \frac{|\operatorname{Im}\kappa_0|}{4\sqrt{N_{\text{flux}}}}\,. \tag{D.21}$$

As an example, for the $\mathbb{WP}^4_{[1,1,1,1,4]}$ model, we have $N_{\text{flux}} = 972$ and $2|\operatorname{Im}\kappa_0| \approx 2.9$, which implies

$$\xi_{\min} = \mathcal{O}(10^{-2})\,. \tag{D.22}$$

In the case of the constrained ensemble, the previous argument does not apply. In the limit $\xi \to 0$ with $f_A^0 = h_A^0 = h_A^z = 0$ and

$$f_0^B = f_A^z \, k_z + \frac{h_0^B}{2(h_z^B)^2}\left[2h_z^B(f_z^B + f_A^z \, k_{zz}) - f_A^z \, h_0^B \, k_{zzz}\right],\tag{D.23}$$

the LCS parameter ξ can be used to parametrize no-scale solutions. This leads to a flat direction along $\operatorname{Im}\tau \approx (\xi_0/\xi)^{1/3}\,|f_A^z/h_z^B|$, where $\xi_0 \equiv (3/2^4)|\operatorname{Im}\kappa_0|k_{zzz}^2$, which allows solutions arbitrarily close to the LCS/weak-coupling limit.

D.3 Maximum value consistent with small instanton corrections

In this section, we give an upper bound $\xi_{\max}$, independent of the flux vector N, by requiring the instanton corrections to the metric of the complex structure moduli space to remain small. As we mentioned above, the numerical analysis shows that the field space metric is typically the object where these corrections have the largest effect, and thus it is particularly suitable for estimating the regime of validity of the EFT. For convenience we will split the prepotential as

$$\mathcal{F}(z) = \hat{\mathcal{F}}(z) + \mathcal{F}_*(z) + \dots, \tag{D.24}$$

where $\hat{\mathcal{F}}$ is the perturbative part of the prepotential, and $\mathcal{F}_*$ denotes the leading term of the instanton contributions $\mathcal{F}_{\text{inst}}$. In the case of the octic model, near the LCS point the prepotential is given by (5.2) and (5.3), which have the form

$$\hat{\mathcal{F}}(z) = \frac{i}{6}\kappa_3 z^3 + \frac{1}{2}\kappa_2 z^2 + i\kappa_1 z + \frac{1}{2}\kappa_0\,, \qquad \mathcal{F}_*(z) = -\frac{in_1}{(2\pi)^3}e^{-2\pi z}\,, \tag{D.25}$$

the latter being perturbatively small when compared to $\hat{\mathcal{F}}$ in the LCS regime. The period vector (2.9) is then split as

$$\Pi = \begin{pmatrix} 1 \\ iz \\ 2\mathcal{F} - z\partial_z\mathcal{F} \\ -i\partial_z\mathcal{F} \end{pmatrix} = \begin{pmatrix} 1 \\ iz \\ 2\hat{\mathcal{F}} - z\partial_z\hat{\mathcal{F}} \\ -i\partial_z\hat{\mathcal{F}} \end{pmatrix} + \begin{pmatrix} 0 \\ 0 \\ 2\mathcal{F}_* - z\partial_z\mathcal{F}_* \\ -i\partial_z\mathcal{F}_* \end{pmatrix} \equiv \hat{\Pi} + \Pi_*\,. \tag{D.26}$$

Keeping only to leading instanton contribution, the Kähler potential (2.13) is then

$$e^{-K_{cs}} = i\,\Pi^\dagger \cdot \Sigma \cdot \Pi \approx i\,\hat{\Pi}^\dagger \cdot \Sigma \cdot \hat{\Pi} + i\,\hat{\Pi}^\dagger \cdot \Sigma \cdot \Pi_* + i\,\Pi_*^\dagger \cdot \Sigma \cdot \hat{\Pi}$$
$$= e^{-\hat{K}} - 2\,\mathrm{Im}(\hat{\Pi}^\dagger \cdot \Sigma \cdot \Pi_*)\,. \tag{D.27}$$

Defining $\mathcal{I} \equiv \mathrm{Im}(\hat{\Pi}^\dagger \cdot \Sigma \cdot \Pi_*)$ we obtain to leading order

$$K_{cs} \approx \hat{K} + 2\mathcal{I}e^{\hat{K}}\,. \tag{D.28}$$

Denoting the zeroth order metric and its leading instanton correction as

$$G_{z\bar{z}} \equiv \partial_z \partial_{\bar{z}} \hat{K}\,, \qquad g_{z\bar{z}} \equiv \partial_z \partial_{\bar{z}} (2\mathcal{I}e^{\hat{K}})\,, \tag{D.29}$$

we find that the field space metric is given by

$$\partial_z \partial_{\bar{z}} K_{cs} \approx G_{z\bar{z}} + g_{z\bar{z}}$$
$$= G_{z\bar{z}} + 2e^{\hat{K}} \left(G_{z\bar{z}}\mathcal{I} + \hat{K}_z \hat{K}_{\bar{z}}\,\mathcal{I} + \hat{K}_{\bar{z}}\mathcal{I}_z + \hat{K}_z \mathcal{I}_{\bar{z}} + \mathcal{I}_{z\bar{z}} \right)\,, \tag{D.30}$$

where subindices denote partial derivatives. Letting e_z^1 be a *real vielbein* with respect to the zero-order metric $G_{z\bar{z}}$ (so that $G_{1\bar{1}} = 1$), we then find

$$g_{1\bar{1}} = 2e^{\hat{K}} \left(\left(1 + (\hat{K}_1)^2\right) \mathcal{I} + \hat{K}_1 \left(\mathcal{I}_1 + \mathcal{I}_{\bar{1}}\right) + \mathcal{I}_{1\bar{1}} \right)\,, \tag{D.31}$$

where we used $\hat{K}_1 = e_1^z \hat{K}_z = e_1^{\bar{z}} \hat{K}_{\bar{z}} = \hat{K}_{\bar{1}}$. The value of $\mathcal{I}$ and its partial derivatives are found by direct computation. Defining $\theta = 2\pi\mathrm{Im}(z)$ and using (4.2), we get

$$\mathcal{I} = -\frac{n_1}{4\pi^3} e^{-2\pi\mathrm{Re}(z)} (1 + 2\pi\mathrm{Re}(z)) \cos(\theta)\,, \tag{D.32}$$

$$\mathcal{I}_1 + \mathcal{I}_{\bar{1}} = \frac{2n_1}{\pi} e^{-2\pi\mathrm{Re}(z)} \frac{\mathrm{Re}^2(z)}{x} \cos(\theta)\,, \tag{D.33}$$

$$\mathcal{I}_{1\bar{1}} = \frac{2n_1}{\pi} e^{-2\pi\mathrm{Re}(z)} \frac{\mathrm{Re}^2(z)}{x^2} \cos(\theta)\,. \tag{D.34}$$

From the analysis in section 4, we know that the relations

$$e^{\hat{K}} = \frac{1}{2|\mathrm{Im}\,\kappa_0|} \frac{\xi}{1+\xi}\,, \qquad \hat{K}_1 = -\sqrt{\frac{3}{1-2\xi}}\,, \tag{D.35}$$

$$x^2 = \frac{3(1-2\xi)}{(1+\xi)^2}\,, \qquad \mathrm{Re}\,z = \left(\frac{3|\mathrm{Im}\,\kappa_0|}{2\kappa_3}\right)^{1/3} \frac{1}{\xi^{1/3}} \tag{D.36}$$

hold. Thus, substituting (D.32) through (D.36) into (D.31), and defining $\alpha \equiv \left(\frac{3|\mathrm{Im}k_0|}{2k_3}\right)^{1/3}$, we get

$$g_{1\bar{1}} = -\frac{n_1 \cos\theta}{6\pi^3 |\mathrm{Im}\,\kappa_0|} \frac{(2-\xi)\xi^{1/3}}{(1+\xi)(1-2\xi)} e^{-\frac{2\pi\alpha}{\xi^{1/3}}} \left((2\pi\alpha)^2 (1+\xi) + 3\xi^{2/3} + 6\pi\alpha\xi^{1/3} \right)\,.$$

Requiring the relative corrections to the canonically normalised metric to remain below 20% (or equivalently $|g_{1\bar{1}}| \le 0.2$, since $G_{1\bar{1}} = 1$), we find

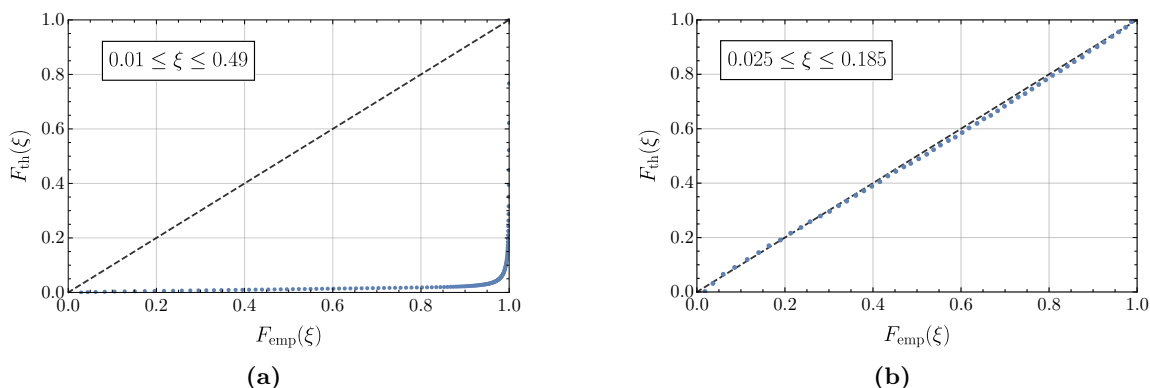$$\xi \le \xi_{\mathrm{max}} \approx 0.2\,. \tag{D.37}$$

Figure 16. P-P plots of the theoretical distribution of ξ, (6.8), versus the data obtained within the generic ensemble for (a) $0.01 \leq \xi \leq 0.49$ and (b) $0.025 \leq \xi \leq 0.185$. For reference, we plot the curve $F_{\text{th}}(\xi) = F_{\text{emp}}(\xi)$ corresponding to perfect agreement with a dashed line. We find that the distribution only fits the data within the range plotted in (b).

D.4 Accuracy of the statistical description

The statistical description of the flux ensemble presented in section 6 relies on two assumptions: first that the prepotential defining the EFT (5.2) contains only polynomial terms (we neglect instanton contributions, $\mathcal{F}_{\text{inst}} \equiv 0$), and second that the flux vector N can be regarded as a *continuous* random variable. These two conditions were imposed to make the problem analytically tractable, and also to simplify the numerical analysis so that the homotopy continuation methods could be applied. Thus, it is expected that, in regimes of parameter space where the vacua fail to be consistent with these assumptions, we should observe discrepancies between the theoretical probability distributions and the histograms obtained from the numerical scan. Here, we present the method we used to identify these deviations in the data in a systematic way. For definiteness we will focus the discussion on the distribution of the LCS parameter ξ, whose theoretical distributions for the generic and constrained ensembles are given by (6.8) and (6.17), respectively.

As we discussed above, the predicted distribution cannot be applied in the whole domain of ξ. Vacua near the conifold point $\xi_{\text{cnf}} \approx 0.39$ are prone to big instanton corrections while, for the generic ensemble, those in the LCS limit $\xi \to 0$ are expected to be suppressed due to the breakdown of the continuous flux approximation. Thus, we will now establish empirical bounds where the theoretical distributions for ξ are applicable. A widely used graphical method to verify how an empirical data distribution performs against a reference distribution is that of *P-P* plots (see, e.g., [136]). The method consists in plotting the empirical and theoretical cumulative distributions functions, $F_{\text{em}}(\xi)$ and $F_{\text{th}}(\xi)$, one against the other. If the agreement is perfect then the resulting plot is a straight line at 45 degrees.

As shown in figure 16, in the generic ensemble case, the best agreement with the Denef-Douglas distribution was found for

$$0.025 \leq \xi \leq 0.185 \,. \tag{D.38}$$

The large discrepancy observed in figure 16 (a) is due to the deficit of vacua near the LCS point in the generic ensemble. Note that these bounds are in very good agreement with the estimates (D.22) and (D.37) obtained above, which correspond to the limits of applicability of the continuous flux approximation and of the EFT, respectively.

A similar analysis shows that for the constrained ensemble, the theoretical and empirical distributions agree in the interval

$$5 \cdot 10^{-5} \le \xi|_{N_A^0 = 0} \le 0.185\,. \tag{D.39}$$

As can also be seen in the histograms of section 6, the Denef-Douglas distribution (6.3) provides an accurate description of the LCS parameter and other physical quantities (Yukawa couplings, scalar and fermion masses...) within the limits established above.

References

[1] S. Kachru, R. Kallosh, A.D. Linde and S.P. Trivedi, *de Sitter vacua in string theory*, *Phys. Rev. D* **68** (2003) 046005 [hep-th/0301240] [INSPIRE].

[2] V. Balasubramanian, P. Berglund, J.P. Conlon and F. Quevedo, *Systematics of moduli stabilisation in Calabi-Yau flux compactifications*, *JHEP* **03** (2005) 007 [hep-th/0502058] [INSPIRE].

[3] J.P. Conlon, F. Quevedo and K. Suruliz, *Large-volume flux compactifications: Moduli spectrum and D3/D7 soft supersymmetry breaking*, *JHEP* **08** (2005) 007 [hep-th/0505076] [INSPIRE].

[4] V. Balasubramanian and P. Berglund, *Stringy corrections to Kähler potentials, SUSY breaking, and the cosmological constant problem*, *JHEP* **11** (2004) 085 [hep-th/0408054] [INSPIRE].

[5] A. Westphal, *de Sitter string vacua from Kähler uplifting*, *JHEP* **03** (2007) 102 [hep-th/0611332] [INSPIRE].

[6] A. Giryavets, S. Kachru, P.K. Tripathy and S.P. Trivedi, *Flux compactifications on Calabi-Yau threefolds*, *JHEP* **04** (2004) 003 [hep-th/0312104] [INSPIRE].

[7] A. Giryavets, S. Kachru and P.K. Tripathy, *On the taxonomy of flux vacua*, *JHEP* **08** (2004) 002 [hep-th/0404243] [INSPIRE].

[8] O. DeWolfe, A. Giryavets, S. Kachru and W. Taylor, *Enumerating flux vacua with enhanced symmetries*, *JHEP* **02** (2005) 037 [hep-th/0411061] [INSPIRE].

[9] F. Denef, M.R. Douglas and B. Florea, *Building a better racetrack*, *JHEP* **06** (2004) 034 [hep-th/0404257] [INSPIRE].

[10] J. Louis, M. Rummel, R. Valandro and A. Westphal, *Building an explicit de Sitter*, *JHEP* **10** (2012) 163 [arXiv:1208.3208] [INSPIRE].

[11] J.J. Blanco-Pillado, M. Gomez-Reino and K. Metallinos, *Accidental Inflation in the Landscape*, *JCAP* **02** (2013) 034 [arXiv:1209.0796] [INSPIRE].

[12] M. Cicoli, D. Klevers, S. Krippendorf, C. Mayrhofer, F. Quevedo and R. Valandro, *Explicit de Sitter Flux Vacua for Global String Models with Chiral Matter*, *JHEP* **05** (2014) 001 [arXiv:1312.0014] [inSPIRE].

[13] R. Bousso and J. Polchinski, *Quantization of four form fluxes and dynamical neutralization of the cosmological constant*, *JHEP* **06** (2000) 006 [hep-th/0004134] [inSPIRE].

[14] M.R. Douglas, *The Statistics of string/M theory vacua*, *JHEP* **05** (2003) 046 [hep-th/0303194] [inSPIRE].

[15] F. Denef and M.R. Douglas, *Distributions of flux vacua*, *JHEP* **05** (2004) 072 [hep-th/0404116] [inSPIRE].

[16] F. Denef and M.R. Douglas, *Distributions of nonsupersymmetric flux vacua*, *JHEP* **03** (2005) 061 [hep-th/0411183] [inSPIRE].

[17] M.R. Douglas, *Statistics of string vacua*, hep-ph/0401004 [inSPIRE].

[18] M. Tegmark, *What does inflation really predict?*, *JCAP* **04** (2005) 001 [astro-ph/0410281] [inSPIRE].

[19] R. Easther and L. McAllister, *Random matrices and the spectrum of N-flation*, *JCAP* **05** (2006) 018 [hep-th/0512102] [inSPIRE].

[20] D. Battefeld, T. Battefeld and S. Schulz, *On the Unlikeliness of Multi-Field Inflation: Bounded Random Potentials and our Vacuum*, *JCAP* **06** (2012) 034 [arXiv:1203.3941] [inSPIRE].

[21] M.C.D. Marsh, L. McAllister, E. Pajer and T. Wrase, *Charting an Inflationary Landscape with Random Matrix Theory*, *JCAP* **11** (2013) 040 [arXiv:1307.3559] [inSPIRE].

[22] A. Masoumi, A. Vilenkin and M. Yamada, *Inflation in random Gaussian landscapes*, *JCAP* **05** (2017) 053 [arXiv:1612.03960] [inSPIRE].

[23] G. Wang and T. Battefeld, *Random Functions via Dyson Brownian Motion: Progress and Problems*, *JCAP* **09** (2016) 008 [arXiv:1607.02514] [inSPIRE].

[24] F.G. Pedro and A. Westphal, *Inflation with a graceful exit in a random landscape*, *JHEP* **03** (2017) 163 [arXiv:1611.07059] [inSPIRE].

[25] B. Freivogel, R. Gobbetti, E. Pajer and I.-S. Yang, *Inflation on a Slippery Slope*, arXiv:1608.00041 [inSPIRE].

[26] T. Bjorkmo and M.C.D. Marsh, *Manyfield Inflation in Random Potentials*, *JCAP* **02** (2018) 037 [arXiv:1709.10076] [inSPIRE].

[27] M. Dias, J. Frazer and M.c.D. Marsh, *Seven Lessons from Manyfield Inflation in Random Potentials*, *JCAP* **01** (2018) 036 [arXiv:1706.03774] [inSPIRE].

[28] A. Masoumi, A. Vilenkin and M. Yamada, *Initial conditions for slow-roll inflation in a random Gaussian landscape*, *JCAP* **07** (2017) 003 [arXiv:1704.06994] [inSPIRE].

[29] A. Masoumi, A. Vilenkin and M. Yamada, *Inflation in multi-field random Gaussian landscapes*, *JCAP* **12** (2017) 035 [arXiv:1707.03520] [inSPIRE].

[30] J.J. Blanco-Pillado, A. Vilenkin and M. Yamada, *Inflation in Random Landscapes with two energy scales*, *JHEP* **02** (2018) 130 [arXiv:1711.00491] [inSPIRE].

[31] S. Paban and R. Rosati, *Inflation in Multi-field Modified DBM Potentials*, *JCAP* **09** (2018) 042 [arXiv:1807.07654] [inSPIRE].

[32] T. Bjorkmo and M.C.D. Marsh, *Local, algebraic simplifications of Gaussian random fields*, *JCAP* **12** (2018) 022 [arXiv:1805.03117] [INSPIRE].

[33] J.J. Blanco-Pillado, K. Sousa and M.A. Urkiola, *Slepian models for Gaussian Random Landscapes*, *JHEP* **05** (2020) 142 [arXiv:1911.07618] [INSPIRE].

[34] L.L. Feng, S. Hotchkiss and R. Easther, *The distribution of vacua in random landscape potentials*, *JCAP* **01** (2021) 029 [arXiv:2004.04429] [INSPIRE].

[35] S.K. Garg and C. Krishnan, *Bounds on Slow Roll and the de Sitter Swampland*, *JHEP* **11** (2019) 075 [arXiv:1807.05193] [INSPIRE].

[36] H. Ooguri, E. Palti, G. Shiu and C. Vafa, *Distance and de Sitter Conjectures on the Swampland*, *Phys. Lett. B* **788** (2019) 180 [arXiv:1810.05506] [INSPIRE].

[37] N. Arkani-Hamed, L. Motl, A. Nicolis and C. Vafa, *The String landscape, black holes and gravity as the weakest force*, *JHEP* **06** (2007) 060 [hep-th/0601001] [INSPIRE].

[38] E. Palti, *The Swampland: Introduction and Review*, *Fortsch. Phys.* **67** (2019) 1900037 [arXiv:1903.06239] [INSPIRE].

[39] T.D. Brennan, F. Carta and C. Vafa, *The String Landscape, the Swampland, and the Missing Corner*, *PoS* **TASI2017** (2017) 015 [arXiv:1711.00864] [INSPIRE].

[40] P. Candelas and X. de la Ossa, *Moduli Space of Calabi-Yau Manifolds*, *Nucl. Phys. B* **355** (1991) 455 [INSPIRE].

[41] P. Candelas, X.C. De La Ossa, P.S. Green and L. Parkes, *A Pair of Calabi-Yau manifolds as an exactly soluble superconformal theory*, *Nucl. Phys. B* **359** (1991) 21 [INSPIRE].

[42] S. Hosono, A. Klemm, S. Theisen and S.-T. Yau, *Mirror symmetry, mirror map and applications to complete intersection Calabi-Yau spaces*, *Nucl. Phys. B* **433** (1995) 501 [hep-th/9406055] [INSPIRE].

[43] S. Gukov, C. Vafa and E. Witten, *CFT's from Calabi-Yau four folds*, *Nucl. Phys. B* **584** (2000) 69 [*Erratum ibid.* **608** (2001) 477] [hep-th/9906070] [INSPIRE].

[44] S.B. Giddings, S. Kachru and J. Polchinski, *Hierarchies from fluxes in string compactifications*, *Phys. Rev. D* **66** (2002) 106006 [hep-th/0105097] [INSPIRE].

[45] A. Klemm, *Topological string theory on Calabi-Yau threefolds*, *PoS* **RTN2005** (2005) 002 [INSPIRE].

[46] V. Braun, *On Free Quotients of Complete Intersection Calabi-Yau Manifolds*, *JHEP* **04** (2011) 005 [arXiv:1003.3235] [INSPIRE].

[47] A. Braun, A. Lukas and C. Sun, *Discrete Symmetries of Calabi-Yau Hypersurfaces in Toric Four-Folds*, *Commun. Math. Phys.* **360** (2018) 935 [arXiv:1704.07812] [INSPIRE].

[48] B.R. Greene and M.R. Plesser, *Duality in Calabi-Yau Moduli Space*, *Nucl. Phys. B* **338** (1990) 15 [INSPIRE].

[49] D. Gallego, *On the Effective Description of Large Volume Compactifications*, *JHEP* **06** (2011) 087 [arXiv:1103.5469] [INSPIRE].

[50] A. Achucarro, S. Hardeman and K. Sousa, *F-term uplifting and the supersymmetric integration of heavy moduli*, *JHEP* **11** (2008) 003 [arXiv:0809.1441] [INSPIRE].

[51] K. Sousa and P. Ortiz, *Perturbative Stability along the Supersymmetric Directions of the Landscape*, *JCAP* **02** (2015) 017 [arXiv:1408.6521] [INSPIRE].

[52] M. Rummel and Y. Sumitomo, *de Sitter Vacua from a D-term Generated Racetrack Uplift*, *JHEP* **01** (2015) 015 [arXiv:1407.7580] [INSPIRE].

[53] M. Rummel and Y. Sumitomo, *Probability of vacuum stability in type IIB multi-Kähler moduli models*, *JHEP* **12** (2013) 003 [arXiv:1310.4202] [INSPIRE].

[54] A. Maharana, M. Rummel and Y. Sumitomo, *Accidental Kähler moduli inflation*, *JCAP* **09** (2015) 040 [arXiv:1504.07202] [INSPIRE].

[55] M. Cicoli, F. Muia and F.G. Pedro, *Microscopic Origin of Volume Modulus Inflation*, *JCAP* **12** (2015) 040 [arXiv:1509.07748] [INSPIRE].

[56] A. Achúcarro, P. Ortiz and K. Sousa, *A new class of de Sitter vacua in String Theory Compactifications*, *Phys. Rev. D* **94** (2016) 086012 [arXiv:1510.01273] [INSPIRE].

[57] A. Klemm and S. Theisen, *Considerations of one modulus Calabi-Yau compactifications: Picard-Fuchs equations, Kähler potentials and mirror maps*, *Nucl. Phys. B* **389** (1993) 153 [hep-th/9205041] [INSPIRE].

[58] C. Doran, B. Greene and S. Judes, *Families of quintic Calabi-Yau 3-folds with discrete symmetries*, *Commun. Math. Phys.* **280** (2008) 675 [hep-th/0701206] [INSPIRE].

[59] P. Candelas and C. Mishra, *Highly Symmetric Quintic Quotients*, *Fortsch. Phys.* **66** (2018) 1800017 [arXiv:1709.01081] [INSPIRE].

[60] V. Braun, *The 24-Cell and Calabi-Yau Threefolds with Hodge Numbers* $(1,1)$, *JHEP* **05** (2012) 101 [arXiv:1102.4880] [INSPIRE].

[61] V. Batyrev and M. Kreuzer, *Constructing new Calabi-Yau 3-folds and their mirrors via conifold transitions*, *Adv. Theor. Math. Phys.* **14** (2010) 879 [arXiv:0802.3376] [INSPIRE].

[62] C.F. Doran and J.W. Morgan, *Mirror symmetry and integral variations of Hodge structure underlying one parameter families of Calabi-Yau threefolds*, in *Workshop on Calabi-Yau Varieties and Mirror Symmetry*, (2005) [math/0505272] [INSPIRE].

[63] V. Braun, P. Candelas and X. de la Ossa, *Two One-Parameter Special Geometries*, arXiv:1512.08367 [INSPIRE].

[64] P. Candelas, X. de la Ossa, M. Elmi and D. Van Straten, *A One Parameter Family of Calabi-Yau Manifolds with Attractor Points of Rank Two*, *JHEP* **10** (2020) 202 [arXiv:1912.06146] [INSPIRE].

[65] A. Joshi and A. Klemm, *Swampland Distance Conjecture for One-Parameter Calabi-Yau Threefolds*, *JHEP* **08** (2019) 086 [arXiv:1903.00596] [INSPIRE].

[66] A. Font, *Periods and duality symmetries in Calabi-Yau compactifications*, *Nucl. Phys. B* **391** (1993) 358 [hep-th/9203084] [INSPIRE].

[67] C. Brodie and M.C.D. Marsh, *The Spectra of Type IIB Flux Compactifications at Large Complex Structure*, *JHEP* **01** (2016) 037 [arXiv:1509.06761] [INSPIRE].

[68] M.C.D. Marsh and K. Sousa, *Universal Properties of Type IIB and F-theory Flux Compactifications at Large Complex Structure*, *JHEP* **03** (2016) 064 [arXiv:1512.08549] [INSPIRE].

[69] T. Eguchi and Y. Tachikawa, *Distribution of flux vacua around singular points in Calabi-Yau moduli space*, *JHEP* **01** (2006) 100 [hep-th/0510061] [INSPIRE].

[70] G. Torroba, *Finiteness of Flux Vacua from Geometric Transitions*, *JHEP* **02** (2007) 061 [hep-th/0611002] [INSPIRE].

[71] A.P. Braun, N. Johansson, M. Larfors and N.-O. Walliser, *Restrictions on infinite sequences of type IIB vacua*, *JHEP* **10** (2011) 091 [arXiv:1108.1394] [INSPIRE].

[72] U.H. Danielsson, N. Johansson and M. Larfors, *The World next door: Results in landscape topography*, *JHEP* **03** (2007) 080 [hep-th/0612222] [INSPIRE].

[73] T.W. Grimm, C. Li and I. Valenzuela, *Asymptotic Flux Compactifications and the Swampland*, *JHEP* **06** (2020) 009 [*Erratum ibid.* **01** (2021) 007] [arXiv:1910.09549] [INSPIRE].

[74] D. Marsh, L. McAllister and T. Wrase, *The Wasteland of Random Supergravities*, *JHEP* **03** (2012) 102 [arXiv:1112.3034] [INSPIRE].

[75] T.C. Bachlechner, D. Marsh, L. McAllister and T. Wrase, *Supersymmetric Vacua in Random Supergravity*, *JHEP* **01** (2013) 136 [arXiv:1207.2763] [INSPIRE].

[76] T.W. Grimm and J. Louis, *The Effective action of $N = 1$ Calabi-Yau orientifolds*, *Nucl. Phys. B* **699** (2004) 387 [hep-th/0403067] [INSPIRE].

[77] M.R. Douglas and S. Kachru, *Flux compactification*, *Rev. Mod. Phys.* **79** (2007) 733 [hep-th/0610102] [INSPIRE].

[78] T.D. Dimofte, *Type IIB Flux Vacua at Large Complex Structure*, *JHEP* **09** (2008) 064 [arXiv:0806.0001] [INSPIRE].

[79] K. Becker, M. Becker, M. Haack and J. Louis, *Supersymmetry breaking and alpha-prime corrections to flux induced potentials*, *JHEP* **06** (2002) 060 [hep-th/0204254] [INSPIRE].

[80] L. Anguelova, C. Quigley and S. Sethi, *The Leading Quantum Corrections to Stringy Kähler Potentials*, *JHEP* **10** (2010) 065 [arXiv:1007.4793] [INSPIRE].

[81] S. Sethi, *Supersymmetry Breaking by Fluxes*, *JHEP* **10** (2018) 022 [arXiv:1709.03554] [INSPIRE].

[82] S. Kachru and S.P. Trivedi, *A comment on effective field theories of flux vacua*, *Fortsch. Phys.* **67** (2019) 1800086 [arXiv:1808.08971] [INSPIRE].

[83] D. Freedman and A. Van Proeyen, *Supergravity*, Cambridge University Press (2012) [INSPIRE].

[84] S.J. Gates, M.T. Grisaru, M. Roček and W. Siegel, *Superspace Or One Thousand and One Lessons in Supersymmetry*, vol. 58 of *Frontiers in Physics* (1983) [hep-th/0108200] [INSPIRE].

[85] R. D'Auria, S. Ferrara, M. Trigiante and S. Vaula, $N = 1$ *reductions of* $N = 2$ *supergravity in the presence of tensor multiplets*, *JHEP* **03** (2005) 052 [hep-th/0502219] [INSPIRE].

[86] A. Achucarro, S. Hardeman and K. Sousa, *Consistent Decoupling of Heavy Scalars and Moduli in* $N = 1$ *Supergravity*, *Phys. Rev. D* **78** (2008) 101901 [arXiv:0806.4364] [INSPIRE].

[87] P. Candelas, X. De La Ossa, A. Font, S.H. Katz and D.R. Morrison, *Mirror symmetry for two parameter models. 1.*, *Nucl. Phys. B* **416** (1994) 481 [hep-th/9308083] [INSPIRE].

[88] P. Berglund et al., *Periods for Calabi-Yau and Landau-Ginzburg vacua*, *Nucl. Phys. B* **419** (1994) 352 [hep-th/9308005] [INSPIRE].

[89] P. Candelas, A. Font, S.H. Katz and D.R. Morrison, *Mirror symmetry for two parameter models. 2.*, *Nucl. Phys. B* **429** (1994) 626 [hep-th/9403187] [INSPIRE].

[90] P. Candelas, X. de la Ossa and F. Rodriguez-Villegas, *Calabi-Yau manifolds over finite fields. 1.*, hep-th/0012233 [INSPIRE].

[91] E. Cremmer et al., *Vector Multiplets Coupled to $N = 2$ Supergravity: SuperHiggs Effect, Flat Potentials and Geometric Structure*, *Nucl. Phys. B* **250** (1985) 385 [INSPIRE].

[92] D. Farquet and C.A. Scrucca, *Scalar geometry and masses in Calabi-Yau string models*, *JHEP* **09** (2012) 025 [arXiv:1205.5728] [INSPIRE].

[93] L. Covi, M. Gomez-Reino, C. Gross, J. Louis, G.A. Palma and C.A. Scrucca, *de Sitter vacua in no-scale supergravities and Calabi-Yau string models*, *JHEP* **06** (2008) 057 [arXiv:0804.1073] [INSPIRE].

[94] L. Covi, M. Gomez-Reino, C. Gross, G.A. Palma and C.A. Scrucca, *Constructing de Sitter vacua in no-scale string models without uplifting*, *JHEP* **03** (2009) 146 [arXiv:0812.3864] [INSPIRE].

[95] H. Abe, T. Higaki and T. Kobayashi, *Remark on integrating out heavy moduli in flux compactification*, *Phys. Rev. D* **74** (2006) 045012 [hep-th/0606095] [INSPIRE].

[96] D. Gallego and M. Serone, *An Effective Description of the Landscape — I.*, *JHEP* **01** (2009) 056 [arXiv:0812.0369] [INSPIRE].

[97] D. Gallego and M. Serone, *An Effective Description of the Landscape — II*, *JHEP* **06** (2009) 057 [arXiv:0904.2537] [INSPIRE].

[98] I. Bena, E. Dudas, M. Graña and S. Lüst, *Uplifting Runaways*, *Fortsch. Phys.* **67** (2019) 1800100 [arXiv:1809.06861] [INSPIRE].

[99] M. Demirtas, M. Kim, L. Mcallister and J. Moritz, *Vacua with Small Flux Superpotential*, *Phys. Rev. Lett.* **124** (2020) 211603 [arXiv:1912.10047] [INSPIRE].

[100] M.C.D. Marsh, B. Vercnocke and T. Wrase, *Decoupling and de Sitter Vacua in Approximate No-Scale Supergravities*, *JHEP* **05** (2015) 081 [arXiv:1411.6625] [INSPIRE].

[101] D. Gallego, M.C.D. Marsh, B. Vercnocke and T. Wrase, *A New Class of de Sitter Vacua in Type IIB Large Volume Compactifications*, *JHEP* **10** (2017) 193 [arXiv:1707.01095] [INSPIRE].

[102] A. Sen, *Orientifold limit of F-theory vacua*, *Phys. Rev. D* **55** (1997) R7345 [hep-th/9702165] [INSPIRE].

[103] A. Klemm, B. Lian, S.S. Roan and S.-T. Yau, *Calabi-Yau fourfolds for M-theory and F-theory compactifications*, *Nucl. Phys. B* **518** (1998) 515 [hep-th/9701023] [INSPIRE].

[104] F. Denef, *Les Houches Lectures on Constructing String Vacua*, *Les Houches* **87** (2008) 483 [arXiv:0803.1194] [INSPIRE].

[105] D. Lüst, P. Mayr, S. Reffert and S. Stieberger, *F-theory flux, destabilization of orientifolds and soft terms on D7-branes*, *Nucl. Phys. B* **732** (2006) 243 [hep-th/0501139] [INSPIRE].

[106] A. Collinucci, F. Denef and M. Esole, *D-brane Deconstructions in IIB Orientifolds*, *JHEP* **02** (2009) 005 [arXiv:0805.1573] [INSPIRE].

[107] M. Alim, M. Hecht, H. Jockers, P. Mayr, A. Mertens and M. Soroush, *Hints for Off-Shell Mirror Symmetry in type-II/F-theory Compactifications*, *Nucl. Phys. B* **841** (2010) 303 [arXiv:0909.1842] [INSPIRE].

[108] Y. Honma and H. Otsuka, *On the Flux Vacua in F-theory Compactifications*, *Phys. Lett. B* **774** (2017) 225 [arXiv:1706.09417] [INSPIRE].

[109] Y. Honma and H. Otsuka, *F-theory Flux Vacua and Attractor Equations*, *JHEP* **04** (2020) 001 [arXiv:1910.10725] [INSPIRE].

[110] D. Bates, D. Brake and M. Niemerg, *Paramotopy: Parameter homotopies in parallel*, in *International Congress on Mathematical Software*, pp. 28–35, Springer (2018) [DOI].

[111] A.J. Sommese and C.W. Wampler, *Numerical algebraic geometry*, *Lect. Appl. Math.* **32** (1996) 749.

[112] A.J. Sommese and C.W. Wampler, *The Numerical Solution of Systems of Polynomials Arising in Engineering and Science*, World Scientific (2005) [DOI].

[113] D. Martinez-Pedrera, D. Mehta, M. Rummel and A. Westphal, *Finding all flux vacua in an explicit example*, *JHEP* **06** (2013) 110 [arXiv:1212.4530] [INSPIRE].

[114] Y.-H. He, D. Mehta, M. Niemerg, M. Rummel and A. Valeanu, *Exploring the Potential Energy Landscape Over a Large Parameter-Space*, *JHEP* **07** (2013) 050 [arXiv:1301.0946] [INSPIRE].

[115] M. Kac, *On the average number of real roots of a random algebraic equation*, *Bull. Am. Math. Soc.* **49** (1943) 314.

[116] S.O. Rice, *Mathematical analysis of random noise*, *Bell Syst. Tech. J.* **23** (1944) 282.

[117] R.J. Adler and J.E. Taylor, *Random fields and geometry*, Springer Science & Business Media (2009).

[118] S. Ashok and M.R. Douglas, *Counting flux vacua*, *JHEP* **01** (2004) 060 [hep-th/0307049] [INSPIRE].

[119] J.P. Conlon and F. Quevedo, *On the explicit construction and statistics of Calabi-Yau flux vacua*, *JHEP* **10** (2004) 039 [hep-th/0409215] [INSPIRE].

[120] I. Broeckel, M. Cicoli, A. Maharana, K. Singh and K. Sinha, *Moduli Stabilisation and the Statistics of SUSY Breaking in the Landscape*, *JHEP* **10** (2020) 015 [arXiv:2007.04327] [INSPIRE].

[121] A. Aazami and R. Easther, *Cosmology from random multifield potentials*, *JCAP* **03** (2006) 013 [hep-th/0512050] [INSPIRE].

[122] D. Mehta, M. Niemerg and C. Sun, *Statistics of Stationary Points of Random Finite Polynomial Potentials*, *J. Stat. Mech.* **1509** (2015) P09012 [arXiv:1504.02786] [INSPIRE].

[123] J. von Neuman and E. Wigner, *Über merkwürdige diskrete Eigenwerte. Über das Verhalten von Eigenwerten bei adiabatischen Prozessen*, *Phys. Z.* **30** (1929) 467.

[124] T. Guhr, A. Müller-Groeling and H.A. Weidenmüller, *Random matrix theories in quantum physics: Common concepts*, *Phys. Rept.* **299** (1998) 189 [cond-mat/9707301] [INSPIRE].

[125] J.P. Conlon, *The QCD axion and moduli stabilisation*, *JHEP* **05** (2006) 078 [hep-th/0602233] [INSPIRE].

[126] T. Banks and L.J. Dixon, *Constraints on String Vacua with Space-Time Supersymmetry*, *Nucl. Phys. B* **307** (1988) 93 [INSPIRE].

[127] R. Kallosh, A.D. Linde, D.A. Linde and L. Susskind, *Gravity and global symmetries*, *Phys. Rev. D* **52** (1995) 912 [hep-th/9502069] [INSPIRE].

[128] T. Banks and N. Seiberg, *Symmetries and Strings in Field Theory and Gravity*, *Phys. Rev. D* **83** (2011) 084019 [arXiv:1011.5120] [INSPIRE].

[129] D. Junghans, *Weakly Coupled de Sitter Vacua with Fluxes and the Swampland*, *JHEP* **03** (2019) 150 [`arXiv:1811.06990`] [InSPIRE].

[130] M. Demirtas, M. Kim, L. Mcallister and J. Moritz, *Conifold Vacua with Small Flux Superpotential*, `arXiv:2009.03312` [InSPIRE].

[131] R. Álvarez-García, R. Blumenhagen, M. Brinkmann and L. Schlechter, *Small Flux Superpotentials for Type IIB Flux Vacua Close to a Conifold*, `arXiv:2009.03325` [InSPIRE].

[132] C. Crinò, F. Quevedo and R. Valandro, *On de Sitter String Vacua from Anti-D3-branes in the Large Volume Scenario*, *JHEP* **03** (2021) 258 [`arXiv:2010.15903`] [InSPIRE].

[133] J. Otto, A.G. Forbes and J. Verschelde, *Solving polynomial systems with phcpy*, `arXiv:1907.00096`.

[134] J. Gray, Y.-H. He, A. Ilderton and A. Lukas, *STRINGVACUA: A Mathematica Package for Studying Vacuum Configurations in String Phenomenology*, *Comput. Phys. Commun.* **180** (2009) 107 [`arXiv:0801.1508`] [InSPIRE].

[135] D.J. Bates, J.D. Hauenstein, A.J. Sommese and C.W. Wampler, *Bertini: Software for numerical algebraic geometry*, DOI (2013).

[136] J. Klemelä, *Smoothing of Multivariate Data: Density Estimation and Visualization*, Wiley (2009) [DOI].